
Masters Theses

Student Theses and Dissertations

Fall 2018

New nanoparticle water-based drilling fluid formulation with enhanced thermal stability and inhibition capabilities in the Woodford shale

Jose Aramendiz Pacheco

Follow this and additional works at: https://scholarsmine.mst.edu/masters_theses



Part of the [Petroleum Engineering Commons](#)

Department:

Recommended Citation

Aramendiz Pacheco, Jose, "New nanoparticle water-based drilling fluid formulation with enhanced thermal stability and inhibition capabilities in the Woodford shale" (2018). *Masters Theses*. 7818. https://scholarsmine.mst.edu/masters_theses/7818

This thesis is brought to you by Scholars' Mine, a service of the Missouri S&T Library and Learning Resources. This work is protected by U. S. Copyright Law. Unauthorized use including reproduction for redistribution requires the permission of the copyright holder. For more information, please contact scholarsmine@mst.edu.

NEW NANOPARTICLE WATER-BASED DRILLING FLUID
FORMULATION WITH ENHANCED THERMAL STABILITY AND
INHIBITION CAPABILITIES IN THE WOODFORD SHALE

By

JOSE ARAMENDIZ PACHECO

A THESIS

Presented to the Faculty of Graduate School of the
MISSOURI UNIVERSITY OF SCIENCE AND TECHNOLOGY

In Partial Fulfillment of Requirements for the Degree

MASTER OF SCIENCE

in

PETROLEUM ENGINEERING

2018

Approved by:

Dr. Abdulmohsin Imqam. Advisor
Dr. Shari Dunn-Norman
Dr. Ralph Flori

© 2018

Jose Aramendiz Pacheco

All Rights Reserved

ABSTRACT

Drilling fluid design for unconventional reservoirs aims at preventing formation instability problems associated with fluid invasion, shale swelling, and cuttings dispersion. Although oil-based mud (OBM) can be used to achieve these goals, environmental and economic concerns limit its application. This experimental study evaluated the potential use of nanoparticles (NP) to improve water-based mud (WBM) inhibition capabilities and its ability to enhance the overall drilling fluid thermal stability while providing a cleaner technology to the industry.

Characterization of Woodford shale was completed with X-ray diffraction, cation exchange capacity, and scanning electron microscopy, silica, and graphene NP were characterized with aqueous stability tests and zeta-potential. Selected NP were added at a low concentration (0.1 – 1 % wt.), and standard filtration (LTLP & HTHP), rheology, dispersion and swelling tests were conducted to investigate the inhibition improvements of the new NP-WBM. In addition, optimum formulation of the new NP-WBM was aged at different conditions (150°F, 200°F, 250°F) for thermal and rheological stability. Conventional KCL/PHPA fluid was used for comparison purposes.

The NP showed a reduction of the chemical interactions between the WBM and Woodford shale samples, reducing the swelling and dispersion effects. Also, a synergistic effect was observed between NP and conventional additives indicating that NP had the capability to improve the WBM temperature resistance. Thus, offering an eco-friendly alternative with enhanced thermal and rheological stability of the overall WBM formulation and providing more efficient drilling and wellbore stability.

ACKNOWLEDGMENTS

First, I would like to thank God for giving me this unique opportunity and support me every single day of my life. Nothing can be achieved without his grace and mercy.

I would like to express my feeling of gratitude to my advisor Dr. Abdulmohsin Hussain Imqam for the opportunity of being part of his research group. His support, motivation, and understanding in the most difficult moments help me complete this research.

I would also like to thank my advisory committee: Dr. Shari Dunn-Norman and Dr. Ralph Flori for their guidance and assistant during my master's program and research. I also thank Dr. David Wronkiewicz and Dr. Lana Alagha for their technical advice on specific tasks during this research.

There are no words to express my deep gratitude to my wife, parents, and sister. Their endless love and support gave me the strength needed to pursue this goal and I dedicated this work to them. Furthermore, I express my gratitude to my friend in Rolla that make this experience unforgettable.

Finally, I would like to thanks to all my colleagues in the wellbore stability and hydraulic fracturing research group for their invaluable help, enthusiasm, and advice during the entire project.

TABLE OF CONTENTS

	Page
ABSTRACT.....	iii
ACKNOWLEDGMENTS	iv
LIST OF ILLUSTRATIONS.....	x
LIST OF TABLES.....	xv
NOMENCLATURE	xvii
 SECTION	
1. INTRODUCTION	1
1.1. STATEMENT AND SIGNIFICANCE OF THE PROBLEM.....	1
1.2. EXPECTED IMPACTS AND CONTRIBUTIONS	4
1.3. RESEARCH OBJECTIVES	5
1.4. SCOPE OF THIS WORK	6
2. LITERATURE REVIEW.....	8
2.1. DEFINITION OF UNCONVENTIONAL SHALE RESOURCES.....	8
2.2. SHALE HYDRATION MECHANISM.....	10
2.3. WELLBORE INSTABILITY IN SHALE	15
2.4. CLASSIFICATION OF CONVENTIONAL DRILLING FLUIDS.....	19
2.4.1. Non-Aqueous Drilling Fluids (NADF).....	21
2.4.2. Water-Based Drilling Fluid.....	22
2.4.2.1. Amine water-based drilling fluid.....	22
2.4.2.2. KCL/PHPA water-based drilling fluid.....	22

2.4.2.3. Glycol water-based drilling fluids	23
2.4.2.4. Aluminum water-based drilling fluids.....	24
2.4.2.5. Silicate water-based drilling fluid.....	25
2.5. FUNCTIONS OF DRILLING FLUIDS	26
2.5.1. Rheology of Drilling Fluids.....	27
2.5.2. General Considerations of Filtration in Drilling Fluids.....	31
2.5.3. Temperature Effects on Drilling Fluids.....	32
2.6. DRILLING FLUIDS CHALLENGES IN UNCONVENTIONAL SHALES ...	33
2.7. INTRODUCTION TO NANOTECHNOLOGY	35
2.7.1. Definition of Nanoparticles.....	36
2.7.2. Properties of Nanoparticles.....	36
2.8. NANOTECHNOLOGY IN OIL & GAS INDUSTRY	37
2.9. NANOTECHNOLOGY APPLIED TO DRILLING FLUIDS IN SHALES	39
2.9.1. Impact of NP in the Reduction of Fluid Invasion in Shales.....	40
2.9.2. Importance of NP Stability in Drilling Fluids.....	44
2.9.3. Impact of NP in the Rheology of Drilling Fluids.....	48
2.9.4. Impact of NP in the Inhibition of Shale Cuttings.....	51
2.9.5. Impact of NP in Wellbore Strengthening.....	52
3. NEW NANOPARTICLE WATER-BASED DRILLING FLUID FORMULATION WITH ENHANCED THERMAL STABILITY AND INHIBITION CAPABILITIES IN THE WOODFORD SHALE.....	56
3.1. EXPERIMENTAL METHODOLOGY AND DESCRIPTION	56
3.1.1. Shale Analysis Techniques.....	57
3.1.1.1. X-Ray diffraction and clay mineralogy composition.....	57

3.1.1.2. Shale pore determination through SEM.....	64
3.1.1.3. Cation exchange capacity test.....	68
3.1.1.4. Shale porosity measurement.....	71
3.1.2. Nanoparticle Analysis Technique.....	77
3.1.2.1. NP aqueous stability test.....	78
3.1.2.2. NP Zeta-potential measurement.....	81
3.1.3. NP-WBM and KCL/PHPA WBM Analysis Technique.....	86
3.1.3.1. Drilling fluid compositions.....	87
3.1.3.2. Concentration limits for LCM and NP material.....	93
3.1.3.3. NP-WBM preparation procedure.....	94
3.1.3.4. NP-WBM screening criteria.....	97
3.1.3.5. API standard test evaluation.....	97
3.1.3.6. Drilling fluid-formation chemical interaction tests.....	105
3.1.3.7. Dynamic aging test of WBM.....	109
3.2. RHEOLOGICAL MODEL OF THE NP-WBM.....	110
4. RESULTS & DISCUSSION.....	112
4.1. WOODFORD SHALE CHARACTERIZATION.....	112
4.1.1. XRD Analysis.....	113
4.1.2. SEM Analysis.....	115
4.1.3. CEC Analysis.....	119
4.1.4. Porosity Analysis.....	120
4.2. SiO ₂ & GRAPHENE OXIDE (GO) NP CHARACTERIZATION.....	121
4.2.1. Aqueous Stability Test.....	121

4.2.1.1 Effect of salt on SiO ₂ & GO nanoparticle.....	122
4.2.1.2. Effect of pH on SiO ₂ & GO nanoparticle.....	124
4.2.2. SiO ₂ and GO Nanoparticle Zeta Potential Analysis.	125
4.3. NP-WBM DRILLING FLUID CHARACTERIZATION	126
4.3.1. NP-WBM Density and pH.....	127
4.3.2. Effect of Nanoparticle on Static LTLP Filtration Test.	129
4.3.3. Effect of Nanoparticle on Static HTHP Filtration Test.	130
4.3.4. Effect of Nanoparticle on the Rheology Behavior.....	130
4.3.5. Selection of Optimum Nanoparticle Concentration.....	132
4.3.5.1. LTLP and HTHP filtration final screening of NP-WBM.	133
4.3.5.2. Rheology behavior for the final screening of NP-WBM.	133
4.3.5.3. Filtration behavior of optimum NP-WBM.	134
4.3.5.4. Rheology behavior of the optimum NP-WBM.....	138
4.3.6. NP-WBM Inhibition Capabilities in the Woodford Shale.....	139
4.3.6.1. NP-WBM dispersion test analysis.	140
4.3.6.2. NP-WBM visual swelling analysis.	141
4.3.6.3. NP-WBM bulk swelling analysis.....	144
5. NP-WBM VS. KCL-PHPA WBM AT AGING CONDITIONS.....	146
5.1. FILTRATION CAPABILITIES	146
5.2. RHEOLOGICAL BEHAVIOR ANALYSIS.....	150
5.3. INHIBITION CHARACTERISTICS ON THE WOODFORD SHALE.....	158
6. CONCLUSION AND RECOMMENDATIONS.....	162
6.1. CONCLUSIONS.....	162

6.2. RECOMMENDATION FOR FUTURE WORK..... 165

REFERENCES 167

VITA..... 177

LIST OF ILLUSTRATIONS

	Page
Figure 1.1. US Energy production history & projection (EIA 2017).	1
Figure 1.2. US Net energy trade (EIA 2017).	2
Figure 1.3. The Scope of the Research.	7
Figure 2.1. Oil and gas pyramid resources (Aguilera, 2014).	9
Figure 2.2. Directional drilling and hydraulic fracturing in shales.	10
Figure 2.3. Structure of clay mineral groups.	11
Figure 2.4. Representation of micro-shale structure.	13
Figure 2.5. Crystalline swelling mechanism.	14
Figure 2.6. Osmotic swelling mechanism.	14
Figure 2.7. Wellbore stability problems in shales reservoirs.	15
Figure 2.8. Filter cake in conventional and unconventional reservoirs.	16
Figure 2.9. Shale cutting dispersion in the wellbore.	18
Figure 2.10. Drilling fluid classification.	20
Figure 2.11. Newtonian and non-newtonian rheological behavior.	28
Figure 2.12. Representation of different rheological models.	29
Figure 2.13. The scale of items referenced to a nanometer.	36
Figure 2.14. Particle-size scale (Cai 2012, adapted from Abrams 1977).	41
Figure 2.15. Nanoparticle unstable process.	44
Figure 2.16. Relationship of mud pressure and borehole failure.	52
Figure 2.17. Contact area between the drill string and the mud cake.	53

Figure 3.1. X-Ray theory based on Bragg's law.....	58
Figure 3.2. XRD goniometer outline.	59
Figure 3.3. XRD sample preparation.	61
Figure 3.4. XRD samples at different conditions.	62
Figure 3.5. SEM scheme and process.	65
Figure 3.6. SEM samples preparation.....	67
Figure 3.7. FESEM Hitachi S-4700 Missouri S&T.....	68
Figure 3.8. CEC shale slurry preparation.....	69
Figure 3.9. Materials and steps for CEC procedure.....	70
Figure 3.10. Spot test for the end point of shale CEC.	71
Figure 3.11. Pycnometer sketch.....	73
Figure 3.12. Ultrapyc 1200e Missouri S&T.	74
Figure 3.13. Materials and core procedure.	75
Figure 3.14. Displacement setup for bulk density and volume determination.	76
Figure 3.15. Sample preparation for aqueous stability test.....	79
Figure 3.16. Stern model distribution in the solid-liquid interface (Hoxha, 2016).	81
Figure 3.17. Schematic representation of zeta-potential (Malvern Technical Note).....	82
Figure 3.18. Zeta-potential sample preparation.	85
Figure 3.19. Zetasizer nano (Malvern) Missouri S&T.	85
Figure 3.20. Conventional LCM graphite.....	90
Figure 3.21. SEM image of silica NP (courtesy of US Research Nanomaterials Inc.). ...	91
Figure 3.22. SEM image of graphene NP (Courtesy of Nanographene Inc.).	93
Figure 3.23. Equipment used to prepare and mix the basic A fluid.....	95

Figure 3.24. Equipment used to prepare and mix NP dispersion.....	96
Figure 3.25. Mud balance instrument. Missouri S&T.	98
Figure 3.26. pH meter and buffer solutions. Missouri S&T.	99
Figure 3.27. 8-speed OFITE viscometer. Missouri S&T.....	100
Figure 3.28. API LTLF filtrate press. Missouri S&T.	102
Figure 3.29. HTHP filtrate press. Missouri S&T.....	103
Figure 3.30. Graphical representation of spurt loss.	104
Figure 3.31. Cutting dispersion test.	106
Figure 3.32. Experimental set-up for the bulk swelling test.	108
Figure 4.1. XRD analysis of the Woodford shale.	114
Figure 4.2. Ternary diagram of the Woodford shale.	114
Figure 4.3. Mineral composition of the Woodford shale.....	115
Figure 4.4. SEM Images of Woodford shale sample No 1.	116
Figure 4.5. Pyrite framboid detected with BSE.	116
Figure 4.6. SEM image of the Woodford shale No 2.	117
Figure 4.7. Estimation of pore size distribution in the Woodford shale.	118
Figure 4.8. CEC test result for Woodford shale sample.	119
Figure 4.9. Effect of salt concentration and type on silica nanoparticles.	122
Figure 4.10. Effect of salt concentration and type on graphene NP.	123
Figure 4.11. Effect of pH on nanoparticles.....	124
Figure 4.12. Zeta-potential distribution of silica NP.	126
Figure 4.13. Zeta-potential distribution of graphene nanoplatelets.	126
Figure 4.14. Percentage of reduction in LTLF filtrate for silica and graphene NP.	129

Figure 4.15. Percentage of reduction in HTHP filtrate for silica and graphene NP.	130
Figure 4.16. LTLP and HTHP filtration of the final screening for the NP-WBM.	133
Figure 4.17. Final NP-WBM LTLP and HTHP filtrate.	135
Figure 4.18. LTLP filtrate cake thickness and description.	136
Figure 4.19. HTHP filtrate thickness and description.	137
Figure 4.20. Woodford shale dispersion in distilled water and NP-WBM.	140
Figure 4.21. Woodford shale visual analysis.	141
Figure 4.22. Micro-fracture in the Woodford shale due to water interaction No 1.	142
Figure 4.23. Micro-fracture in the Woodford shale due to water interaction No 2.	142
Figure 4.24. NP effect on the Woodford shale visual swelling analysis No 1.	143
Figure 4.25. NP effect on the Woodford shale visual swelling analysis No 2.	143
Figure 4.26. Bulk swelling of the Woodford shale in distilled water and NP-WBM.	144
Figure 5.1. LTLP filtrate at aging conditions of KCL/PHPA and NP-WBM.	146
Figure 5.2. HTHP filtrate at aging conditions of KCL/PHPA and NP-WBM.	147
Figure 5.3. KCL/PHPA and NP-WBM filter cakes at HTHP after aging conditions.	149
Figure 5.4. Rheogram of KCL/PHPA fluid at different aging conditions.	150
Figure 5.5. Rheogram of NP-WBM at different aging conditions.	151
Figure 5.6. KCL/PHPA PV and YP at different aged conditions.	152
Figure 5.7. NP-WBM PV and YP at different aged conditions.	152
Figure 5.8. NP-WBM gel strength at different aging conditions.	154
Figure 5.9. KCL/PHPA gel strength at different aging conditions.	154
Figure 5.10. Woodford shale dispersion in KCL/PHPA.	158

Figure 5.11. Woodford visual swelling in KCL/PHPA. 159

Figure 5.12. Micro-fractures exposed due to KCL/PHPA fluid. 159

Figure 5.13. Bulk swelling of the Woodford shale in KCL/PHPA. 161

LIST OF TABLES

	Page
Table 2.1. Physical and chemical properties of nanoparticles.	37
Table 3.1. Conventional additives used in WBM.	88
Table 3.2. Base fluid for the NP-WBM formulation.	89
Table 3.3. KCL/PHPA formulation.	89
Table 3.4. Graphite properties (courtesy of Asbury Graphite Mills, Inc).....	90
Table 3.5. Silica nanoparticle properties (courtesy of US Research Nanomaterials Inc.).....	91
Table 3.6. Graphene nanoparticle properties (Courtesy of Nanographene Inc.).	93
Table 3.7. Screening criteria design for the NP-WBM.....	97
Table 4.1. Grain volume and density of the Woodford shale samples.	120
Table 4.2. Bulk volume and bulk density of the Woodford shale samples.	120
Table 4.3. Total porosity of the Woodford shale samples.	121
Table 4.4. Zeta-potential measurements of silica and graphene nanoparticle.	125
Table 4.5. Density and pH values of drilling fluids with and without NP.....	128
Table 4.6. Rheology results for silica and graphene NP at 120 °F.	131
Table 4.7. Final screening criteria for NP-WBM.	132
Table 4.8. Rheology results for the final screening of NP-WBM at 120 °F.	134
Table 4.9. Rheological properties with optimum NP-WBM and graphite at 120 °F.	138
Table 4.10. Optimum NP-WBM formulation.....	139

Table 5.1. Aging conditions summary for KCL/PHPA and WBM.	148
Table 5.2. Herschel-Bulkley constants at different aging conditions for NP-WBM.	156
Table 5.3. Herschel-Bulkley constants at different aging conditions for KCL/PHPA. ..	157

NOMENCLATURE

<u>Symbol</u>	<u>Description</u>
τ	Shear stress (Dyne/cm ²)
μ	Fluid viscosity (cp)
γ	Shear rater (sec ⁻¹)
τ_o	Yield stress (lb _f /100ft ²)
n	Flow behavior index (dimensionless)
K	Consistency index (lb _f – sec ⁿ /100ft ²)
ζ	Zeta-potential (mV)
PV	Plastic viscosity (cP)
YP	Yield point (lb _f /100ft ²)
λ	Wavelength of radiation (nm)
d	d-spacing (Å)
ω	Incident angle
Vb	Total volume or bulk volume (g)
Vg	Grain volume (g)
Vp	Pore volume (g)
\emptyset	Total porosity (%)
μ_e	Electrophoretic mobility
V	Particle velocity (μm/sec)
E	Electric field strength (Volt/cm)

ϵ_r	Dielectric constant (dimensionless)
ϵ_0	Permittivity of vacuum (Fm^{-1})
$f(Ka)$	Henry's function
D_h	Hydrodynamic diameter
k	Boltzmann's constant (J/K)
T	Absolute temperature (K)
$[\text{H}^+]$	Hydrogen ion concentration
$[\text{OH}^-]$	Hydroxyl ion concentration
V_s	Spurt loss volume (ml)
W_{Dry}	Shale dry weight (g)
W_{Immersed}	Shale immersed weight (g)
ρ	density (g/cc)

1. INTRODUCTION

1.1. STATEMENT AND SIGNIFICANCE OF THE PROBLEM

As conventional oil & gas reserves face depletion, development of unconventional shale plays have brought a solution for the steady increase in high-energy demands during the last decade. Figure 1.1 presents the historic production of different type of energy in the United States from 1980 to 2016 and a projection until 2040. The increment trend observed for oil & gas since 2006 was supported in the development of the unconventional reservoirs.

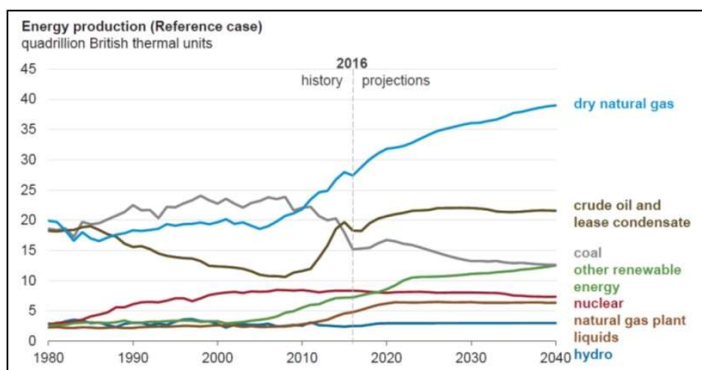


Figure 1.1. US Energy production history & projection (EIA 2017).

This positive scenario helped the United States to decrease its energy dependence from importations by 25% and set the country in a position close to gas demand self-sufficient (Charlez & Delfiner, 2016). Figure 1.2 compares the net energy trade in the United States. Since 1980 the country was dealing with a yearly increase in energy

importations until 2006 when unconventional shale reservoirs became a decisive player in the United States economy.

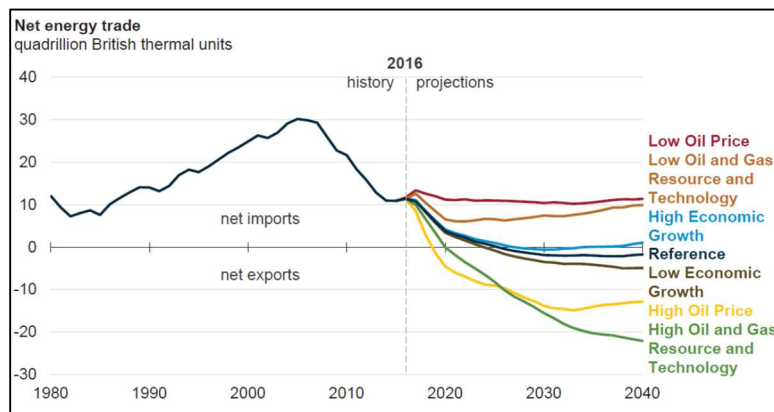


Figure 1.2. US Net energy trade (EIA 2017).

In the next decades, the United States will continue to support their energy plans on the unconventional shale reservoirs. Many improvements have been done on the two techniques applied to develop the unconventional shales, horizontal drilling, and hydraulic fracturing (Arthur, 2009). However, wellbore stability problems related to shale formations still represent the major problem to overcome during the drilling operations (Gazaniol et al., 1995) and is thought that the main reason is due to the undesirable interaction between shale formations and water-based drilling fluids (Hoelscher et al., 2012; Lal, 1999).

The latter represents a challenge, since 75% of the total drilled length worldwide has been accounted to shale formations (Lal, 1999) and these are responsible for about 90% of wellbore stability problems (Cai, 2012; Mody & Hale, 1993) with an estimated cost for

industry operations in hundreds (500 to 1000) of millions of U.S. dollars per year (Bol, 1994; Zeynali, 2012).

Drilling fluids apart to control formation pressure and remove drilled cuttings have the responsibility to minimize formation damage due to the fluid invasion, clay swelling and cutting dispersion. Although oil-based mud (OBM) can be used to achieve these goals, environmental and economic concerns limit its applications. Thus, researchers started to focus on the design of high-performance water-based muds (WBM) to drill through shale plays (Mody & Hale, 1993).

In recent years, researchers have been evaluating the use of Nanoparticles (NP) in different oil & gas applications including drilling fluids (El-Diasty & Ragab, 2013; Muili Feyisitan Fakoya & Shah, 2017). NP can be defined as a particle with a diameter size less than 100 nm. Due to its size, it is believed that NP can plug the shale nanopores reducing the factors that lead to the wellbore instability (Boul, 2016; Cai et al., 2012; Contreras, 2014).

In order to evaluate the potential of NP in WBM for shale plays, shale-fluid interaction, and nanoparticles stability need to be studied in detail. The best approach is to follow a methodology that characterizes the shale rock, then select the appropriate NP and evaluate it under different environmental conditions and finally observed the overall drilling fluid performance by means of rheology, filtration, and inhibition capabilities.

This project was an effort to include for the first time two different nanoparticles in a single WBM formulation as principal additives to reduce fluid invasion, cuttings dispersion, and water adsorptions in the Woodford shale.

1.2. EXPECTED IMPACTS AND CONTRIBUTIONS

Results achieved from this research will encourage the application of silica and graphene NP in WBM to drill through unconventional shale plays due to their ability to reduce filtrate invasion, formation damage, and cuttings dispersion. The methodology suggested in this research can be used to optimize the design of an NP-WBM according to the specific shale play that is intended to drill. Described below are relevant information established through the development of this research:

- 1.) Techniques to describe the pore structure of the Woodford shale were studied. This support the size selection of the NP as well as their shape. Also, the compositional analysis of the rock helped to identify the main mechanism of hydration that the specific shale under this research could experience and based on this support the inclusion of other conventional additives in the NP-WBM.
- 2.) The factors that could affect the NP performance were studied individually. These factors can be found during drilling operations and include changes in pH and the presence of salt in water formation (NaCl, CaCl₂).
- 3.) NP thermal effect on WBM was studied through aging tests. The different conditions allowed to understand the impact that NP might have on conventional additives and on the rheological and filtration stability of the overall drilling fluid system.
- 4.) Evaluation of non-modified nanoparticles at low concentration blended with conventional WBM additives allowed to consider that a possible synergistic effect that can take place. Thus, the concentration of NP can be reduced by avoiding higher concentration usually suggested in the literature.

The results obtained from this research provide a clear understanding about the steps needed to optimize NP-WBM formulation to drill unconventional shales as it is required to reduce the overall cost of the drilling fluid but at the same time improving the hole quality.

1.3. RESEARCH OBJECTIVES

The principal objective of this research was to formulate an NP-WBM to reduce the fluid invasion, cutting dispersion and swelling effect in the Woodford shale while using a low concentration. Standard drilling fluid tests, as well as chemical-interaction tests, were carried out to better understand the effect of NP in the filtration, rheology, and inhibition properties of the new NP-WBM.

This investigation analyzed the application of silica and graphene nanoparticles as principal agents in the design of the new NP-WBM for unconventional shale plays. Graphite was included in the formulation as a conventional LCM additive. To develop the research the consequent objectives were established:

- 1.) Characterize Woodford shale through scanning electron microscopy (SEM), X-ray diffraction (XRD), cation exchange capacity (CEC), and total porosity estimation to identify the hydration mechanism and select size and shape of the NP that best fit the shale structure.
- 2.) Evaluate NP stability through aqueous stability test (pH, salts) and zeta-potential measurements to warranty the solution dispersion based on the degree of attraction/repulsion forces of the NP in a colloidal system.

- 3.) Analyze the NP-WBM rheological and filtration properties based on API recommended practice 13-B at fresh and aged conditions and compare the its behavior against the KCL/PHPA conventional WBM.
- 4.) Investigate the NP-WBM ability to control the cuttings dispersion and hydration of clays present in the Woodford shale by means of bulk swelling test, dispersion test and visual swelling and compare the benefits in inhibition capabilities respect to the conventional KCL/PHPA WBM.
- 5.) Study the effect of NP on thermal and rheology stability of WBM through aging tests at different temperatures (150 °F, 200 °F, and 250 °F) and examine the NP's capability to reduce the degradation rate of polymers at high temperatures respect to the stability of the conventional KCL/PHPA WBM.

1.4. SCOPE OF THIS WORK

This research was primarily a laboratory investigation that was performed to evaluate the inclusion of silica and graphene NP in the design of a drilling fluid to reduce fluid invasion and improve the inhibition capabilities of an NP-WBM for the Woodford shale. Characterization of the rock and nanoparticles helped to refine the design of the NP-WBM. Standardized drilling fluid tests, dispersion test, and aging tests assist to evaluate the potential benefit of NP on WBM in terms of rheology and filtration. Finally, the comparison with a conventional KCL/PHPA serves to evaluate the performance of the new NP-WBM with the intention to move to friendlier technologies that can reduce the footprints of OBM. Figure 1.3 shows the scope of work of the main tasks design to accomplish the research objectives.

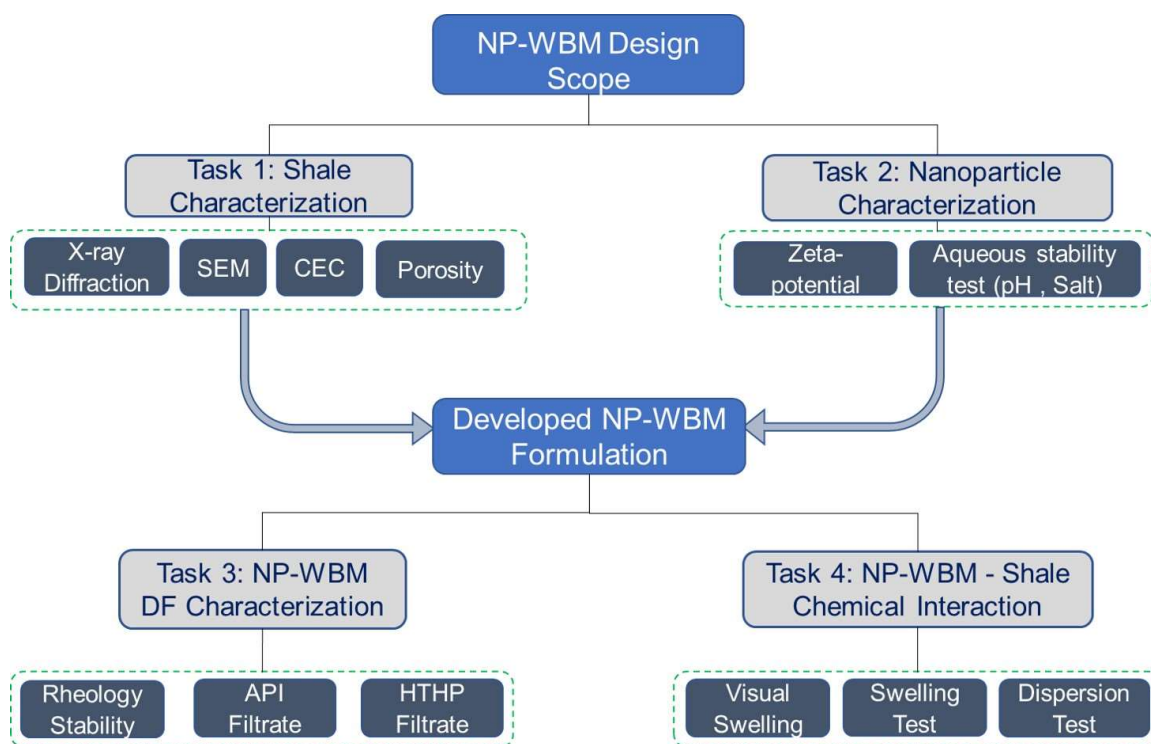


Figure 1.3. The Scope of the Research.

2. LITERATURE REVIEW

2.1. DEFINITION OF UNCONVENTIONAL SHALE RESOURCES

Unconventional reservoirs have been playing an important role in the oil & gas industry to increase reserves and fulfill energy demands, especially in the United States as described in the previous chapter. On the other hand, the singular characteristics, and challenges to accessing these types of reservoirs created the need of optimizing available techniques or even developing new ones, changing the view of how engineers, scientists, and industry, in general, define these reservoirs.

In 2007, the Society of Petroleum Engineers (SPE) published the ‘Petroleum Resources Management System’ (SPE-PRMS, 2007) to redefine and update the classification of reserves and resources. SPE-PRMS defines “unconventional” resources as:

Unconventional resources exist in petroleum accumulation that are pervasive throughout a large area and that is not significantly affected by hydrocarbon influences (also called ‘continues-type deposits’). Examples include coalbed methane (CBM), basin-centered gas, shale gas, gas hydrates, natural bitumen, and oil shale deposits. Typically, such accumulations require specialized extraction technology (e.g. dewatering of CBM, massive fracturing programs for shale gas, steam and/or solvents to mobilize bitumen for in-situ recovery, and, in some cases, mining activities).

In other words, unconventional reservoirs are those energy deposits that are geologically complex and difficult to develop and requires the assistance of advanced technologies to allow them to produce at an attractive and economic flow rate (Holditch,

2009; Miskimins, 2009). Figure 2.1 presents the progression and classification of oil and gas resources. In the case of unconventional shale plays its definition is based on its rock characteristics that make them unique deposits.

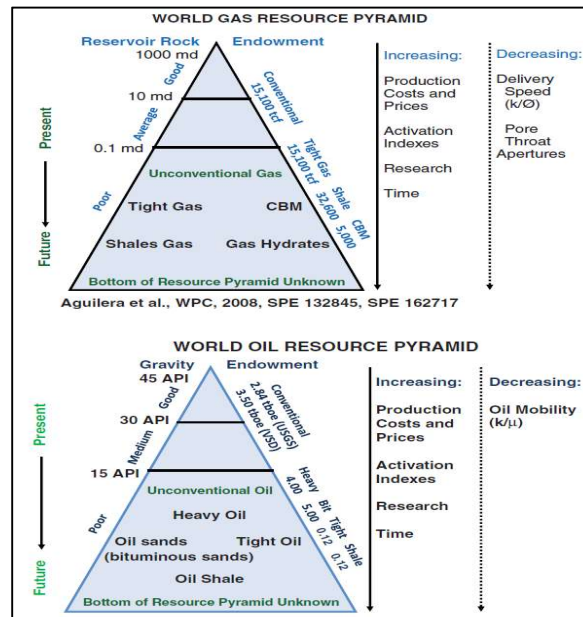


Figure 2.1. Oil and gas pyramid resources (Aguilera, 2014).

Shale rocks can be categorized as a fine-grained sedimentary rock that acts as rock source, reservoir and as a seal rock and is composed with a significant amount of clay that tends to react in different levels with water experiencing wellbore instability (Bol et al., 1994; Lal, 1999; van Oort et al., 1996). Its unique and complex porosity network has been evaluated by different researches finding pore-throat sizes at nanoscales with its largest pore size population below 100 nm (Al-Bazali, 2005), as well as extremely low permeabilities with ranges between 1×10^{-6} to 1×10^{-12} Darcy (Bol et al., 1994; Gazaniol et al., 1995).

These particular conditions do not allow these reservoirs to produce with conventional techniques and as stated before the need of directional drilling techniques to maximize the exposed reservoir area as well as the implementation of hydraulic fracturing to increase its permeability to make them economically attractive are the circumstances that cataloged them under the classification of unconventional reservoirs. Figure 2.2. presents an example of the application of directional drilling and hydraulic fracturing to unconventional shale reservoirs.

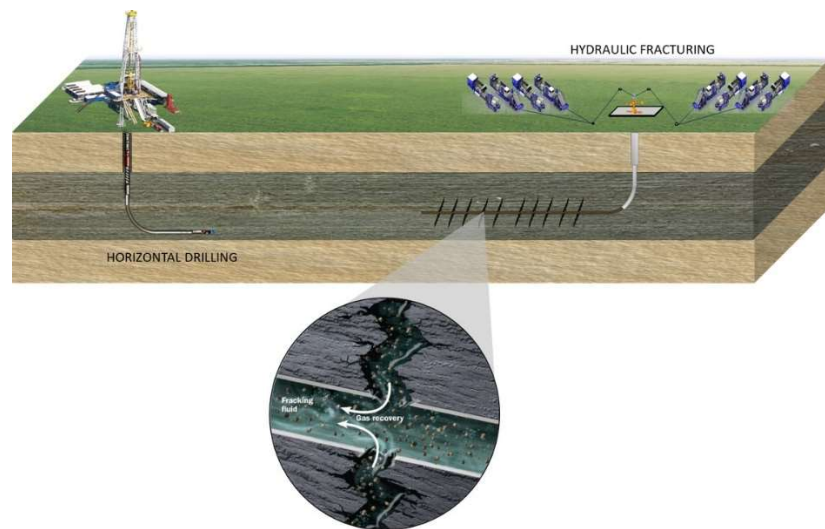


Figure 2.2. Directional drilling and hydraulic fracturing in shales.

2.2. SHALE HYDRATION MECHANISM

As previously described, shales are composed of different types of clays along with other minerals as quartz, calcite, feldspar, dolomite. The basic structure of these clays can be defined as a thin sheet-like form of alternating layers of silica tetrahedron and alumina octahedron (Schlemmer et al., 2003). According to their unit structure, clays can be

classified into specific groups as clay minerals. Important ones of interest to the oil & gas industry are smectite, illite, chlorite, and kaolinite.

The principles of the interlayer bond (strong or weak) in their single units define why ones are more water-like than others (Craig, 2013), which also generate different experiences in terms of hydration and at the end in wellbore instability (Martin E. Chenevert, 1970), In order of most reactive to less reactive clays: smectite (surface area 750 m²/gm), illite (surface area 80 m²/gm), chlorite (surface area 40 m²/gm), kaolinite (surface area 25 m²/gm). Figure 2.3 shows the different unit structure of the clay minerals.

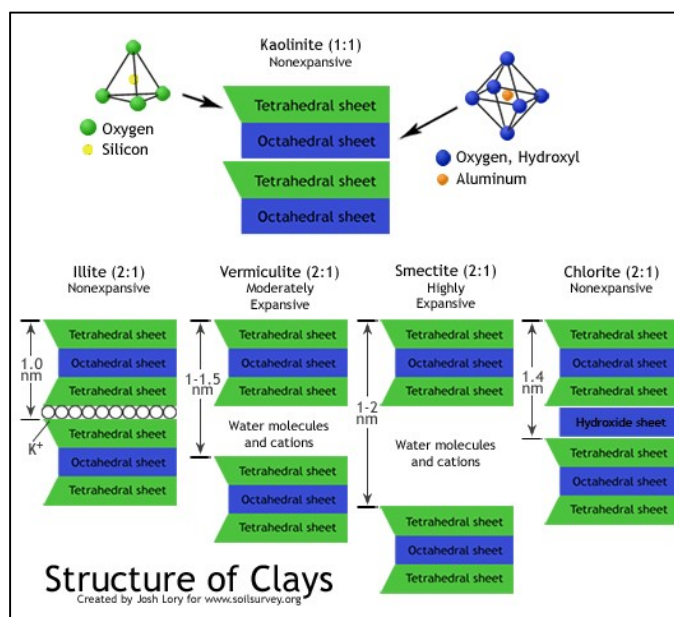


Figure 2.3. Structure of clay mineral groups.

Kaolinite is composed of 1 layer of silica tetrahedron and 1 alumina octahedrons. Illite and smectite have a common structural unit composed of two outside layers of silica tetrahedrons and the central layer of alumina octahedrons. Layers of each individual unit

are adjacent to layers of the neighboring unit; the difference is that the illite group has potassium cations as interlayer connectors instead of water molecules that are present in the smectite group. This difference is the reason the illite group is not as reactive as the smectite group.

It is important to mention that during the depositional process of shale rock some of the original cations associated with the basic structure (silicon or aluminum) were replaced by others (i.e. iron, magnesium). This condition caused the initial imbalance charge in the clay structure, resulting in a negative surface charge for the clay (Salles, 2007).

Despite that clays release water during the depositional process some water remains partially hydrating the structures. The first type is called inter-crystalline water which is associated with cations of the basic structure. The second type is called osmotic water which can be described as a thin layer attached to the negative surface between clay interlayers. Finally, the third type is described as free water normally found inside the pores. Not all the 3 types of water are present in clays. Nevertheless, this condition gives to them a high level of water diffusion effect that can produce a swelling displacement and adversely affect rock strength in the presences of WBM (Anderson et al., 2010; Martin E. Chenevert, 1970). Figure 2.4 shows a representation of the micro-shale structure.

The shale hydration mechanism is based on two different types of swelling processes: crystalline swelling related to the interlayer pore and clay surface, and osmotic swelling associated with clay unit and the intramatrix pores. Crystalline swelling occurs closer to the negatively charged silicate surfaces of the clay particles inside the interlayer region. When the sediments compaction took place, free water was released from the

interlayer of the clays leaving behind the connate water in the nanopores and the cohesive forces between layers kept them together under dry conditions (Martin E. Chenevert, 1970).

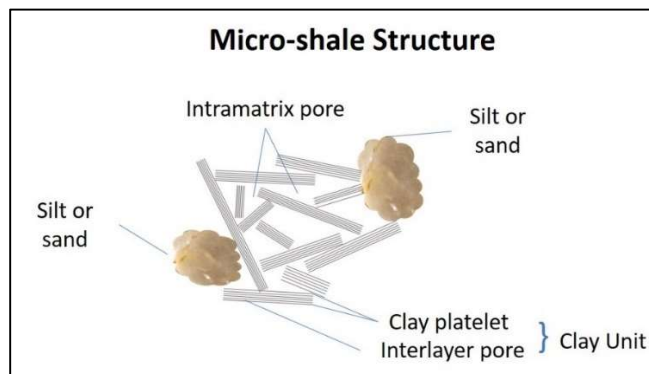


Figure 2.4. Representation of micro-shale structure.

When the shale is again exposed to moisture (water), a potential chance for water molecules adsorption at crystalline level (<1 nm) can occur until an initial chemical balance between the water at the clay surface and the water in the interparticle zone is reached or the interchangeable ions in the surface hydrated. Nevertheless, this initial volume of water is very low (up to 4 water molecular layers) as well as the separation of clay interlayers ($9 - 20 \text{ \AA}$) and mostly the imbalance in the clay structure might continue and the second swelling mechanism might be experienced (Rohel, 1982, Lal, 1999, Wong, 2001, Bui and Tutuncu, 2018). Figure 2.5 illustrates the crystalline swelling mechanism.

Osmotic swelling starts once the crystalline swelling took place usually generating large changes in the clay particle dimensions. This type of swelling is limited to clays that have interchangeable cations in the interlayer regions (e.g. smectite, illite, mixed layers).

If the concentration of the cations in this region is higher than the surrounding medium, water molecules due to their slightly negative nature will tend to get absorbed into the interlayer trying to restore the equilibrium. This is the reason behind significant interlayer expansion from 20 Å to 130 Å and the principal cause of shale instability during drilling operations with WBM (Anderson et al., 2010; Bui & Tutuncu, 2018). Figure 2.6 illustrates the osmotic swelling mechanism.

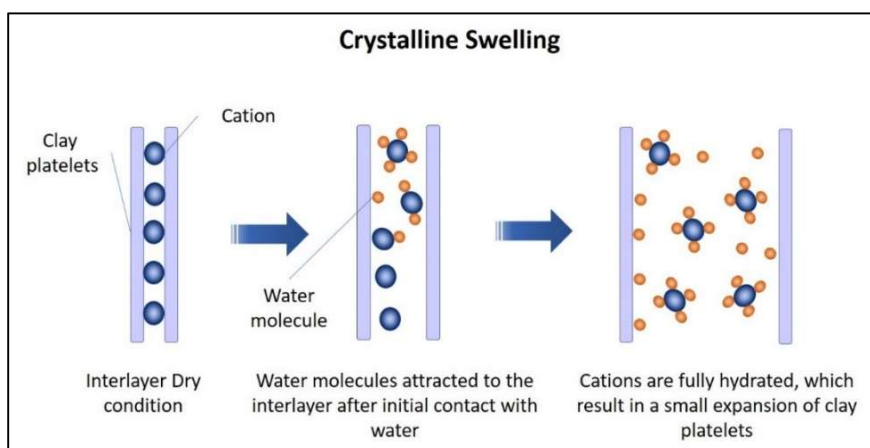


Figure 2.5. Crystalline swelling mechanism.

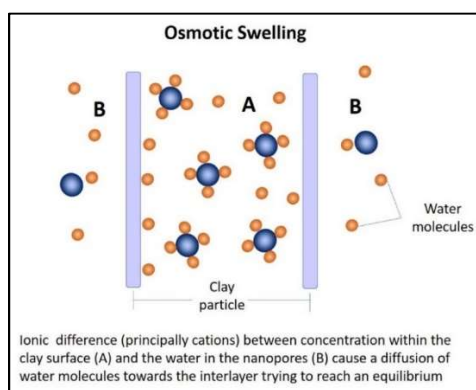


Figure 2.6. Osmotic swelling mechanism.

2.3. WELLBORE INSTABILITY IN SHALE

Clay fractions and types can be very different between two shale plays (e.g. soft shales ‘ductile’, hard shales ‘brittle’). These variations cause shales to experience different degrees of hydration that altered stress distribution, reduce strength, and potentially destabilize the borehole wall in different ways (Zhang, 2008). Figure 2.7 exposes different wellbore stability problems related to shale formations.

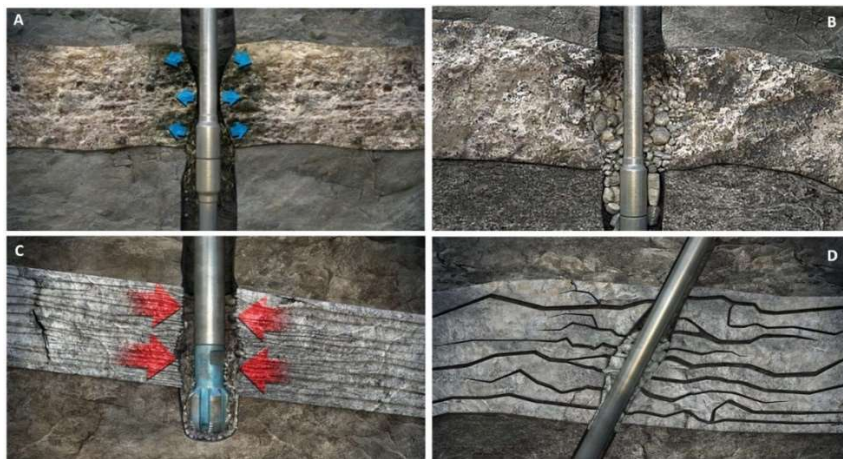


Figure 2.7. Wellbore stability problems in shales reservoirs.

A) Tight spots (soft shales), B) Pack-off with excessive cavings. C) sloughing of wellbore wall (Hard – brittle shales). D) fluid losses due to open/creation of fractures (Hard – brittle shales).

Shale conditions of extremely low permeabilities and pore sizes limited the micronized particles and polymers in WBM to effectively form a filter cake up on the wellbore wall causing filtrate to invade the nanopores (Bol et al., 1994). However, before the fluid invasion through hydraulic flow can take place; the chemical imbalance condition between the WBM and the very proximity of the wellbore wall experience a diffusion of

water molecules or ion present in the aqueous phase of the drilling fluid (crystalline and osmotic swelling).

Eventually, this condition increases the pore pressure causing cohesive forces inside the clay units to reduce as well as affecting the boundary cementation between the clay units and other minerals present in the rock (e.g. quartz, mica, calcite, feldspar), initiating the alteration of the effective stress at the wellbore wall and finally inducing the rock failure (O'Brien & Chenevert, 1973). Figure 2.8 illustrates the effect of micronized particles in conventional and unconventional reservoirs.

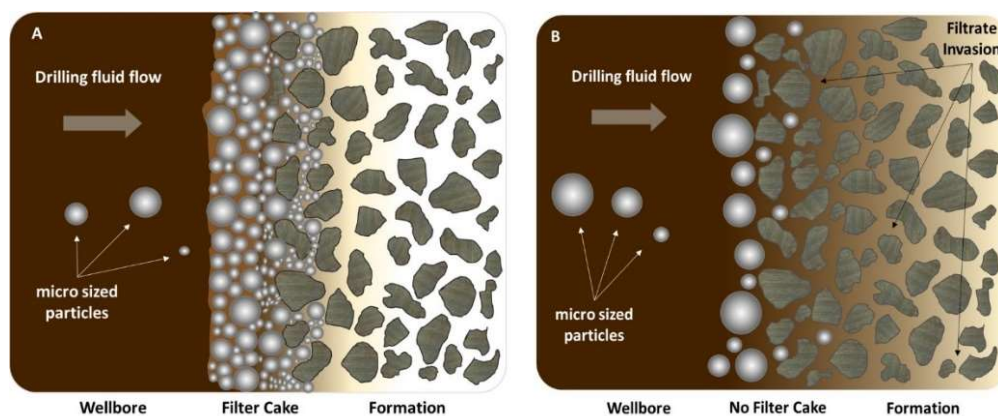


Figure 2.8. Filter cake in conventional and unconventional reservoirs.
A. Filter Cake in a conventional reservoir. B. No filter cake and fluid invasion in unconventional shale reservoir.

Normally, before any instability problems related to WBM and shale formation interactions can be noticed, a long period of time has already passed. This is because the chemical reactions that take place are very slow. For instance, the first two mechanisms of swelling might prevail during the first 24 hrs. After this period of time, pore pressure can continue to increase due to the hydraulic flow invasion or due to the dissolution of the

interparticle bounding that exposed more formation area and allows for deeper invasion of the filtrate or fluid and the cycle starts again (Gazaniol et al., 1995). Finally, the effective stress exceeds the failure envelop and destabilization of the wellbore wall occurs. This is detrimental when poor hydraulics and inappropriate fluid rheology also take place

One important thing to notice is that shale bedding planes are confined in the subsurface by the overbounded pressure of formation layers above it. Which suggest that stresses that might develop in shales due to drilling fluid interactions can be released only by the failure of the shale toward the wellbore.

Usually, old shales are hard and brittle, this condition is due to the low content of swellable clays as mentioned before. These type of shales still can suffer from a low degree of hydration. However, the mechanism that is most common to reduce the mechanical strength of the shale rock is the invasion of the fluids to the pores and subsequent increase in pore pressure. The situation for these specific shales aggravates when natural micro-fractures are present because these defects will increase the invasion of filtrate deeper into the shale matrix and also create a connection between the micro-cracks accelerating the hydration and splitting process along the bedding plane and subsequently slough occurs (He et al., 2016; O'Brien & Chenevert, 1973).

The same conditions related to the destabilization of the wellbore wall in shale formations applied to cuttings generated while drilling. The dispersion of cuttings can be referred to as a continuous and rapid disintegration of shale layers from the very external 'shell' towards the cutting center. Excluding mechanical crushing, cuttings will fail in tension as a result of stress relief and pressure pore penetration since there is no confining stress (e.g. overbounded) to preclude the failure, eventually leading to a grain-grain

dispersion that can generate excessive buildup of low-gravity solids (LGS). Then, drilling fluid density will increase as well as the hydraulic flow increase to the formation creating a very dangerous cycle that is difficult to control once it has started. Figure 2.9 illustrates the cutting dispersion phenomena and its effect on the wellbore stability.

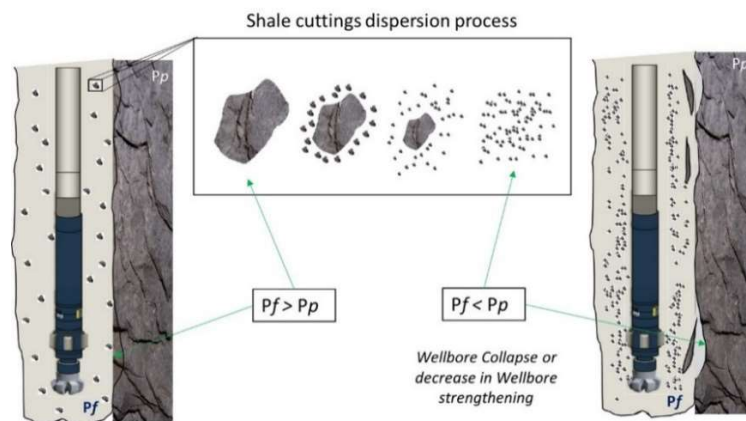


Figure 2.9. Shale cutting dispersion in the wellbore.

Finally, one can summarize the wellbore instability in shales in three main stages (Chenevert & Osisanya, 1989) and as explained before, not all of them can be experienced in a specific shale. These three stages are:

1st stage: Crystalline & Osmotic Swelling. The initial exposure to water-based drilling fluid is experienced and the diffusion of water molecules and ions started to increase pore pressure as well as expanded the clay layers. This period can take 1 to 24 hours.

2nd stage: Hydraulic Flow from the wellbore to the shale matrix. Filtrate initiated its invasion into the intramatrix pores and the pore pressure increased at a faster rate. Dissolution of grain boundary take place exposing natural micro-fractures or create new

ones. Finally, pore pressure exceeds hydrostatic pressure exerted by drilling fluid column and wellbore instability is experienced.

3rd stage: Cutting disintegrations. Cuttings and caving experienced dispersion 'melting' into the drilling fluids. LGS % increase affecting density and rheological properties of the drilling fluid. The last stage of the hydration process is then the dispersion experienced by the cavings. If this issued cannot be controlled the entire cycle is repeated again until the wellbore experiences a total collapse.

Based on all this information the ideal drilling fluid to drill through shales must keep the confining effect stress over the wellbore wall and cuttings high enough to avoid rock failure. This can be achieved by providing an ionic equilibrium on the aqueous phase of the drilling fluid especially for swellable clays, but more important by selecting appropriate 'plugging' agents that can decrease the shale permeability at the wellbore wall reducing the effect of the hydraulic flow to the shale matrix.

2.4. CLASSIFICATION OF CONVENTIONAL DRILLING FLUIDS

Drilling fluids are mainly composed of a mixture that includes different liquids, gases, emulsions, and solids, some of them dispersible some not (Vasii, 2008). Drilling fluids are a vital component during the well construction process to reach reservoirs with different characteristics while carrying out the cuttings generated and providing a medium to stabilize the wellbore wall.

Its origins can go as early as the third century BC when in China water was first used to 'softening' the underground layers to drill wells of hundreds of feet in depth (Darley and Gray, 1988). Its modern history started in Spindletop Field in south Beaumont, Texas

in 1901 when a kind of muddy water was used to drill through unconsolidated sands (Mitchell and Miska, 2011)

Nowadays, Industry has already understood that the correct design and application of drilling fluids depends mostly on the characteristics of the formations to drill, especially when its average cost can be about 5% to 15% of the total cost to drill a well (Patel, 2007; van Oort et al., 1996). Therefore, with improvements in research, different additives have been developed and tested to enhance the drilling fluid performance in order to satisfy the requirements of each specific reservoir while reducing costs associated with non-productive times.

Drilling fluids are typically classified according to their base material into liquids composed by water-based drilling fluids (WBM), and non-aqueous based drilling fluids (oil-based, OBM and synthetic-based, SBM), gas or a gas/fluid mixture (Pneumatic-based drilling fluids) Figure 2.10 shows a common classification of drilling fluids.

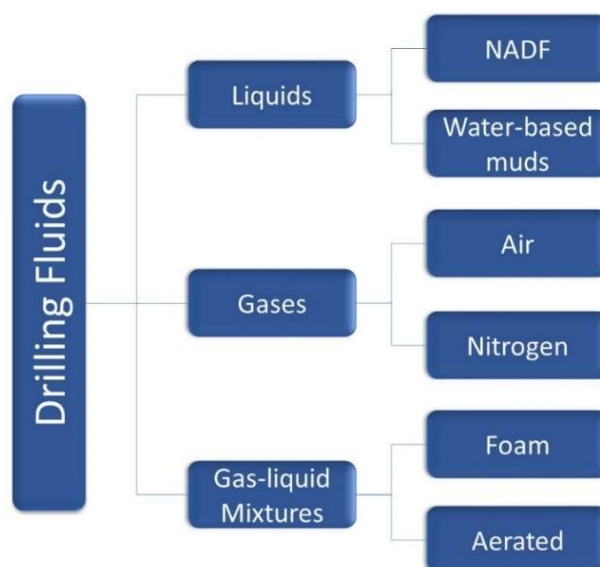


Figure 2.10. Drilling fluid classification.

OBM and WBM have been the main conventional systems that oil & gas industry has been used to drill problematic shale formations. The following section briefly describes the main characteristics of the different WBM and Non-aqueous drilling fluids, NADF (OBM, SBM) applied to shale formations.

2.4.1. Non-Aqueous Drilling Fluids (NADF). NADF has been the preferred system to drill through shale plays. These fluid system support their effectiveness in the capillary entry pressure, due to the interfacial tension created between two immiscible fluids. Oil or synthetic fluid act as a non-wetting phase and the fluid inside the shale pores (brine/water) as a wetting phase. The low permeability and nanopores generate very high capillary pressures (15 MPa in pore-network of 10 nm) which restrict the NADF to displace the pore fluids and interact chemically with the shale formation at the same time that controls any pore pressure build up (van Oort et al., 1996). The water phase in NADF is usually a calcium chloride solution with water activity (a_w) equal or less than the water activity of the connate water inside the shale pores creating a chemical balance that restrict the diffusion of water molecules and ions in or out of the formation that could affect the stability of the wellbore wall (Oleas, 2008).

The main advantage of this system is their exceptional shale stabilization at HTHP condition by avoiding the chemical interaction between the drilling fluid and formation. Also, its excellent lubricity improves the drilling process in the horizontal sections generating less tortuosity, avoid bit balling and increased ROP compared to WBM.

Despite all the advantages that NADF's have their main disadvantages compare to WBM are the higher cost associated to prepare, maintain, and dispose of the fluids and oil-impregnated cuttings after drilling operations. Also, governments and environmental

organizations have requested in the past to reduce the footprint of the E&P operations and the implementation of more environmental-friendly WBM solution (Deville, 2011).

2.4.2. Water-Based Drilling Fluid. WBM have a wide spectrum based on their chemical design or principle to control shales hydration, some of them are based on shale/fluid chemistry interactions (e.g. ion exchange) while other due plugging effect based on precipitates on an attempt to mechanically obstruct shale nanopores and micro-fractures.

2.4.2.1. Amine water-based drilling fluid. Amine systems were introduced to the market in the late 1980's (Beihoffer, 1990). The amine molecules can enter the clay structure and act as a hydration suppressant preventing hydratable clays from swelling and expanding in the presence of water. (Patel et al., 2007)

- **Amine WBM advantages.** Amine system has shown the ability to control clays with high absorption capacity. Its compatibility with most drilling fluids additives is a plus as well as its low marine toxicity, which makes it suitable for offshore applications.

- **Amine WBM disadvantages.** These fluids do not perform well in a high concentration of reactive shale cuttings. Experience difficulties to disperse or 'dehydrated' already hydrated clay particles, to some degree are salinity-dependent and can present foam problems due to pH alterations (Patel et al., 2007). Furthermore, amine WBM might not be the most appropriate drilling fluid to drill through unconventional shales that have low cation exchange capacity (CEC), since this is not the failure mechanism in these type for shales with less hydratable clay fractions and the amine molecules cannot control the hydraulic flow into the shale matrix.

2.4.2.2. KCL/PHPA water-based drilling fluid. KCL/PHPA systems had been widely applied for years in conventional and unconventional shales showing an acceptable

performance by reducing drilling fluid – shale formation interactions based on the cation exchange principle (van Oort et al., 1996). The combination with PHPA polymer help to control cuttings dispersion in the drilling system.

- **KCL/PHPA advantages.** The main advantage is its ability to exchange hydratable cations with the clay structure, which reduce shale hydration and swelling. Also, the combination of the PHPA enhances cutting removal due to an encapsulation mechanism. Thus, reduce cutting dispersion. Is a system with a relatively low cost and can be designed for freshwater or sea water up to 16 ppg.

- **KCL/PHPA disadvantages.** high salt concentration above the optimum point will tend to dehydrate the shale affecting formation strength until wellbore collapse can be experienced (Mody & Hale, 1993). PHPA need to be added continuously due to its removal with the coated cuttings. High salt concentrations can lead to corrosion problems in the drill string and in some cases misreading in logs. Similarly, water and high conductive cutting resulting from the application of KCL/PHPA WBM represent an environmental concern in terms of waste disposal. Lastly, polymers tend to experience high degradation rates at HTHP conditions (Abdo & Haneef, 2012; Boul et al., 2016).

2.4.2.3. Glycol water-based drilling fluids. Glycol systems have become widely used. Their mechanisms rely on cloud point temperature (CPT). Glycol is dissolved in the aqueous phase of the WBM but is designed to come out of solution experiencing a ‘cloudy’ effect. Once out of solution the glycol is assumed to precipitate and displace the connate water, blocking shale pores, and reducing further fluid invasion which tent to stabilize the wellbore wall. The temperature at which it occurs is determined by salinity, glycol

molecular weight, and concentration in the system. An increase in any of these three parameters will decrease the CPT (McGill, 1997).

- **Glycol WBM advantages.** Reduce pore pressure transmission, which tends to stabilize wellbore walls experiencing some hardening effect (M.S. Aston & Elliott, 1994). The system can coat the cuttings reducing the dispersion. Its preservation is easier due to fewer dilution rates required while drilling and improve lubricity in the system.

- **Glycol WBM disadvantages.** These systems are high salt-dependent which becomes impractical in terms of fluid and cuttings disposal affecting the idea of an eco-friendly system. Furthermore, irreversible pore blocking increases formation damage, which is not desirable in a drill-in fluid for unconventional shale plays.

2.4.2.4. Aluminum water-based drilling fluids. Aluminum WBM system is a complex aluminum salt soluble in water. Aluminum remains soluble and stable in the aqueous phase of the drilling fluid under alkaline condition ($\text{pH} > 10$) but once it encounters a system with a lower pH, such as the connate water in the shale pores and microfractures ($\text{pH} 4-5$), it will precipitate as aluminum hydroxide in the form of a crystalline mineral, blocking the shale pores. Pore pressure transmission is then reduced and an increase in the shale strength can be experienced, preventing the wellbore from experience swelling or wellbore collapse (Benaissa, 1997).

- **Aluminum WBM advantages.** Control pore pressure build-up due to the pore blocking ability and cation exchange is also present in the system which improves the overall performance covering hydratable clays.

- **Aluminum WBM disadvantages.** The system dependency on pH can be a problem while drilling because any sudden change in pH can lead to a sudden precipitation inside

the wellbore, directional tools, mud pits and/or filter mud pumps; eventually leading to tight spots, excessive torque and drag, bit balling or any non-productive time conditions. Additionally, higher pH environments have become a hazard in the oil & gas industry (van Oort et al., 1996). Furthermore, aluminum WBM systems support its efficiency in the irreversible precipitation of the aluminum hydroxide in the pore network, thus this system should present difficulties to treat unconventional shales as a reservoir rock, affecting future operations and oil & gas production.

2.4.2.5. Silicate water-based drilling fluid. Silicate system was impractical at its early stage due to high rheology problems presented while drilling and was suspended in 1940. The system was introduced again in the mid-1960's with lower concentrations and in combination with a salt (KCl, K₂CO₃, NaCl). The adjustments showed to be an effective solution to inhibitive shale formations and control cutting dispersion. This system is based on pore plugging due to silicate precipitation in gel form once experiencing the pH difference between the drilling mud system and the connate water in the shale pores.

- **Silicate WBM advantages.** Avoid further fluid invasion into the shale matrix due to the pore plugging that acts as a physical block and also produce a dehydration effect in the shale providing kind of formation hardening. Efficiently control cuttings dispersions and also can work in the presence of shale micro-fracture structure by filling the small cracks and pressure-seal them.

- **Silicate WBM disadvantages.** The high concentration of salt needed to achieve a good performance runs against the cost-efficiency and environmental regulations. Also, the alkalinity level (pH = 11-12.5) is high enough to represent a hazard condition. Its permanent precipitation in gel form in pores and micro-fractures increase formation

damage, thus are not recommended to apply as drill-in fluid in shales (van Oort et al., 1996). Also, silicate WBM low tolerance to LGS produces a negative rheological effect. Even more, when commercial thinners cannot be applied to disperse drilling fluid, the system may lead to a silicate gelation in the wellbore or in any place of the drill string or rig circulation system (Ward, 1999).

In summary, OBM still represents a good option to drill unconventional shale plays, but environmental regulations and higher cost associated to their application weaken the decision to use it, leading scientists, and engineers to continuously search for a better WBM option. On the other hand, available WBM systems have a great spectrum of operations but most of them are designed to specifically drill through non-productive shale formations. The introduction of NP in the oil & gas industry allows researchers to study and evaluate new perspectives that might help to fill the gap of an eco-friendly WBM with high performance that might efficiently drill unconventional shale plays as reservoir rocks.

2.5. FUNCTIONS OF DRILLING FLUIDS

Drilling fluids are capable to perform different tasks during the well construction. Nevertheless, the main two functions of drilling fluids in every well are controlling effectively the formation pressure while carrying the cuttings up to the surface (Baker Hughes, 2006). Other functions related to drilling fluids are highlighted in this section:

- 1.) Provide mechanical stability: Maintaining wellbore stability is very critical for the success of each drilling operation. Drilling fluid density, rheology, and chemical composition are vital to maintaining the in-situ stress condition of the wellbore

walls in different types of formations until casings and the cement jobs can protect these formations.

- 2.) Cool the bit and the drill string: Considerable heat is generated by rotation of the bit and the drill string. Drilling fluids can dissipate the heat generated thereby extending the drilling tools efficiency and time life.
- 3.) Reduce formation damage: Drilling fluids should be able to effectively form a filter cake in the wellbore wall to minimize the fluid-loss into the formations that tend to reduce the permeability (skin factors) or initiate hydration process in shales.
- 4.) Transmit Hydraulic power to drilling tools (e.g. bit, mud motor): Once the drilling bit generates cuttings, those cuttings should be removed from under the bit to avoid re-drilled cutting conditions and poor hole cleaning. Also, drilling fluids help to increase the ROP with its hydraulic impact and provide hydraulic energy to directional tools.
- 5.) Minimize corrosion: Corrosion in drilling fluids is the result of some kind of contamination. It can be related to the presence of hydrogen sulfide, CO₂, salt in the drilled formations or from a poor pH environment that tends to generate a bacterial action affecting all the equipment involved in the drilling operations. Mud corrosion is controlled by alkalinity or by addition of corrosion inhibitors.

2.5.1. Rheology of Drilling Fluids. Rheology is the science that studies the relationship between the flow of matter and the deformation experience. In drilling operations, rheology is one of the most important characteristics to describe the drilling fluid behavior at various flow conditions. The drilling fluid rheology and analysis can have

a further impact on the capabilities to increase the hole cleaning efficiency, borehole stability, and ROP if not designed properly.

Different rheological models tried to describe the behavior of the drilling fluids at dynamic conditions. When shear stress and shear rate in the drilling fluid are directly proportional the fluid behavior will be linear and can be defined as a Newtonian fluid (e.g. water, alcohols) in which its slope described a constant effective viscosity (μ) On the other hand, when the relationship does not follow the same proportion, the fluid will behave as a non-Newtonian fluid (Figure 2.11). Most drilling fluids fit the last group. (Baker Hughes Drilling fluids reference manual, 2006).

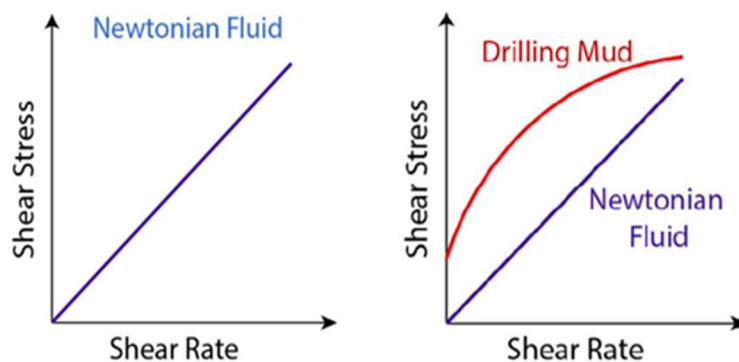


Figure 2.11. Newtonian and non-newtonian rheological behavior.

There are different mathematical models that have the intention to describe the non-Newtonian behavior of most drilling fluids as the Bingham plastic model, Power law model, and the Herschel-Bulkley model (Figure 2.12). A brief description of each model is summarized below.

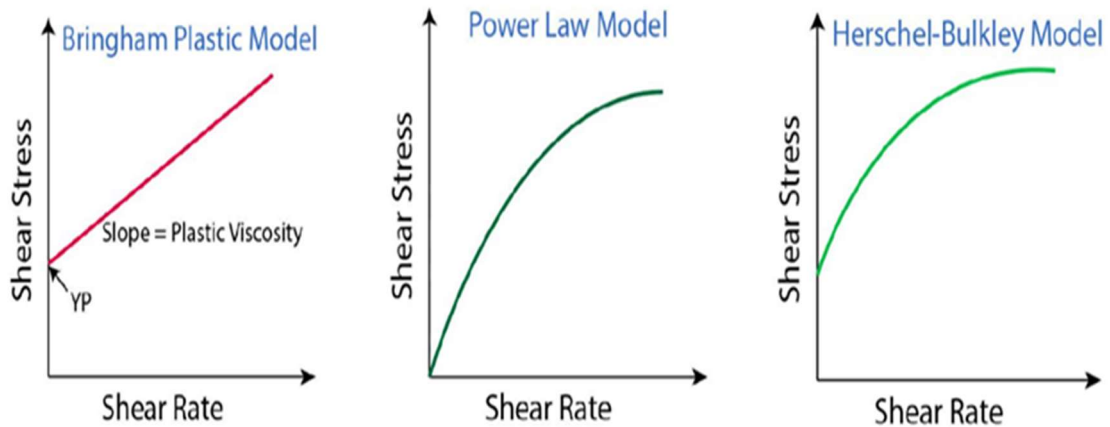


Figure 2.12. Representation of different rheological models.

- 1.) Newtonian Model. This model is the basis from which the later models were developed. Mathematically, the Newtonian model is expressed as:

$$\tau = (\mu) * (\gamma) \quad (1)$$

Where, τ (lbf/100ft²) is the Shear stress, γ (sec⁻¹) is the Shear rate, and μ (cp) is the fluid viscosity

- 2.) Bingham Plastic Model. In the early 1990's, Bingham observed that certain types of fluid exhibited a plastic behavior that did not fit the Newtonian conditions. These fluids required an initial stress known as yield stress before they start to flow. After this shear stress, the fluid will follow the behavior of Newtonian fluids. Bingham Plastic Model is given by,

$$\tau = \tau_o + (\mu_{\infty}) * (\gamma) \quad (2)$$

Where, τ is the shear stress, τ_o (lbf/100ft²) is the yield stress, γ is the shear rate, and μ_∞ (cp) is the fluid plastic viscosity.

3.) Power Law Model. The relationship between shear stress and shear rate are non-linear according to this model. The Power Law model aims to eliminate the defects of the Bingham model at low shear rates. This model requires two parameters to perform the drilling fluid characterization, K (Consistency Index) and n (Flow behavior Index). The mathematical model is defined as:

$$\tau = K * \gamma^n \quad (3)$$

where τ is the shear stress, K is the consistency index, γ is the shear rate, and n is the flow behavior index. K describes the thickness conditions of the fluid, somehow analogous to the effective viscosity, while n , expresses the degree to which a certain fluid will behave as a Newtonian ($n = 1$) or non-Newtonian fluid, either pseudo-plastic ($n < 1$) or dilatant ($n > 1$).

4.) Herschel-Bulkley Model. This model is considered a modified Power Law Model that includes an initial yield stress parameter in the calculations. As a consequence, this model is more widely used than previous models, since it can describe more accurately the shear stress/shear rate relationship of drilling fluids. The model is defined as:

$$\tau = \tau_o + K * \gamma^n \quad (4)$$

where τ_0 is the shear stress at zero shear rate (yield stress). K is the consistency index, γ is the shear rate, and n the flow behavior Index.

2.5.2. General Considerations of Filtration in Drilling Fluids. Drilling fluids are usually composed of liquid and solid phases. Filtration refers to the invasion of the liquid phase into the formation when the drilling bit exposes new formation and the drilling fluid comes in contact with it. Initially, a small volume of mud can invade the formation before the actual filtration process takes place, this volume is known as mud spurt. However, there are certain cases where the bridging materials in the drilling fluid cannot control the fluid invasion and total lost circulation is experienced (Walker, 1993).

Bridging agents of a certain size can plug the pores in the near-wellbore region. These bridging agents should be at least 1/3 to 1/7 of the average pore size of the formation (Abrams, 1977). Larger particles cannot plug the pores and the mud flow will sweep them again into the main fluid stream. Smaller particles will tend to invade the formation creating an internal filter-cake that can generate a skin factor. The appropriate selection of the primary bridging agent will permit the particles to efficiently plug the smaller pores and eventually the other particles in the drilling fluid can be trapped forming a low-permeable seal that reduces the filtrate invasion into the formation. (Chesser et al., 1994).

Filtration occurs under both dynamic and static conditions during drilling operations. Filtration under dynamic conditions occurs while the drilling fluid is circulating. Static filtration occurs during connections, trips or when the fluid is not circulating. It is logical to think that thinner and durable filter-cakes can have lower permeabilities than thicker and erodible filter-cakes. The thinner the filter-cake the less volume of filtrate that invades the formation. Nevertheless, there are some factors that affect both, the build-up of the

filter-cake and the filtrate invasion (B.G. Chesser et al., 1994; Mi-Swaco, 1998) Some of these factors are: time and temperature, differential pressure, compressibility of the filter-cake, permeability of the filter-cake, viscosity of drilling fluid and filtrate, solids composition and percentage, and particle size distribution.

2.5.3. Temperature Effects on Drilling Fluids. One of the most challenging problems for drilling fluids is the temperature operational range of the chemicals use to mixed it. The temperature at the bottom of the hole increases as the well deepens, and it is important that the drilling fluid maintains acceptable rheological and filtration properties. These properties of the mud are strongly related to the temperature effects and under downhole conditions may be very different from the ones measured at the surface leading to misinterpretations that can generate future undesirable wellbore conditions (e.g. wellbore instability, tripping difficulties). When drilling fluids are exposed to high temperatures, the portion of the fluid that is at the lower part of the wellbore becomes excessively thick, a situation that becomes worse under static conditions in which the prolonged heating may cause the drilling fluid to experiences a solidification process (Al-marhoun, 1990).

The effect of temperature on drilling mud can be attributed to the complicated interplay of several causes, some of which are more dominant than others. Factors such as reduction in the degree of hydration of the polymers, reduction of the viscosity of the suspending medium, increased dispersion of clay particles, and an increase in the degradation rate of additives. Since all these processes take place in the drilling fluid simultaneously as the temperature is varied, an interpretation of the observed results will

only be possible in cases whereby some of the effects are predominant and as such be easily identified.

One immediate effect of high temperatures is the detrimental effect on drilling fluid rheology, which can increase cuttings settling and affect the hydraulic capabilities as well as experiencing some degree of flocculation in the drilling mud. The latter will lead to a poor quality-filter cake, thick enough to increase the risk of differential stuck pipe due to the larger contact area between the drill string and the filter cake.

On the other hand, the poor permeability condition of the filter-cake will increase the filtrate into the formation. Thermal degradation of filtrate control-additives and viscosifiers aggravate the problem previously described. As an example, at temperatures below 300 °F, starches in the drilling fluid start to experience hydrolysis and depolymerization of thinners or irreversible chemical reactions can take place leading to a complete degradation of the drilling mud (Chesser & Enright, 2013).

Finally, the temperature should be treated as one important contaminant in drilling fluids. It is complicated to assimilated such condition, however, its detrimental effect on polymer hydration, clay flocculation, and rheological problems as described previously are a few points that support this claim. The most interesting part of all of this is that temperature has no treatment. The initial design of the drilling fluid with the appropriate chemicals is the only preventive solution to the problem.

2.6. DRILLING FLUIDS CHALLENGES IN UNCONVENTIONAL SHALES

Most of the problems related to drilling operations in unconventional shales are due to an incorrect design of the drilling fluid. Failures during drilling operation can lead to

non-productive time (NPT) producing excessive overall costs, loss of tools, reduce the productivity of wells, increase the time for investments returns, and poor performance in the operations (Zamora, 2000; Zamora & Roy, 2000). Increasing the compatibility between drilling fluids and shale formation can reduce the risk associated with the operations. Below is a brief description of 5 challenges that drilling fluids face when dealing with unconventional shale formations and are related to this research.

- 1.) Environmental Issues. Preserving the ecosystems of the world is a very sensitive topic nowadays. As mentioned before, NADF's have been the main option to drill unconventional shales. However, the footprint of this technique related to cuttings disposals, dewatering operations and/or eventually surface spills represent a drawback for the industry.
- 2.) Formation Damage. Conventional drilling fluids applied in shales are based either, on cation exchange capacity or irreversible pore plugging. An incorrect selection of the chemicals can reduce the permeability of the formation reducing the performance of hydraulic fracturing. Furthermore, conventional additives cannot efficiently build a filter cake in the near wellbore region due to the nanopore structure of the shales. Thus, the fluid invasion is even higher.
- 3.) Wellbore stability. This can be the main problem when drilling through complex shale formations. Drilling fluids can disturb shale formations both, chemical and mechanically. Any formation can collapse if the mud is not properly designed according to the mechanical stresses (mud weight window). On the other hand, an incompatibility with the drilling fluid can generate sloughing or caving (e.g. pack-off, tight holes) or either excessive dehydration

that can lead to the same problem due to further hydraulic invasion into the shale matrix.

- 4.) Stuck pipe. Drill string can experience a stuck pipe due to the different responses of the shale formation to the drilling fluid as mention before. Still, most of the well path designs to develop unconventional shale reservoirs are extremely complex (e.g. horizontal, multilateral). This tends to increase the torque and drag and dogleg severities increasing the risk of a mechanical stuck pipe. This problem aggravates when poor lubrication and hole cleaning are experienced.
- 5.) Temperature effects. High temperatures in shale reservoirs represent a challenge for WBM to keep rheological, filtration and chemically stability. Conventional polymers tend to suffer from a high degradation rate as temperatures increase above > 200 °F. Under this environment, their efficiency is reduced to a point where polymer structure suffers a breakdown (e.g. hydrolysis) affecting the entire drilling operation.

2.7. INTRODUCTION TO NANOTECHNOLOGY

Nanotechnology principally covers the fields related to nanomaterials, from their synthesis to their exploitation going through a meticulous characterization. To understand the region of nanomaterials application, one can refer to a very tiny scale, in which a nanoparticle size can be in the range of 10^{-7} m to 10^{-12} m (El-Diasty & Ragab, 2013). Nanomaterials behavior are basically the bridge between the molecules and the infinite bulk systems. The importance of NP relies on its unique chemical and physical properties

that are not related either to the bulk materials or to the atomic-molecular level. Therefore, nanomaterials with their amazing characteristics in contrast to the traditional materials expand the research opportunities to new frontiers.

2.7.1. Definition of Nanoparticles. A particle of a size between 1 to 100 nm or at least with one side's structure in this range is cataloged as a nanoparticle. NP are far smaller than the daily structures of the world subject to Newton's law of motion but bigger than a single atom or molecule (Horikoshi & Serpone, 2013). Figure 2.13 shows different materials at the nanometer level.

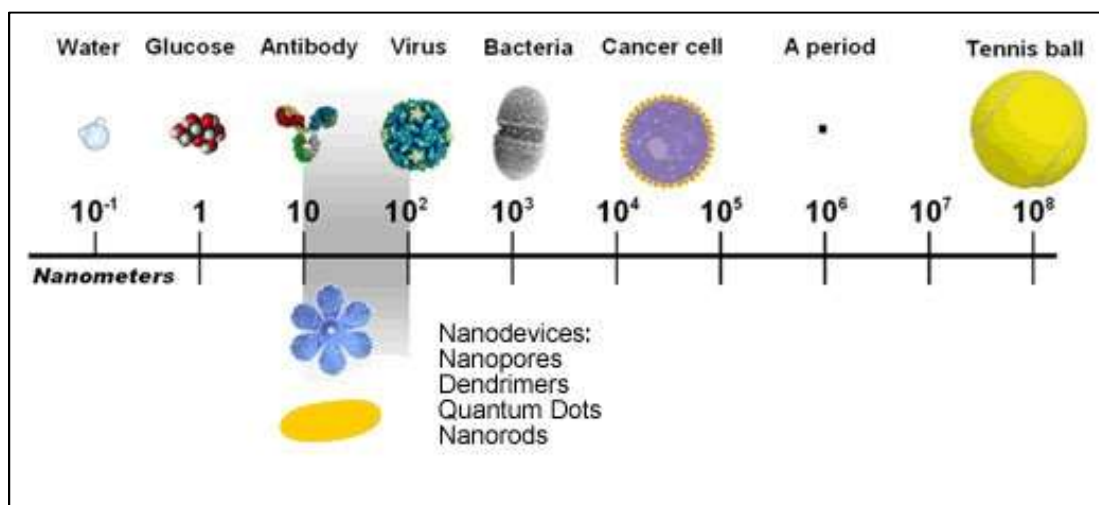


Figure 2.13. The scale of items referenced to a nanometer.

2.7.2. Properties of Nanoparticles. As described before, nanoparticles have the singular characteristics that cannot be found in their original material which is in the micro or macro scale. Table 2.1 illustrates a brief summary of the principal chemical and physical properties related to NP (Cademartri & Geoffrey, 2009, Gogotsi, 2006).

Table 2.1. Physical and chemical properties of nanoparticles.

PHYSICAL PROPERTIES	CHEMICAL PROPERTIES
Shape, size, aspect ratio, increase the surface area	Increase reaction rate, solution stabilization
Reduction of melting point	Chemistry of surface (charge, zeta-potential)
The increase of mechanical strength	Improve biocompatibility
Experience superparamagnetic behavior	Lipophilicity/hydrophilicity
Improve optical properties	photocatalytic properties
Improve electrical conductivity	Increase thermal conductivity
Improve aggregation/agglomeration rate	Improve solubility under correct conditions

2.8. NANOTECHNOLOGY IN OIL & GAS INDUSTRY

The continuous effort to understand nanoparticles behavior, their properties and advantages have to lead to several applications, especially in cosmetics, medical, electronics, food, fabric, painting, and coating industries. The oil & gas industry has been aware of this research topic and different investigations have been performed covering NP application in exploration, reservoir, production, completion, drilling, and refinery.

In oil & gas explorations, NP serves to designed sensors that improve the formation of imaging contrast (Krishnamoorti, 2006). Other researchers used NP's ability to resist HTHP conditions in deep wells and apply them to gather reservoir characterization, flow monitoring and recognition of different types of fluids presented (Esmaeili, 2009). NP has

been used to improve PDC bit technology. Nanodiamond particles have been applied to PDC cutters so the unique surface obtained is complete homogeneously with the PDC matrix. However, the improvements in performance are still under review (Chakraborty, 2012).

The nanotechnology has been extremely successful in the construction of completion devices such as fracturing balls used in each fracture stage. The introduction of controlled electrolytic metallic (CEM) nanostructures allow the application of fracturing balls that will disintegrate in the presences of the appropriate fluid. The latter, reduce time and risk to the hydraulic fracture operations while maintaining the necessary strength on the ball used to support the pressure observed during the fracture treatment and correctly isolated each stage (El-Diasty and Salem, 2013).

Other researchers have evaluated the application of nano-emulsion for cementing jobs to improve hole cleaning and reverse the formation wettability to achieve a better adhesion with the cement slurry (Maserati et al., 2010). Also, acceleration in cement hydration processes, increases in compressive strength, reduction in fluid loss and gas migration have been investigated by applying different NP as nano silica, nano alumina, carbon nanotubes among others (Santra, 2012).

Ni-Fe nanoparticle (50 nm) has been suggested to use in the production and recovery of gas hydrated based on the size particle and their ability to rise temperature inside the formation needed to disturb the thermodynamic equilibrium in this unconventional reservoir and allowing the recovery of the associated gas (Bhatia & Chacko, 2011).

Researchers have studied different NP in drilling fluids at the lab scale for diverse purposes. Silica NP as fluid loss additive in shale formation (Cai et al., 2012; Zakaria, 2012). CuO and ZnO NPs to improve the thermal and electrical behavior of WBM (Ponmani, 2016). NP to inhibit cutting (Boul, 2016). As an HTHP additive to maintain rheological properties (Abdo & Haneef, 2012; Ponmani, 2016), and to provide wellbore strengthening in shales, among others (Contreras, 2014).

The advantage that nanoparticle size can fit and efficiently plug the shale nanopores represent a possible solution to improve the development of unconventional shale plays without the risk to deal with irreversible plug techniques offered by the conventional WBM. Hence, NP-WBM has the potential to replace OBM in sensitive areas, improve the drilling fluid inhibition capabilities and increase the thermal resistance of conventional drilling fluids additives, thus offering a WBM eco-friendly alternative to drill unconventional shale plays.

2.9. NANOTECHNOLOGY APPLIED TO DRILLING FLUIDS IN SHALES

Drilling fluids have an extremely important role in the entire drilling operations in every well, from the spud mud until the completion fluid used in the final displacement prior to continuing with further operations. In the literature, it is possible to find different modifications of conventional WBM or OBM used to drill shale formations. However, as previously discussed, a good result due to one modification cannot be generalized and extended as a rule to other formations. Even more, environmental concerns are factors to have in mind when the intention is to achieve the real success that might represent a touchable and valuable technique for the oil & gas industry.

The sensitive condition of most shales formations and the need to pursue an eco-friendly drilling fluid system is where the nanotechnology in drilling fluids can make a great difference. Advantages such as reduction of formation damage, the creation of thin filter-cakes, control of fluid invasion or filtrate, reduction in cutting dispersion, enhancement of rheological and thermal properties, as well as the strengthening of wellbore walls, are among other benefits that have proved their potential.

The present literature review has the intention to provide a better exposure of nanoparticles as principal additives in the drilling fluid system while at the same time provide information why some previous projects leads to excellent results that support NP as an effective solution, but other aspects of the technique need to be reviewed, and thus the journey to a better and suitable drilling fluid formulations based on NP is still under construction.

2.9.1. Impact of NP in the Reduction of Fluid Invasion in Shales. The principal advantage of the nanoparticle as an additive for drilling fluids in shale plays is its size. Conventional additives use to control filtration have a particle size distribution at the micro or macro scale (Figure 2.14). These particles are larger than the nanopore structure of the shale formations. The differences in size clearly explain the reason these products cannot build a filter cake and control the fluid or filtrate invasion from the wellbore to the shale matrix in the near-wellbore region (Cai, 2012).

Nanoparticle offers a solution to this problem, as their size fits perfectly to the nanopore structure of shales following Abram's plugging theory which suggests that the bridging material should have a median particle size between $1/7$ to $1/3$ or slightly more than the median pore throat size of the formation to protect (Abrams, 1977). Also, NP can

create a thin filter cake in the shale wellbore walls that control the water influx avoiding further drilling problems (Hoelscher, 2012).

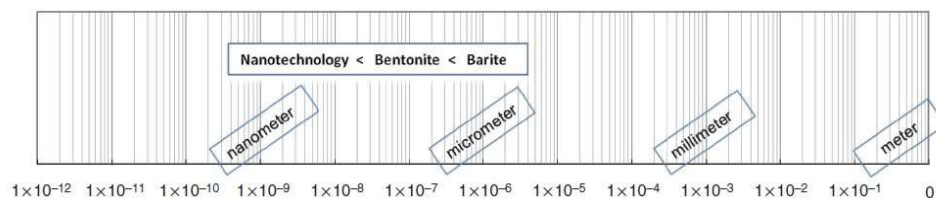


Figure 2.14. Particle-size scale (Cai 2012, adapted from Abrams 1977).

Researchers found in previous studies that NP are able to create an external filter cake instead of internal cake that causes formation damage and is impossible to remove prior to cementing jobs. The ability of NP-WBM to form an external filter cake with less % of solid helps to remove them easily with pre-flush fluid prior to the cement job generating a better bonding between cement and formations (Amanullah, 2011; Salih, 2016). Additionally, when the filter cake is not totally removed formation damage can be experienced before hydraulic fracturing, thus, the fracture conductivity can be affected. Preventing formation damage is more desirable than reduced production as it increases the operational cost associated with a remediation operation, especially for low permeability reservoirs such as the shale plays.

On the other hand, NP filter cake had proved to be strong and thin enough to reduce even the spurt filtrate and avoid solids or aqueous phase to invade the formation generating damage. The spurt loss can be defined as the volume of filtrate that invades the formation prior to a mud cake is established (extrapolate time to 0s). In other words, is the medium that carries solid particles inside formation causing irreversible formation damage, once

those particles start to be deposited in the internal pore structure of the rock an internal filter cake is formed blocking the pores with time affecting future production (Zakaria, 2012).

Usually, in sandstone, the spurt volume can deposit fine material that blocks the pores and in the case of shales as the amount of spurt volume increase, the more like the shale formation can swell if high smectite content is present or the pore pressure can rise faster in the case of less hydratable shales. The advantages of NPs to reduce solid concentration in the drilling fluid system, control spurt losses, filtrate volume and build thinner and no-erodible filter cakes make them an extremely convenient additive for drill-in fluids in shale plays.

A first attempted to include silica nanoparticle in a drilling fluid system used 20 nm silica NP with a concentration of 10 wt. % as the principal additive to decrease water influx in Atoka shales, with reductions up to 72%. The results presented the effect of applying NP in WBM to successfully protect shales formations. The results suggested a reduction of permeability by a factor between 5 to 50 (Al-Bazali, 2005; Sensoy, 2009). However, the biggest concern about this study was the conclusion that at least 10 wt. % of functionalized NPs is needed to achieve favorable results, which increase the cost of NP-WBM.

After the promising results achieved with silica NP as a plugging agent in the analysis performed in Atoka shale (Sensoy, 2009) many researchers started to extend the technique to other shales plays such as Mancos (Hoxha, 2017; Ji et al., 2012), Yanchang Shale (Kang, 2016), Fracture Shale gas (Riley et al., 2012) varying the type and concentration of the nanomaterial (non-modified, and functionalized) to evaluate how effective NP can be in shale plays with dissimilar clay content.

In order to reduce the cost associated with functionalized NP researchers had evaluated the ability of non-modified SiO₂ NP to reduce the permeability in Atoka. The results indicated that the minimum nanoparticle concentration to effectively plug the shale nanopores was also close to 10% by weight (Cai et al., 2012) showing no difference between previous works with the functionalized NPs.

Nonetheless, a 10% wt. of NPs modified or non-modified still too much to consider it viable for an Oil & Gas application. Further researchers have reduced the concentration up to wt. 3% (10.5 ppb in field units) and still obtained good results in the transition pressure test (Ji et al., 2012; Riley et al., 2012). Despite the good results, the condition of surface modified nanoparticles increases the cost associated with the NP-WBM which play against the goal of an affordable technique to replace the so preferred OBM system.

Other researchers evaluate In-house NP (generated inside the drilling fluid) showing the same ability to reduce both, spur and filtrate loss when compare them to conventional LCM material. The reduction was close to 40% under different conditions demonstrating superior plugging properties than conventional LCM products (Zakaria et al., 2012)

One of the weakness observed with NP-WBM was their poor performance in shale plug with natural micro-fractures. When the NP-WBM was applied to high-fractured gas shale the results in permeability reduction were negatives, even with a high concentration of NP (as high as 30 wt. %). These suggest that NP-WBM would have a low performance dealing with shale plays with natural micro-fractures while drilling (Sharma, 2012). A possible solution could be studied based on the analysis of the shale pore size distribution as well as for micro-fracture both, natural or induced. These will allow selecting a specific

shape of NP (e.g. nanoplatelets). Furthermore, the inclusion of conventional LCM materials such as graphite to heal faster the wellbore walls should be considered. The last indicates that further studies should focus to established an optimum balance between non-modified NPs as they are cheaper than the functionalized ones conventional LCM material to evaluate the potential cooperation for the design of NP-WBM.

2.9.2. Importance of NP Stability in Drilling Fluids. One major concern with nanoparticle solutions is to maintain the system stability. In other words, to avoid the formation of NP aggregates that might precipitate and cause rheology problems (Figure 2.15). NP are prone to face stability issues at high temperatures and salty environments, both conditions can be encounter either while drilling shale formations or in the drilling fluids systems itself (Mcelfresh, 2012; Metin, 2011). Screening test for salt, temperature, and pH tolerance should be conducted previous inclusion of the NP to the drilling fluid formulation to evaluate their stability as a future main additive in an alternative NP-WBM.

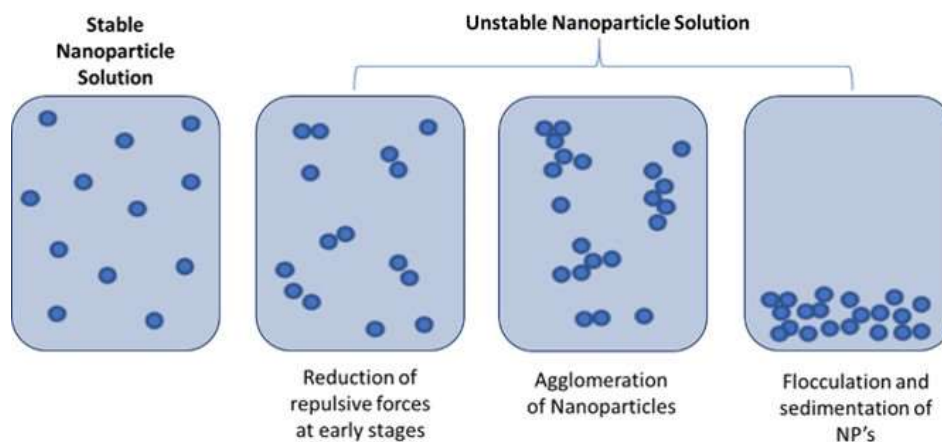


Figure 2.15. Nanoparticle unstable process.

The mechanism of how NP plugged shale Nanopore goes beyond than just a physical seal. NP application not only depend on the particle size that is able to plug the shales nanopores, there are other factors such as surface charge density, zeta-potential, NP shape and concentration, salt content and pH among others that define how stable an NP-WBM can be (Hoxha et al., 2017).

Recent studies suggested that the surface of NP can change its surface charge based on the medium conditions (e.g. pH). If the Van der Waals attraction forces between the shale surface and the NPs surface are higher than the repulsion forces, the adhesion behavior of NPs to the shale pores will increase as well as the rate of deposition and the bond strength. In other words, the plugging capacity of the NP will improve. Contrary, if the repulsion forces between NP are weak the more probable that the solution starts to form aggregates affecting the stability of the NP-WBM and reducing its ability to seal the Nanopores (Hoxha, 2016; Taraghikhah, 2015).

To know how stable a NP solution is, Zeta-potential (ζ) measurements give us a degree of the solution dispersion. In other words, the result shows the potential difference between the disperse medium and the immobile charges layer attached to the surface of the disperse nanoparticles (Chilingar, 2014). ζ values that fall between -30 mV to +30 mV indicated that the attraction forces in the system are greater than the repulsion forces and the system might experience aggregation of NP and later flocculation and sedimentation. The goal is to keep a magnitude of ζ value above 30 mV, ($\zeta > 30$ mV or -30 mV $< \zeta$) which is considered as a stable colloidal system (Mahmoud, 2016).

By modifying the pH of the solution is possible to alter the zeta potential values of both, nanoparticles and shales which can be beneficial or not depending on the initial

values. For example, if the pH of a system that contains NP with the negative surface is reduced, the surface charge can become neutral and aggregation issues can arise. On the other hand, if the same system becomes more basic (pH increase) repulsion forces will be stronger improving the dispersion of the solution but at the same time the ability to reach the shale surface (shale has also negative surface charge).

The key is to reach a balance between NP-NP repulsion and NP-Shale surface attraction. As stated before, NP solutions can be very sensitive to pH conditions. Previous investigations used SiO₂ NP demonstrated that this nanomaterial can have stable behavior and positively impact rheology and filtration properties in both, low pH (9.4) and high pH environment (11.5) while exhibit good shear thinning capacity compared to the base mud (without NPs) despite different pH conditions (Salih et al., 2016).

NP has shown better dispersion in OBM due to the use of surfactants in the mud formulation itself, despite its environmental concern. Researchers have been evaluating different methods to provide nanoparticle stability in WBM, some with coated or functionalized NP, others by reducing the concentration in the liquid medium, and others analyzing which factors affect the non-modified NP to improve their stability (Ghanbari, 2016). The main goal should focus on how to improve the stability of NP in WBM rather than apply NP to OBM and continue with the environmental concerns of this type of system. Also, surfactants are expensive and can interact with the rock formation affecting its wettability preference leading to production issues in the future. Some studies conclude that when no surfactant is used aggregation issues with NPs start to experience above 2 % wt. (Fakoya, 2014). The last concentration can serve as upper-limit criteria in the design of NP-WBM with no surfactants.

The reduction of interparticle space increases the attraction forces of NP at high concentration, this can explain why the stability of the colloidal solution reduces at higher concentration leading to aggregation issues. On the other hand, extremely low concentrations expose the NP-WBM to experience a non-uniform colloidal suspension (NP get concentrated in one place) in the mud column providing and inadequate filtration capacity and wellbore stability (Hoxha et al., 2017). The inclusion of NP with stable zeta-potential values can help to reduce concentration avoiding focal clustering inside the drilling fluid column.

Thus, future investigations should emphasize their effort in the inclusion of conventional additives (i.e. biopolymers, graphite) with low NP concentration that was previously proved to be stable under different conditions (pH, salt, T). Salt has a negative effect on the stability of NP solutions. As salt concentration increases the double layer in each NP is affected and the repulsion force decrease allowing aggregation to occur. NP can be more easily destabilize in the presence of divalent salts than monovalent salts. Nevertheless, no matter the type of salt, as the concentration of NP or salt increase the aggregation phase will be more easily to achieve (Metin et al., 2011).

Regardless of the different environmental conditions that can influence the NP stability, another technique to protect the NPs is to change their surface. Functionalized NP (coated, modified surface, nanocomposites) present lower tendencies to suffer from aggregation. Essentially, each functionalized NP has a shield in its own surface that increases the repulsive force providing a more stable solution. (Boul, 2016; Jain, 2015; Pham, 2014). Still, modified NP can be extremely expensive affecting the overall cost of the drilling fluid in any drilling operation.

Non-modified NPs if correctly tested against potential instability factors (Salt, and pH) can decrease the economic factor related to the design of a NP-WBM. The effort to assess these experiments will increase the chances to select a proper concentration and type of NP that can be stable under different environmental conditions. At the same time, the NP will gain confidence as an additive to apply in WBM for shale plays and eventually lead the objective to provide a high performance and environmentally friendly WBM for the industry.

2.9.3. Impact of NP in the Rheology of Drilling Fluids. Drilling fluids with good pumpability exhibit lower viscosity at high shear rates and higher viscosities at low shear rates. This condition provides safer trips in and out of the hole (low shear rates) due to the ability of the drilling fluid to support cuttings at static conditions, while at higher shear rates help to reduce friction losses and control the formation of cutting beds in the low side of the wellbore improving drilling fluid hydraulic and hole cleaning.

From the rheology point of view, literature indicated that SiO₂ nanoparticle influences positively the drilling fluid carrying capacity with few exceptions among researchers that experience a decrease in YP (Mahmoud, 2018; Salih, 2017; Wahid, 2015). These studies did not consider the later as a problem which in fact they could suggest that NP-WBM can experience difficulties to transport cutting to the surface, especially for the horizontal sections. However, the reason for these results could be due to an inhibition effect of NPs on the bentonite hydration process or a flocculation due to poor zeta-potential values of the NP in the system. Even though low YP helps to avoid high pump pressures, the key is to reach an optimum range that at the same time does not affect cuttings transport to surface.

Other studies (Aftab, 2017; Ghanbari, 2016) obtained the opposite result in YP with increments in the values over the base fluid. Furthermore, some of the studies showed evidence that SiO₂ NP provides long-term stability to drilling fluids in terms of gel strength at fresh conditions and at aged conditions with no progressive behavior (Li, 2016; Salih, 2016; Taraghikhah, 2015), which is a desirable characteristic in WBM especially at high temperatures where conventional additives tend to degrade at faster rates.

The non-progressive behavior of gel strength supports the idea that NP can reduce the flocculation of bentonite at high temperatures providing a more stable system when compared to the conventional WBM with no NP. Most important, avoiding progressive gels usually experienced with the conventional additives, the NP-WBM warranty lower pressure to restart circulation, lower friction losses in annular spaces and ECD and problems related to formation fractures due to high pump pressures.

Rheology changes in the drilling fluid due to the addition of NP suggested how important is to maintain a correct dispersion in the NP to avoid possible aggregation that might precipitate at downhole conditions and lead to much severe operational problems such as drill string pack-off, well kick due to phase separations, and fluid invasion among others. Prior evaluation of the NP stability against concentration might discard any aggregation problems that can be the cause of the increase in PV. Rheology test with aged NP-WBM varying concentration can reveal the stability of a specific NP-WBM at lab scale giving more safety to the chemical formulation. A higher PV can also affect the ability of the NP-WBM to keep the bit face clean of cuttings and a reduction in ROP can be expected.

A low solid WBM helps to increase ROP in hard formations and at the same time prevent formation damage in productive zones. The extraordinary NP surface area

compared to its volume ratio helps to decrease the concentration of solids in the drilling fluid, less material is then required and a reduction in the interaction between formation-drilling fluids and drilled cuttings can be achieved as well as the effects of high % LGS in the drilling fluid.

Researchers have already tested a low concentration of NP between 0.1% to 0.5 % by wt. (Ponmani, 2016). The principal effect observed was the NP ability to improve the thermal and electrical conductivity of the drilling fluid systems. In other words, researchers found that NP due to their large surface area per unit volume can absorb or dissipate heat while drilling and cooling the directional tools as well as the bit. Also, NP's high thermal conductivity avoid the temperature to affect the hydration of conventional additives keeping the rheology properties more stable and at some point serve as a 'shield' to polymers that might suffer from high degradation rate at those high temperatures. Based on the last statement NP can lead to a possible reduction of conventional additives concentration for WBM, providing a drill-in fluid with fewer solids and at the same time reducing the effects of solids in the viscosity of the entire system.

Selection of the optimum concentration of NP is a key parameter to avoid further rheology issues (excessive PV/YP/Gels). In the past, researchers found that once the NP concentration goes above the optimum value agglomeration can easily occur which not only generates rheology negative conditions but at the same time increases filtration into the shale formation (Amanullah, 2011; Fakoya, 2014). Therefore, avoiding aggregation and flocculation tendencies of NP is one of the most important points to correctly design a stable NP-WBM.

2.9.4. Impact of NP in the Inhibition of Shale Cuttings. In the literature, the majority of the test focuses on the NP ability to stop the water influx to shale samples. Few researchers had analyzed the effect of NP-WBM to avoid cuttings dispersions (Boul, 2016; Jain et al., 2015). Usually, if shale cuttings dispersion is not controlled the problems associated to increments in the fluid density and rheology, will tend to increase hydraulic flow into the shale formation. This will lead to a condition of underbalance and finally to wellbore instabilities (cavings, shale sloughing) or even worst, wellbore collapse.

If NPs shows an ability to keep the integrity of shale cuttings avoiding their dispersion it will prove that the NP-WBM inhibitive properties go beyond that just plugging the shales Nanopores. In the last years, researchers have been trying to reduce the Silica NP's concentration below 10% wt. previously suggested as the minimum required. Concentration around 1 % w/v of Silica NP without further treatment showed a respectful performance preventing problems such as swelling, cuttings dispersion, and delamination of microfractures in shales (Taraghikhah, 2015).

Swelling and dispersion test evaluates the ability of NP-WBM to effectively inhibit shale formations and cuttings. An important key for NP-WBM is to warranty a strong attraction between NPs and shale surface, so they can maintain attached to shale pores and cuttings surfaces and avoid a further fluid invasion that can cause swelling, microfracture, and cutting dispersion.

Researchers proved that SiO₂ NP helps to reduce cutting erosion in shale formations (Mancos) both in fresh and salt water at a low concentration in this specific investigation, the silica NP was functionalized to keep them dispersed in the system. Nevertheless, a stable dispersion of NP with non-modified surface should reach acceptable results. Also,

the friendlier condition of silica NP to work at lower pH and salt concentration compared to conventional WBM support the NP-WBM to reduce the footprints of the chemicals needed for cuttings treatment and water disposals while generating less corrosive effects in the WBM (Boul, 2016).

2.9.5. Impact of NP in Wellbore Strengthening. Previous investigations based on pressure transient test showed that NP can prevent pore pressure build up by controlling the influx of drilling fluid to the formation (Cai, 2012). In other words, NP help to maintain the overbalance of the drilling column in the safe mud window by avoiding the invasion of water to the formation that can increase the pore pressure and lead to wellbore collapse. At the same time, NP-WBM has lighter weight minimizing the chances to experience fractures due to excessive overbalance (Figure 2.16).

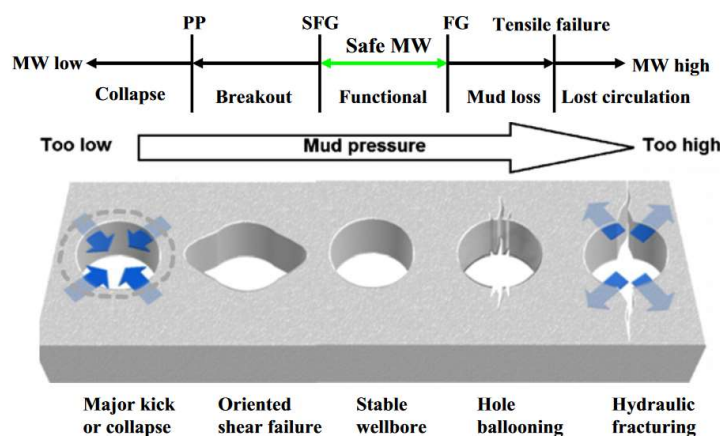


Figure 2.16. Relationship of mud pressure and borehole failure.

In recent years horizontal wells have been one of the most important techniques to develop the unconventional shale plays in the United States. Wellbore collapse in this type

of trajectories represents a serious operational issue that might lead to increments in the overall operational project cost due to Lost in hole (LIH) of tools, extra cement operation (ST) and third parties cost or even a 100% well lost. The dynamic load experience with the vibration and impact of drill bits and tools against the wellbore walls can aggravate this problem especially when we face high tortuosity trajectories normally encounter in horizontal wells. NP can reduce T&D and also increase the wellbore strengthening in shales (Contreras, 2014).

The ability of NP to create thin, flexible, and no-erodible mud cake while drilling shale formation indicated its potential to reduce drilling problems such as excessive T&D or potential stuck pipe in the long lateral sections. A homogeneous external filter cake in the horizontal section helps to reduce the drill string area that is in contact with the low side of the well which decreases the risk of stuck pipe (Figure 2.17). This thin filter cake and the NP itself help to reduce the friction resistance, generating less tortuosity of the wellbore while increasing the ROP, so desirable in extended reach wells or multilateral sections. (Amanullah, 2011; Taraghikhah, 2015).

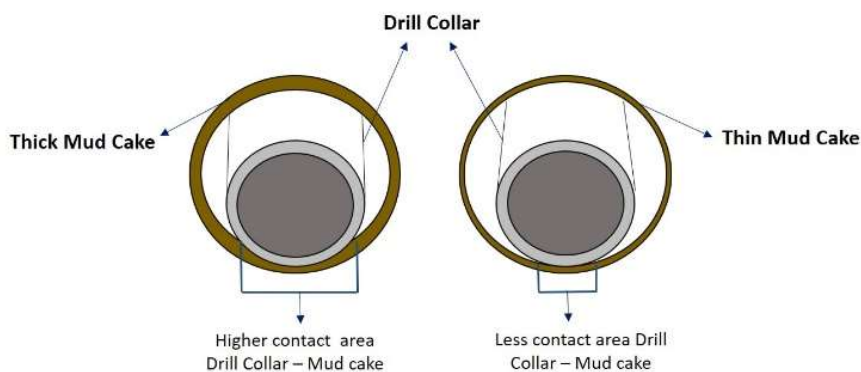


Figure 2.17. Contact area between the drill string and the mud cake.

Several types of research have been evaluating the advantages of NP related to WS, some of them used modified (Boul, 2016; Sensoy, 2009) other non-modified (Cai, 2012; Fakoya, 2014; Srivatsa, 2012). These studies include the analysis of spurt and filtrate volumes of the API static filtration test as well as the HTHP and related them to the increase of rock samples fracture pressure (Contreras, 2014).

Application of NP in OBM showed an increase in the range of 20% to 30% in the fracture pressure (Contreras, 2014). This research showed an important reduction in NP concentration between 0.5% to 2 % by wt. which imply a positive impact in terms of cost and stability for NP drilling fluids. Nonetheless, the based fluid for those tests was OBM which reduce interaction with the shale matrix due to capillarity possibly hiding the real effect of the NP. Similar studies need to be addressed with WBM to prove their capabilities and support the intention of a friendlier drilling fluid.

However, is important not to assume that Darcy flow can be applied to shales. Instead, transient pressure test can give a better analysis of the ability of NP to reduce permeability and increase wellbore strength while drilling. From the literature, we can establish that NP has the ability to increase the strength in shales. However, wellbore strengthening based on NP-WBM not only depends on the NP presence. The stability of the NP solution is vital to keep them disperse conserving their original shape as well as reduce the aggregation tendency. This will keep as much as possible the original structure of the NP and consequently effectively plug the nanopores increasing the wellbore strengthening (Hoxha, 2017).

On the other hand, there are still some specific doubts about NP's ability to seal micro or Nano fractures (Sharma et al., 2012), the results indicated a poor performance,

but if the concentration of NP and shape is optimum a combination with conventional LCM products such as graphite can represent a solution for the NP-WBM formulations when trying to provide wellbore strengthening to shales formations that have natural microfractures.

Finally, we can conclude that the application of NP-WBM to shale formation is an integral design in which each benefit is strongly attached to the other. There cannot be an increase in WS with a high fluid loss of the NP-WBM. At the same time, stable rheology and enhanced inhibition properties work together to avoid cuttings dispersion reducing the risk of density increments. The key is to understand the formation and select materials that are stable enough under different condition. Thus, the design should include not only a deep characterization of shale but, also a characterization of the nanoparticles, and the overall NP-WBM including its chemical interactions with the rock.

This research has the intention to cover the characterization of specific NPs (silica and graphene oxide) and mix them with conventional additives to design a NP-WBM that can fit the specific needs of the Woodford shale.

3. NEW NANOPARTICLE WATER-BASED DRILLING FLUID FORMULATION WITH ENHANCED THERMAL STABILITY AND INHIBITION CAPABILITIES IN THE WOODFORD SHALE

3.1. EXPERIMENTAL METHODOLOGY AND DESCRIPTION

This chapter outline the different research methodologies used to address the research objectives listed in chapter 1. In addition, samples preparation, procedures, materials as well as laboratory tests will be presented in detail. The proposed methodology was classified in 3 main task, shale rock characterization, nanoparticle characterization, and, drilling fluid performance evaluation. The task sequence proposed is important to follow since the design of drilling fluids should be based on the type of formation that is intended to be drilled.

The shale rock characterization allowed to describe the structural and compositional characteristics of the rock, gathering relevant information that indicated the features needed in the NP. Analyzing the characteristics of NP, provided an insight into their stability at different environmental conditions to support their use in the drilling fluid. The performance of drilling fluids was evaluated following standardized guidelines API RP 13-I and API RP 13 B-1. Concentration for materials was studied to establish an operational limit to save cost and materials, and, inhibition capabilities were examined through a series of swelling and dispersion test.

Finally, dynamic aging tests were included to evaluate the effect of different temperature conditions on the stability of drilling fluids, in terms of filtration and rheological properties and KCL/PHPA fluid was used for comparison purposes.

3.1.1. Shale Analysis Techniques. Laboratory characterization of the reservoir rock is an important part to correctly design a drilling fluid and should be the first step in the drilling fluid customization process. The shale rock analysis was performed through four different techniques, X-ray Diffraction (XRD), scanning electron microscopy (SEM), cation exchange capacity (CEC), and, porosity measurements.

Through XRD analysis it is possible to determine the rock mineral composition, its clay content, and the specific type of each clay, which is a crucial information from the design perspective of water-based mud formulations (Deville, 2011). SEM technique is an advanced imaging method that can be used to understand the complex rock pore system, particularly in unconventional shales where its pore network is known to be composed from micro to nano-scale. Another important parameter to be determined in shale rocks is the cation exchange capacity, also known as CEC, which indicates the shale reactivity in the presence of water. The last parameter to complete the shale characterization proposed is the porosity measurement. Grain volume and density were obtained through gas pycnometer, while bulk rock properties through immersion test. The difference between these values helped to estimate the total porosity.

3.1.1.1. X-Ray diffraction and clay mineralogy composition. Clay minerals are described as very fine grain material that is impossible to identify with common optical methods. X-Ray Diffraction is a non-destructive technique that can identify the shale rock mineralogy composition and is one of the most precise methods to define clay composition. Knowing the shale rock mineral composition and more specifically its clay content allow to better understand the type of hydration process a specific shale might experience and based on this customized the drilling fluid formulation (Deville, 2011).

The principle behind the X-Ray Diffraction theory is based on the Bragg's Law (1912). X-rays are electromagnetic radiation of exactly the same nature as light but of very shorter wavelength ($10^{-10}\text{m} = 1\text{\AA} = 0.1\text{ nm}$). Thus, X-rays are ideal to measure interatomic distances in crystal solids which are typical of that order of magnitude. When X-rays of known wavelength are directed to the sample, the crystal structure of the material can act as scattering center for the X-rays and generate constructive and destructive interference. The interferences produce a diffracted ray that is then detected, processed, and counted (Cullity, 1978). Only the constructive interferences are of interest in the final process because the destructive interferences cancel each other. Figure 3.1 shows and scheme of the diffraction process.

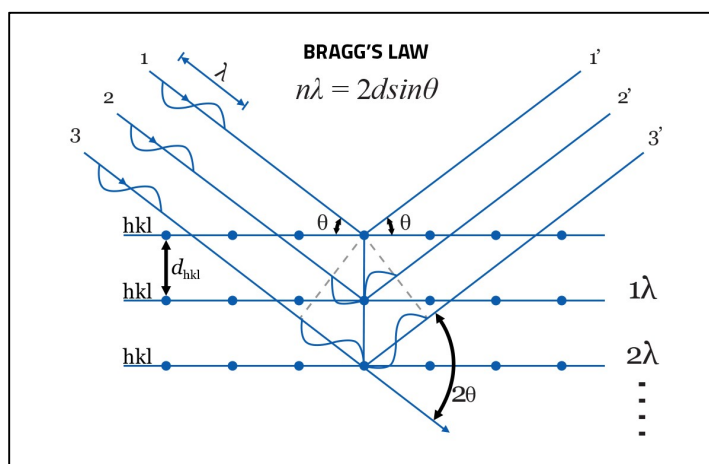


Figure 3.1. X-ray theory based on Bragg's law.

The scattering is related to a specific angle of diffraction based on the d-spacing between atoms in the crystal structure of the sample. The Bragg's law describes the last relationship as:

$$n\lambda = 2d\sin\theta \quad (5)$$

Where n is an integer, λ is the wavelength of the radiation, d is the lattice spacing between atomic layers in the crystal structure of the sample (in angstroms), and θ is the angle of diffraction.

To perform an XRD analysis a mechanical assembly called theta-theta goniometer system is used as shown in Figure 3.2. The system holds and maintains the sample horizontally while the anode x-ray source and the detector tube rotate at a rate $-\theta$ °/min and $+\theta$ °/min respectively. The angle between the X-ray source and the sample is defined as ω (incident angle) and the diffracted angle between the incident beam and the detector tube is defined as 2θ . Diffracted angle, 2θ , is always twice the incident angle, ω . (Rigaku, 1993)

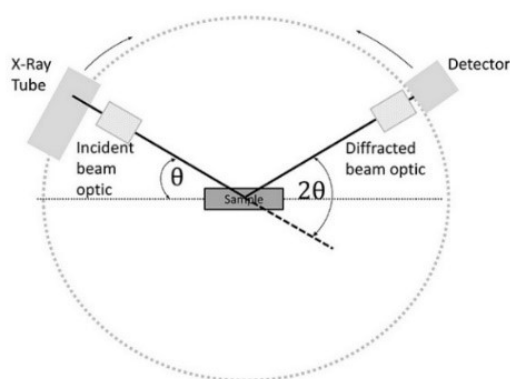


Figure 3.2. XRD goniometer outline.

By scanning the sample through a range of 2θ angles, all possible diffraction directions of the lattice should be attained. Then, conversion of the diffraction peaks to d-

spacings with Bragg's equation allows identification of each mineral because each mineral has a set of unique d-spacings (Moore & Reynolds, 1997).

• **Shale sample preparation.** The reliability of XRD results are based mainly on the quality of the sample preparation, any contamination during this step can affect the validity of the XRD results (Moore & Reynolds, 1997). For the purpose of this research, a semi-quantitative method described by George S. Austin (New Mexico Bureau of Miners & Mineral Resources) and later modified by Dr. David Wronkiewicz at Missouri S&T was selected. The procedure produces a clay mounted sample where the single clay particles are oriented with their c-axis perpendicular to the glass slide. The latter will produce an intense basal reflection during the XRD analysis minimizing the reflections from other crystallographic directions. The preparation consisted of 7 steps described below:

- 1.) Thermally resistant glass slides (600 ° C) were selected and labeled for the XRD analysis.
- 2.) 50 grams of shale sample was weighed and then crushed to a fine powder using a mortar and pestle.
- 3.) 25 grams of the shale powder in step 2 was added to a 100 ml beaker with deionized water and then mixed for 5 minutes. The clay mixed solution was then allowed to stand for 10 minutes.
- 4.) During the stand period, the coarse material should settle, and a clay decanted fraction should remain suspended. If flocculation is observed and the clay particles cannot remain suspended a longer period of settling time should be allowed until the water fraction is clear and can be poured off and new water added and remixed.

- 5.) If after several attempts in step 4 clay still settling. Few drops of hexametaphosphate (CALGON) should be added to the solution and remixed. This product control clay flocculation allowing the clay particles to be dispersed in the solution and remain suspended after the coarse material has been settled.
- 6.) Once the clays particles could remain in suspension after the 10 min. stand period the clay sample was mounted. A pipette was used to withdraw clay-water solution from the top of the suspension and then transferred to the glass slide covering all of it avoiding any overflow.
- 7.) Clay samples mounted in the slides were then covered to protected them from dust contamination and allowed them to dry overnight at room temperature. Figure 3.3 shows the procedure for clay sample preparation.

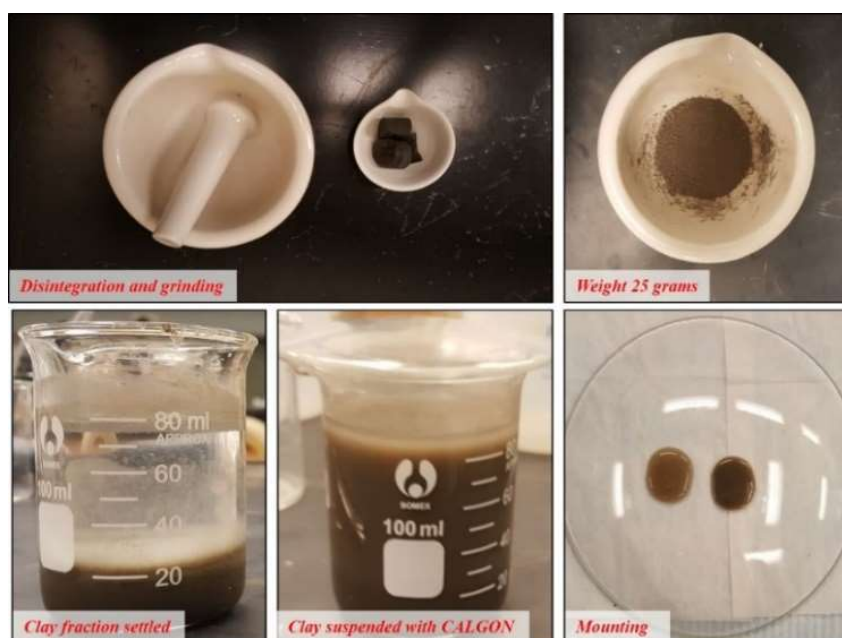


Figure 3.3. XRD sample preparation.

• **Test procedure.** The shale XRD samples were analyzed 3 times under different conditions. Untreated (dry overnight), glycol exposed (24 hrs.) and heat treated at 550 °C for 1 ½ hour (Figure 3.4). The three different analysis were run in sequence order. The equipment used for the XRD investigation was a PANalytical X'Pert Pro (MPD) part of the advanced material characterization laboratory (AMCL) of the Missouri S&T. The equipment has a Bragg-Brentano beam geometry and CuK α X-ray source. The X-ray tube was set to 40 kV accelerating voltage, and 45 mA heating amperage (Figure 3.4).



Figure 3.4. XRD samples at different conditions.

The following procedure explains the conditions and parameters for each type of test:

- 1.) Untreated scan: Initially, the dried overnight sample with no treatment was brought into $\theta:\theta$ goniometer for XRD analysis. Two runs were performed. The first one was named rapid scan, and the analysis was from 2° to 40° 2θ at speed of 2° 2θ /min. Then, a low scan was run on the same sample from 24° to 26° 2θ at speed of

0.4°2θ/min. this one was designed for better differentiation between chlorite and kaolinite peaks.

- 2.) Glycol treatment scan: after the untreated scan, the same sample was put inside a vessel with ethylene glycol for a period of 24 hrs. to allow expandable clays layers to swell for better mineral peak identification. The rapid scan range was from 2° to 40° 2θ at speed of 2°2θ/min and the slow scan from 2° to 15° 2θ at speed of 0.4°2θ/min
- 3.) Heated scan: to better identification of kaolinite and chlorite peaks the previous glycol sample was heated at 550 ° C for 1 ½ hour in the oven. This step helped to identify kaolinite and chlorite since the first become amorphous to X-rays and the peak tends to disappear (Moore & Reynolds, 1997). The rapid scan range was from 2° to 40° 2θ at speed of 2°2θ/min and the slow scan from 2° to 15° 2θ at speed of 0.4°2θ/min.

The qualitative identification process for each mineral and clay peak present in the XRD patterns begins by identifying the peak with the highest intensity. Once the mineral related to this peak is confirmed the second step is to identify the weaker peaks of the same mineral present in the XRD pattern. The same procedure is following for the identification of all minerals and clays present. To precisely identify the 2θ positions of each peak Fityk 0.9.8 software was used. Then the 2θ position where transform with Equation (5) to basal d-spaces and compare with the values corresponding to each mineral in the literature. the quantification process was performed with the Software associated with the XRD equipment.

3.1.1.2. Shale pore determination through SEM. Evaluate the mineralogical structure of unconventional reservoirs as shales is difficult to accomplish due to the nanoscale pore network. The use of SEM has been a priority test to customize the plugging material selection of drilling fluids for shale plays. SEM technique can provide an insight into one of the most important properties to determine in shales rocks, its pore size distribution. Based on SEM image analysis, the size selection of the nanoparticle as a plugging agent can be refined to select the most appropriate material. SEM technique and digital image analyzer (ImageJ) were used to precisely estimate the characteristics of the pore structure in the Woodford shale.

The SEM operates based on the use of an accelerated electron beam, which is directed towards the specimen under examination. An electron gun located at the top of the device generates the beam of highly concentrated electrons. When the incident beam hits the specimen, it emits a radiation consisted of x-ray and electrons. The ejected electrons include backscattered electrons (BSE), and, secondary electrons (SE). The SEM implement an electron detector to catch these rebounding electrons, record them, and after processing them to generate the 2D image of the sample structure.

In addition to topography images generated with the SE to evaluate the pore network, the SEM allows for the determination of other relevant properties of the rock sample, including its surface chemical composition and mineral phases identification when using the BSE (Gree, 2015). Figure 3.5 shows a layout of the SEM process.

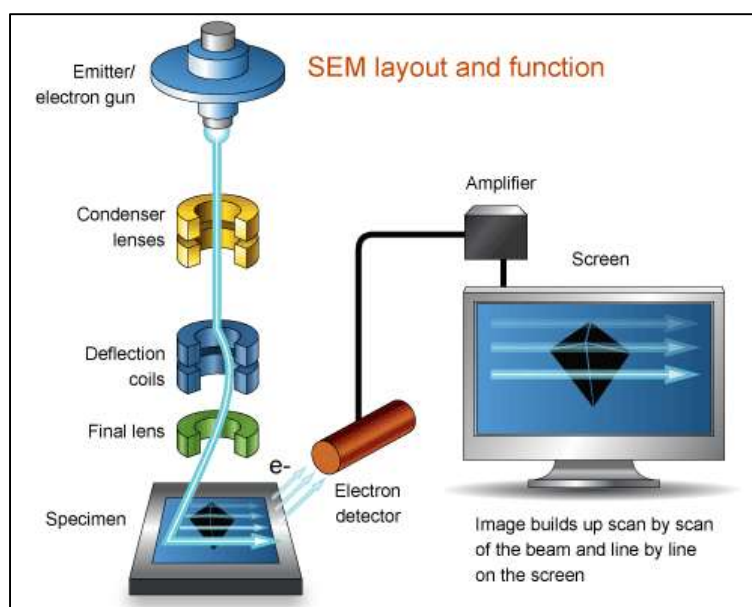


Figure 3.5. SEM scheme and process.

• **Shale sample preparation.** Preparation of shale rock specimens for SEM analysis consisted of 6 steps, sectioning, cleaning, sample ‘cold’ mounting, grinding, polishing, and, sample coating.

- 1.) Sectioning: Shale core of 1 x 1 inches were sectioned with a slow diamond saw perpendicular (circular shape) and parallel (rectangular shape) to the bedding planes with a thickness of approximately $\frac{1}{2}$ inch.
- 2.) Cleaning: Sectioned samples were immersed in a 100 ml beaker with ethanol and then placed inside a Eumax ultrasonic cleaner bath with frequencies > 20 kHz. The ultrasonication process was then held for 5 minutes to agitate the mineral oil molecules and other particles detaching them from the shale surface to reduce sample contamination.

- 3.) Sample 'cold' mounting: Cleaned thin shale slices were positioned inside disposal mounting cups and the acrylic cold solution was then poured filled $\frac{3}{4}$ of the mounting cup. After 12 minutes the acrylic was cured, and the sample demounted from the cups.
- 4.) Grinding: Flat, smooth an unscratched surface is critical to obtain SEM images for quantitative analysis. The grinding process followed use silicon carbide sandpaper with different grits (180-320-400-600-800-1200-1500). Each grit was positioned above a rectangular piece of glass used as a flat surface. Then, the shale sample mounted in acrylic was grit against the sandpaper using mineral oil as a lubricant. Ethanol was used to wash the sample after each grit stage and air to dry it. Optical microscope (120X) was used to evaluate the surface of the sample before continuing to the next grit paper.
- 5.) Polishing: The procedure involved the use of oil-based diamond suspension instead of water-based suspension to avoid the effect of water on the clays. A specific polishing cloth was used for each suspension and lapping oil provide lubrication. 3 um suspensions were followed by 1 um. Ultrasonication process was performed between stages and also after the final polish.
- 6.) Sample coating: Shale rocks are known to be no conductive materials. Therefore, if an uncoated sample is placed in the path of the electron beam, the sample will charge, causing deviation of the electron beam and no image can be generated. The sample must be coated with conductive material, such as carbon, gold, or gold-palladium alloy. Once the sample was polished it was then attached to an aluminum stub using carbon dot tape, for safety reasons carbon tape was also used around the

sample. Coating of gold/palladium was selected to increase the shale sample conductivity using a Denton Vacuum desk IV sputter. This was the last step before mount the shale rock sample on the SEM equipment. Figure 3.6. shows a photo collage of the sample preparation process.



Figure 3.6. SEM samples preparation.

- **Test procedure.** The Investigations were carried out at the advance material characterization laboratory (AMCL) of the Missouri S&T following the internal guidelines for the Hitachi S-4700 scanning electron microscope (Figure 3.7). The coated shale sample was mounted in the SEM equipment and the images were obtained under high vacuum at low voltage electron beam (2 – 5 kV) using the SE and BSE detectors. These parameters provided the best image at high magnification.

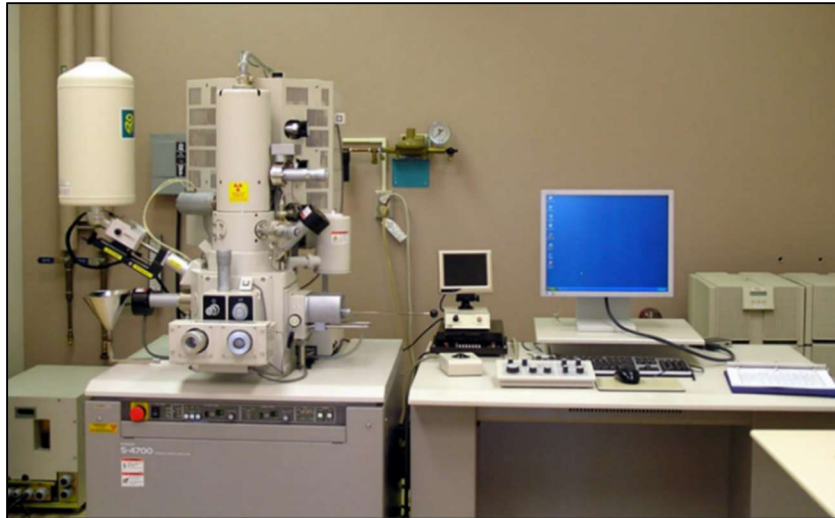


Figure 3.7. FESEM Hitachi S-4700 Missouri S&T.

3.1.1.3. Cation exchange capacity test. Shales rock formation is generally composed of a significant amount of different clays. Depending on the predominant type of clay the reactivity or of the shale exposed to the WBM can be high or low (See section 2.2). Therefore, the determination of CEC in shales is a relevant step in the correct characterization of shale rock and the design of the water-based drilling fluid. Essentially, CEC tests measure the ability of the charged clay surface to interact with cations presented in the aqueous phase of the drilling fluid and retain them attached to its surface, by a positive ion-exchange process (Ali, 2016).

CEC is expressed in milliequivalent weight of exchangeable cations per 100 grams of dry rock. A standardized methylene blue test solution is outlined in API Bulletin RP 13B-1 to calculate the CEC in drilling fluids. However, researchers determined a procedure to extend the methylene blue test to calculated CEC in shales, this method was used for this research (Chevernet & Oslsanya, 1989).

• **Shale sample preparation.** The following steps describe the sample preparation of the shale slurry for CEC.

- 1.) 10 -15 grams of shale samples were disaggregated until obtained shale cuttings < 200 mesh. Then mortar and pestle were used to homogenized and obtained a fine shale powder.
- 2.) 1 gram of the shale powder was then added to 50 ml of distilled water, stirred, and heated for 15 min until obtained the final shale slurry to run the CEC test.

Figure 3.8 illustrates the steps for sample preparation.



Figure 3.8. CEC shale slurry preparation.

• **Test procedure.** CEC Test for shale was measured following the standard CEC test for drilling fluids as described in API RP 13 B-1. A summary of the steps is described below. Figure 3.9 shows materials used for this test.



Figure 3.9. Materials and steps for CEC procedure.

- 1.) 2 ml of the shale slurry was added to 10 mL of distilled water in an Erlenmeyer flask with 15 mL of 3% hydrogen peroxide and 0.5 mL of sulfuric acid the final solution was then boiled gently for 10 minutes. Dilution of the solution was then reached by adding 50 ml of distilled water.
- 2.) Methylene blue solution was added in 0.5ml increments from the pipette to the flask. After each addition of 0.5 ml, the contented was swirl for about 30 seconds and while the solids were still suspended, one drop of the solution was removed with the stirring rod and placed on the filter paper. This process was continuing as necessary until the initial endpoint was reached (dye blue ring appears surrounded by dyed solids).
- 3.) Once the initial blue ring spread from the spot was detected, the solution in the flask was shaken for additional 2 minutes, and another drop was placed on the filter paper

to confirm the endpoint with the evidence of the blue ring. If by chance the ring does not appear the addition of methylene should continue as described in step 3.

Figure 3.10 shows a diagram of the CEC endpoint determination.

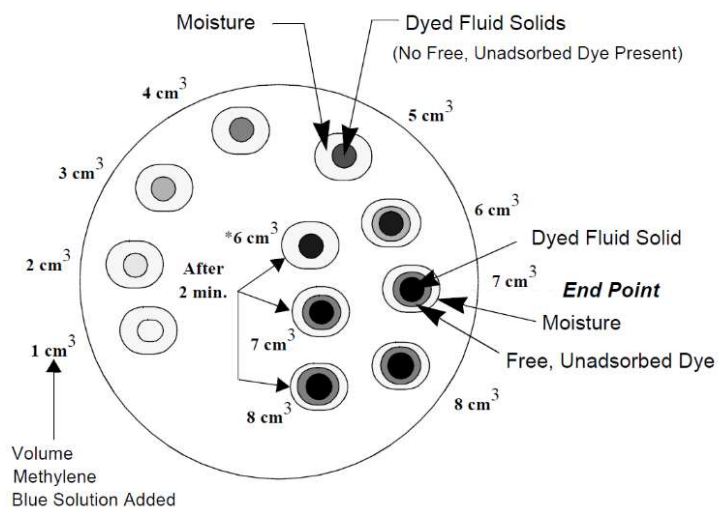


Figure 3.10. Spot test for the end point of shale CEC.

- **Calculation of shale CEC.** The cation exchange capacity of the shale is equal to the methylene blue capacity of the shale slurry, should be reported as meq/100gr and calculated as:

$$CEC = MBT = (ml \text{ of methylene blue}) / (ml \text{ of shale slurry}) \quad (5)$$

3.1.1.4. Shale porosity measurement. Porosity is another critical parameter for the characterization of shale reservoirs, as well as to determine the hydrocarbon content in place. Mathematically, porosity is defined as the open space or void volume of a porous

medium (sedimentary rock) with respect to the bulk volume of the rock sample. Likewise, the bulk or total volume (V_b) is equal to the sum of this pore volume (V_p) plus the grain volume (V_g) of the rock as stated in Equation (7) (Jenkins, 1960).

$$V_b = V_g + V_p \quad (6)$$

Measurement of any two of the three volumes allows for the calculation of the third, and subsequent determination of porosity usually expressed as a percentage of the total volume Equation (8). It is important to emphasize that ‘total porosity’ account for all pores in the rock sample, whether this are interconnected or isolated. Effective porosity includes only the interconnected ones. Only total porosity is considered in this research.

$$\phi = V_p/V_b * 100 \quad (7)$$

From a drilling perspective, the drilling fluid invasion into the shale formation is related to porosity. The rock-fluid interactions can affect the initial porosity, either by altering the clays structure content in the shale (dissolution, swelling or detachments) creating new fluid flow path or by destabilizing the wellbore wall through the opening of natural microfractures and weak bedding planes (Lal, 1999). Thus, the selection of proper plugging material is vital to reduce the rock-fluid interaction effects that can generate the shale porosity alterations that lead to wellbore complex situations.

- **Grain volume and grain density determination.** The gas expansion method based on Boyle’s Law is a non-destructive technique with reasonable accuracy (error of

$\pm 0.1-0.5\%$). The method uses an inert gas (Helium) at low pressures < 20 psi that can reach even the finest pores and eliminate any adsorption or surface chemistry problem with the rock (Jenkins, 1966). Figure 3.11 illustrates a representation of a pycnometer based on Boyle's Law.

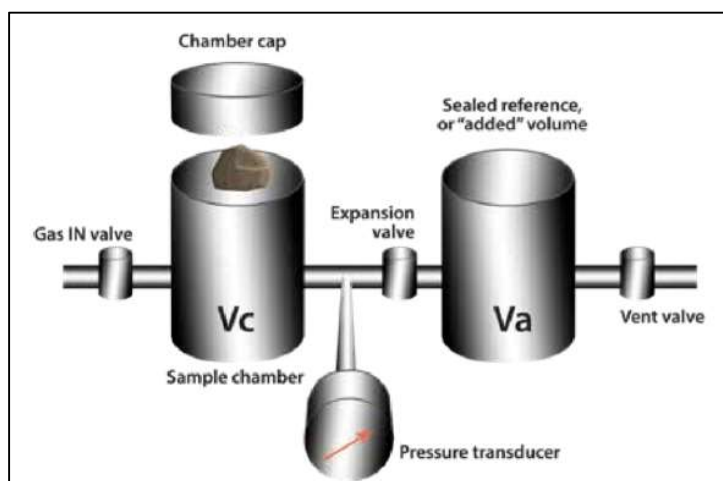


Figure 3.11. Pycnometer sketch.

The first step is to pressurize the sealed sample chamber of known volume with the displacement gas until the pressure stabilized, which means the gas reached the pore spaces. The second step is to open the expansion valve to allow the inert gas to expand to the reference chamber which volume is also known until reach the equilibrium in the entire system at some final pressure. The gas volume difference between the two chambers is a measure of the sample grain volume. For the purpose of this research, a Quantachrome Ultrapycnometer 1200e (Figure 3.12) located in the Engineering Research center was used. Its versatility to test 1'' OD rock cores reduce the error attached to crushed samples.

Moreover, the automatization process of the equipment reduces also the human error and allow to test the same core multiple times for reliability.



Figure 3.12. Ultracyc 1200e Missouri S&T.

• **Sample preparation and test procedure using Ultracyc 1200e.** Shale rock cores of 1-inch diameter were obtained by using a Hilti D220 Drill press with 1.25'' OD / 1'' ID core bit (Figure 3.13). Prior to run the test the core was cleaned and dried at 110 °C. After preparing the shale core, the grain volume test procedure using the Ultracyc 1200e can be summarized as follow:

- 1.) The weight of the 1-inch shale core sample was measured and record using an analytical balance with a resolution of ± 0.001 g precision.
- 2.) Medium cell size (50 cc) in which the 1-inch shale core can fit was selected and the shale core was placed inside the cell and carefully the cup was closed to avoid any gas leakages.

- 3.) Information related to the sample as name, weight, cell volume size, number of runs, and pressure target (18 psi) was introduced in the software as the input data before running the test.
- 4.) Helium tank valve connected to the Ultrapyc 1200e was opened and the run option was selected in the equipment menu. Before analysis, the equipment automatically set a period of time for purge the sample, this step conditioned the sample chamber by removing any contaminants or trapped air inside the cell chamber.
- 5.) After the sample purge, the instrument run the test automatically. Once the test finished the system provided a record of 3 different values for the shale core grain volume (cc) and grain density (g/cc) with its standard deviation.



Figure 3.13. Materials and core procedure.

- **Bulk volume and bulk density determination.** Bulk volume determination was obtained by gravimetric displacement method. The displacement methods are based on Archimedes principle and can be either gravimetric (change in weight) or volumetric (change in volume) measurements of the fluid displaced. Physically, this method observes the loss in weight of a sample of known air-dry weight once it is immersed in a fluid of known density. The difference between the air-dry weight and the immersed weight of the rock sample is then divided by the fluid density to obtain the bulk volume (V_b). It is important to avoid any surface contamination of the sample with the liquid used. Usually, the bulk volume (V_b) obtained through displacement methods yield to an error less than 0.5% (Jenkins, 1966). Figure 3.14. illustrate the setup for the displacement method.

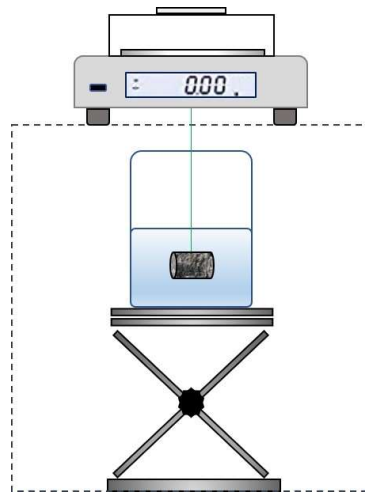


Figure 3.14. Displacement setup for bulk density and volume determination.

The following guide summarizes the steps to obtain the bulk volume for shale cores by applying the gravimetric displacement method:

- 1.) The weight of the hook clip and the plastic wire together, as well as the plastic wrap used to coat the shale sample, was recorded. Then the plastic wire was tied around the protected shale sample.
 - 2.) The air-dry weight of the shale sample was registered by using the hook option of the OHAUS Explorer Analytical balance (resolution of $\pm 0.001\text{g}$).
 - 3.) Distilled water with a density of 0.9982 g/cc ($25\text{ }^\circ\text{C}$) was used as the displaced fluid. a beaker of 400 ml volume capacity was filled with 300 ml of water. Then the beaker was placed on top of a laboratory tray and lifted until the sample was totally immersed in the fluid and the immersed weight was recorded.
 - 4.) The difference between the weights obtained in steps 2 and 3 was then divided by the water density (0.9982 g/cc) to obtain the bulk volume of the shale sample.
 - 5.) Bulk density was calculated in g/cc diving the air-dry weight by the bulk volume obtained in the previous step.
- **Total porosity calculation.** The difference between the bulk volume (V_b) obtained by the gravimetric displacement and the grain volume (V_g) registered with the Ultrapyc 1200e represents the pore volume (V_p) of the shale rock sample. applying equation (8) explained before, the Total porosity (ϕ) of the shale rock was calculated.

3.1.2. Nanoparticle Analysis Technique. The characterization of the nanomaterials for drilling applications allowed us to establish how stable the colloidal system will be. To accomplish this research task a group of tests was designed to characterize the NP based on aqueous stability test that can recreate the different environmental influences that might affect the colloidal system, the analysis of their surface

charge through zeta-potential measurements to understand their ability to keep dispersed in solution (Setia & et al, 2013).

3.1.2.1. NP aqueous stability test. The aqueous stability test is a simple and not expensive observation test that described qualitatively the ability of NPs to withstand different environmental influences such as variance in Ionic strength (e.g. brine formation, polymers, salts) or pH (connate formation water). This test is basically a sedimentation process naturally attached to the effect of gravity. The literature stated that gravity does not have a great effect on sedimentation of particles with a diameter less than 1 μ m. However, when the different surrounded conditions of the colloidal solution affect the nanoparticles, agglomeration of single NP can take place and thus, the particle cluster can destabilize the solution and settle down (Korada, 2017).

- 1.) Salt effects on NP stability were studied with 2 different inorganic salts, a monovalent salt (NaCl) and divalent salt (CaCl₂). The concentrations for NaCl were 0.5% - 1.5% and 3% by wt. In the case of the divalent salt, it is known that this type of salt has a greater impact on NP aggregation (Metin et al., 2011). Thus, a lower concentration of salt was selected, 0.1% 0.3% and 0.5% by wt.
- 2.) pH effect on NP stability was studied by observing how NP dispersions with same concentration were exposed from an acidic condition to an alkali condition, since pH changes can affect NP's double layer charge, increasing the attraction tendency (Metin et al., 2011). The pH range selected for this test was 2, 5, 8 and 10. Is important to mention that this alkali range was selected because usually, WBM as well as the conventional chemicals used have their best performance at this pH conditions.

• **Sample preparation.** The different scenarios of the aqueous stability test follow the same guidelines for sample preparation. Figure 3.15 illustrates the sample preparation and the steps are described below.



Figure 3.15. Sample preparation for aqueous stability test.

- 1.) The aqueous phase used in the solution preparation was deionized water with the density of 0.9982 g/cc. Colloidal solution was prepared by the addition of accurate amounts of specific Nanoparticle material to the aqueous phase in a concentration of 0.1% by wt.
- 2.) NP was weight with the help of weighing paper (non-stick) to reduce the loss of material. 150 ml of deionized water contained in a beaker was in continuous motion with a magnetic stirrer while adding the NP. Then, the colloidal solution was

ultrasonicated (> 40 kHz) for 60 minutes changing the water bath every 20 minutes to avoid evaporation of the NP solution and to assure that NP had been homogeneously dispersed.

- 3.) NP solution was then ready to transfer the desired volume to the test tubes. For this research flat bottom 3.3 borosilicate glass test tubes of 10 ml, volume capacity from Karter scientific was used. Each tube has a black phenolic screw top lined with rubber that resists the effects of temperature and steam. Disposal of the plastic pipette was used for every single tube to avoid cross-contamination.
- 4.) Once each test tube was filled with the NPs solution the sample preparation was ready and then each individual aqueous stability test took place.

• **Test procedure.** Below a detailed description of each aqueous stability test is explained.

Salt effect: Exact concentration of NaCl and CaCl₂ were weighted and added to a single tube contained the NP solution to test. Then, under static conditions, the effect of salt was registered with pictures in different periods of time (1 hour, 12 hours, 48 hours, 72 hours, and 168 hours).

pH effect: Sulfuric acid, H₂SO₄ for acid pH conditions and, potassium hydroxide, KOH for alkali conditions were used to adjust the different pH of each NP solution. 25 ml of the NP solution was poured into a 50 ml beaker and the pH was adjusted dropwise to the desired pH before filled the single 10 ml test tubes. Then under static conditions, the pH effect was registered with pictures in different periods of time (1 hour, 12 hours, 48 hours, 72 hours, and 168 hours).

3.1.2.2. NP Zeta-potential measurement. Zeta-potential measurements provide a method to evaluate the stability of a NP dispersion. Zeta-potential defines these interaction differences as an electrical potential existing between charged particles and the liquid medium that surround them (Chilingar, 2014). Figure 3.16 Illustrates schematically the Stern model association of charges and electrical potential distribution in the solid-liquid interface.

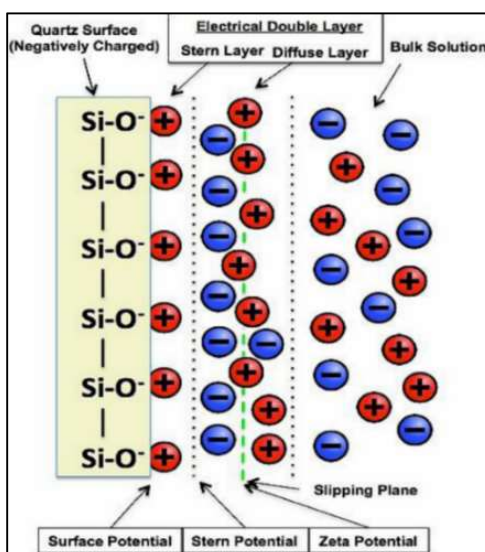


Figure 3.16. Stern model distribution in the solid-liquid interface (Hoxha, 2016).

The bulk solution has different ‘counter-ions’ (opposite in charge to the surface) or ‘co-ions’ (same charge as the surface) that experience attraction or repulsion respectively with the NP surface. In the very close proximity to the surface, the ‘counter-ions’ are strongly attracted to the oppositely charged surface trying to reach a charge balance with it and established an immobile layer across the entire surface, known as stern layer (non-diffuse part of the double layer model) (Chilingar, 2014).

As the distance from the particle surface continues to increase and goes beyond the stern layer some ‘counter-ions’ are still attracted while others are repelled by the stern layer, this further layer is known as the diffuse layer. The density of ‘counter-ions’ started to reduce as the distance from the surface increase until reaching the equilibrium in the bulk solution or liquid medium. On the other hand, the ‘co-ions’ experience a similar phenomenon. Inside the diffuse layer, there is a deficit of ‘co-ions’, because they have the same charge of the surface, so they are repelled. The repulsive force is then compensated due to the interaction with the ‘counter-ions’ inside the diffuse layer until the equilibrium is reached (Zeta-Meter Inc, 1997). The interface between the stern and the diffuse layer is also known as shear or slipping plane. The electric potential drop between this plane and the bulk solution is known as the Zeta-potential (Van Olphen, 1977). Figure 3.17 shows the different electrical potential distribution between each layer.

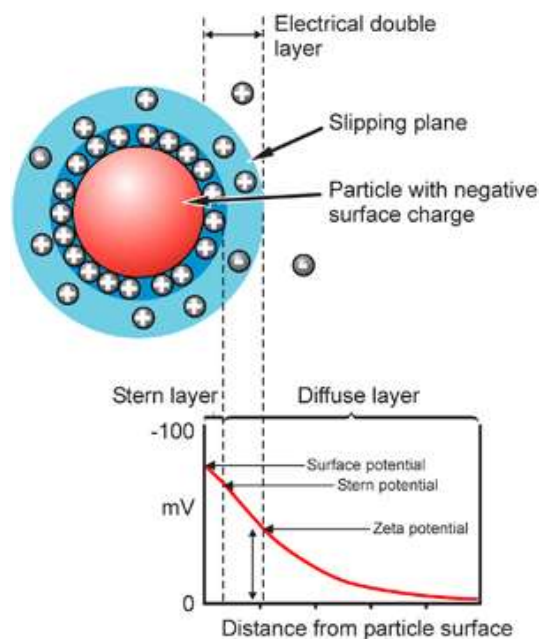


Figure 3.17. Schematic representation of zeta-potential (Malvern Technical Note).

• **Zeta-potential measurements via electrophoresis.** In the proximities of the NP surface electroosmotic process take place. When an electric field is applied to the dispersion, the charged particles will drag fluid with them towards the opposite electrode. The quantification of electrophoretic mobility of the nanoparticle in function of the distance from the opposite electrode is the process which makes possible to measure zeta-potentials (Myers, 1999). Equation 8 described the electrophoretic mobility (μ_e).

$$\mu_e = V/E \quad (8)$$

Where, V is particle velocity ($\mu\text{m}/\text{sec}$) and E is electric field strength (Volt/cm) both quantities known from the experimental setup to find zeta-potential. Once μ_e is found the zeta-potential (ζ) is calculated by solving Henry's equation (9) for ζ .

$$\mu_e = (2\varepsilon_r \varepsilon_0 \zeta f(Ka))/3\eta \quad (9)$$

Where μ_e , is electrophoretic mobility, ε_r , is relative permeability/dielectric constant, ε_0 , permittivity of vacuum, ζ , Zeta-potential, $f(Ka)$, Henry's function, η , viscosity at experimental temperature (Bhattacharjee, 2016).

• **Sample preparation.** The purity of the NP solution for zeta-potential measurements is the key to obtain reliable results. The water used in the sample preparation was ultra-pure deionized water (18 M Ω @ 25 °C). Disposal DTS1070 capillary zeta- cell cuvettes with electrodes on both ends were used for zeta-potential measurements for both,

silica oxide nanoparticles and graphene nanoplatelets. Figure 3.18 is a collage representation of the sample preparation.

The procedure for sample preparation is the same for both nanomaterials and is described below.

- 1.) NP concentration of 0.1mg/ml was selected based on guidelines stated in Malvern Zetasizer user manual (2013).
- 2.) 100 ml of deionized water was added to a 200 ml beaker and the NPs concentration selected in step 1 were weighted. Then, NP was mixed with the water with using a magnetic stirrer. pH of the solution was then measured and recorded.
- 3.) The NP dispersion was allowed to stand overnight (12 Hrs.). Then carefully with the help of disposal plastic pipettes, the supernatant (Top layer of NPs solution) was collected and transfer to 10 ml borosilicate tubes.
- 4.) Glass tubes filled with the NP solution were exposed to ultra-sonication (> 40 kHz) for 30 minutes before the test.
- 5.) The NP solution was then collected with a clean syringe and the capillary Malvern zeta-cell was filled according to Malvern guideline user manual (2013). Is important to check that the cell is free of bubbles before inserting it into the equipment.

• **Test procedure.** NP zeta-potential was performed with the Malvern Zetasizer NANO ZS equipment located in the Mining & Nuclear Engineering laboratory of Dr. Lana Alagha. The equipment measured the electrophoretic mobility of the NP based on a combination of Laser Doppler velocimetry and phase analysis light scattering (PALS)

technique (Bhattacharjee, 2016; Corbett, 2012). Figure 3.19 shows a picture of the Zetasizer Nano ZS.

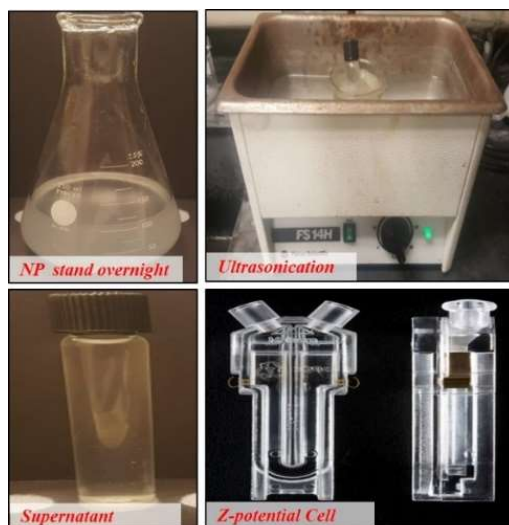


Figure 3.18. Zeta-potential sample preparation.

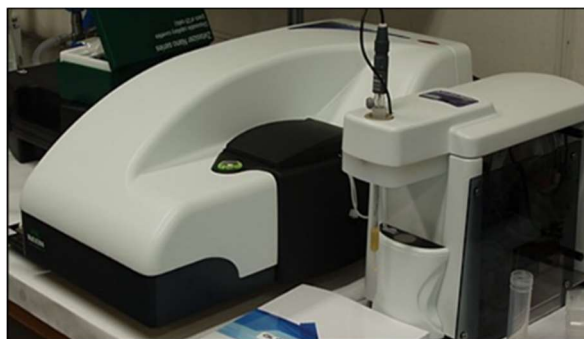


Figure 3.19. Zetasizer nano (Malvern) Missouri S&T.

Internally, a laser beam is divided in two and while one hit the NP in the dispersed solution the other is kept as a reference. Then both laser beams are combined again and quantify the difference in wave frequency (Doppler effect). The velocity on the

nanoparticle is then deduced from this difference and at the end calculate electrophoretic mobility of the nanoparticles and consequently their ζ - potential (Corbett, 2012). The procedure followed to run the test was based on Malvern guideline user manual (2013). A summary is described below:

- 1.) The instrument was switched on 30 minutes before starting the measurement to warm up the laser. A standard solution was run first to validate the data generated with the instrument prior to testing NP solutions.
- 2.) Then, the conditions of the zeta-cell that contained the NPs solution was checked confirming that the electrodes were completely immersed in the NPs solution. The zeta-cell was inserted into the instrument with the Malvern logo oriented towards the front of the instrument.
- 3.) All the input data was reviewed in the software for zeta-potential measurements based and the runs were performed. The instrument performed 3 measurements automatically and the zeta-potential values are recorded and a graphic generated for each NP solution.

3.1.3. NP-WBM and KCL/PHPA WBM Analysis Technique. Drilling fluids are one major component in the success of Oil & Gas drilling operations. Evaluation of all key parameters associated to each specific reservoir should support the correct design of drilling fluid and the costs associated to it. The first part of this section describes the nanomaterials and conventional chemicals used in this research and then define the considerations needed to design and mix a NP-WBM. The second part related the wellbore stability through tests that described the fluid invasions and cutting integrity issues, while the formation damage was analyzed considering the chemical interaction between the

drilling fluids and the shale rock, thus, the tests were oriented to examine the shale water absorption and its consequences.

To accomplish this task, the tests to characterize WBM were grouped into two categories. First, the standardized test category based on the API recommended practices ‘Bulletin RP 13B-1’ to evaluate density, pH, rheology, and static filtration (LTLP and HTHP). The second category provided information about chemical interaction previously mentioned, for the scope of this research the tests that compose this category were the Cutting dispersion test, visual swelling analysis, and bulk swelling test. The laboratory analysis was conducted for 2 different fluids, the new NP-WBM proposed and the conventional KCL/PHPA water-based drilling fluid. Finally, dynamic aging tests (150 °F, 200 °F, 250 °F) was selected to evaluate the impact of temperature on each drilling fluid, in terms of rheology and filtration capabilities.

3.1.3.1. Drilling fluid compositions. The inclusion of nanomaterials in WBM is becoming an important research topic in the pursuit of high-performance drilling fluids capable to control the interaction between WBM and sensitive shale formations as documented in chapter 2. In this work, 2 different nanoparticles were selected, spherical silica oxide nanoparticles, and graphene nanoplatelets. The main advantage of this nanomaterials resides in their size, which can fit the nanopores and microfractures presented in the shale formations respectively.

Conventional additives and LCM were used to design the base fluid to which the NP solutions were later added. The intention to mix conventional additives with the NP was to reduce costs and to evaluate the belief that NP thermal conductivity can ‘shield’ other products in the drilling fluid reducing the premature degradation at high temperatures.

This work also includes the mixing and further analysis of a conventional KCL/PHPA WBM which has been used for years in the industry to drill problematic shale formations (Caen and Chilingar 1996). The results of the KCL/PHPA WBM were then used as a reference to compare and evaluate the performance of the new NP-WBM proposed.

- **Conventional materials.** Deionized water was used as a carrier fluid for the NP-WBM and distilled water for the KCL/PHPA. The reason behind this was to reduce any effect on the surface of the NP that could affect their stability. The conventional chemicals used are shown in table 3.1.

Table 3.1. Conventional additives used in WBM.

Product	Company	Function
Bentonite, Premium Gel	CETCO Drilling fluids	Viscosity/filtrate
Xantham Gum, Kelzan	CP KELCO	Improve rheology
Pre-gelled Starch	Unidentified	Filtrate reduction
PAC – LV	Newpark Drilling fluids	Filtrate Reduction
KCL (99%) purity	Alfa Aesar	control shale hydration
KOH (85%) purity, flakes	Alfa Aesar	to adjust pH
PHPA, Hyperdrill AE853	SNF INC	Reduce cutting dispersion

Also, table 3.2 and 3.3 present the formulation for the Base fluid for the NP-WBM and for the KCL/PHPA WBM, respectively.

Table 3.2. Base fluid for the NP-WBM formulation.

BASE FLUID NP-WBM FORMULATION	
PRODUCT	CONCENTRATION
Bentonite	10 ppb
Xantham Gum	0.25 ppb
Pre-gelled Starch	1.85 ppb
PAC – LV	1.85 ppb

Table 3.3. KCL/PHPA formulation.

KCL/PHPA FORMULATION	
PRODUCT	CONCENTRATION
Bentonite	10 ppb
Xantham Gum	0.75 ppb
Pre-gelled Starch	3 ppb
PAC – LV	1.5 ppb
KCL	7 % wt.
KOH	Needed to raise pH to 9.5
PHPA	0.5% vol.

• **LCM material.** Graphite was selected as a conventional LCM for the new NP-WBM. Since decades the graphite has been identified as a powerful wellbore strengthening agent with minimal affectation in the drilling fluid rheology (Aston, 2007; Contreras, 2014; Goud, 2006). Different concentrations (0.5%, 1.25 %, and 2 % by wt.) were mixed with the basic fluid (table 3.2) the NP-WBM to established the optimum concentration. Examining the graphite performance in the WBM together with NP can support the belief

of a possible synergetic effect between both materials to improve the performance of WBM applied to unconventional shales as will be addressed in upcoming chapters. Figure 3.20 shows the graphite used and table 3.4 its properties.



Figure 3.20. Conventional LCM graphite.

Table 3.4. Graphite properties (courtesy of Asbury Graphite Mills, Inc).

Graphite properties	
Carbon	99.85 %
Ash	0.15% Max.
Moisture	1.16 % Max

- **Silica oxide (SiO₂) NP.** Silicon oxide also known as silica, consists of two atoms of oxygen with a silicon atom having a molecular formula of SiO₂. NP of silica are highly stable, less toxic, and can work effectively in the presence of other molecules. The already optimized and efficient production method allows it to have competitive and affordable prices compare to other nanoparticles (Cademartri & Geoffrey, 2009).

Silica NP is divided into p-type and s-type particle on the basis of their structure. P-type is a porous type, while s-type is spherical non-porous. The area of application of nano silica is very vast. Some of them include plastics, paints, rubber, batteries, adhesives, concrete, fiber, thermal insulators, humidity sensors, electronic substrates, electrical insulators, etc. In the oil & gas industry, its application has been evaluated in different fields (Fakoya, 2017). For this research, s-type silica nanoparticles with no further surface treatment were selected. Figure 3.21 shows an image of nano silica obtained from scanning electron microscopy (SEM) courtesy of the company. Table 3.5 presents the characteristics of the silica NP selected.

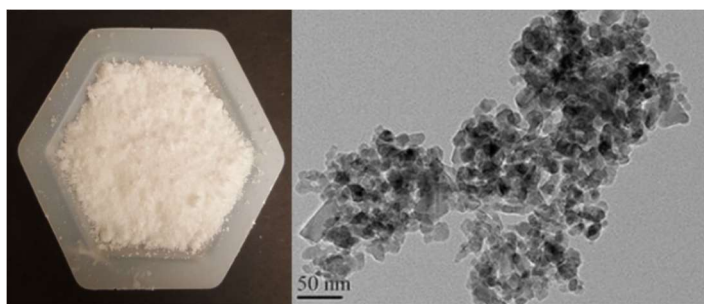


Figure 3.21. SEM image of silica NP (courtesy of US Research Nanomaterials Inc.).

Table 3.5. Silica nanoparticle properties (courtesy of US Research Nanomaterials Inc.).

Silica NP Properties	
Form	Powder
Purity	99.5%
Shape and size	Spherical, non-porous 15 -20 nm
Density	0.1 g/cm ³

- **Graphene oxide (GO) nanoplatelets.** Graphene is defined as a two-dimensional (2D) tightly and thin nanoplatelet consisting of carbon atoms connected with each other in a hexagonal structure. At the atomic scale, the graphene structure looks like a 2D honeycomb lattice. This nanomaterial was studied theoretically back in the 40's and it was not until 1987 that was officially known as graphene.

In 2004, the extraction method of graphene monolayers with a thickness of a few nanometers was established. This achievement represented Nobel prize in physics in 2010 to Andre Geim and Kostya Novoselov and since that time many organizations started to design the best technique to make this 2D nanomaterial commercially available (Taha, 2015). Along with its unique structure, graphene possesses a range of amazing and unusual properties: most notably, the thermal conductivity (3080-5150 W/mK, melting point 4510K), mechanical properties (tensile strength of 130 gigapascals, young modulus of 1 TPa), and electronic properties (Chatterjee et al., 2012; Geng, 2009; Singh et al., 2011).

There have been few investigations in the Oil & Gas industry documented. Recently its application has been evaluated in well cementing (Peyvandi, 2017) and in drilling fluids (Kosynkin et al., 2012; Taha, 2015). The key to introducing graphene to drilling fluids application for unconventional shale reservoirs relies on its ability to form impermeable membranes. Some studies suggested that graphene nanoplatelets can act as an impermeable barrier even to helium gas (Bunch et al., 2008). The latter makes graphene nanoplatelets a great candidate as a bridging agent to plug microfractures. Figure 3.22 shows SEM images of the graphene nanoplatelets used for this work courtesy of the company. Table. 3.6 presents the characteristics of the graphene NP.

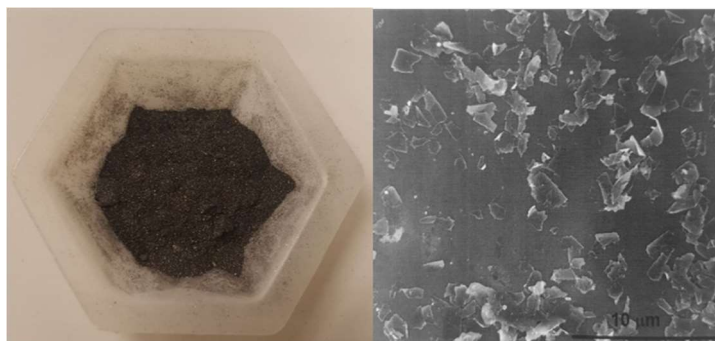


Figure 3.22. SEM image of graphene NP (Courtesy of Nanographene Inc.).

Table 3.6. Graphene nanoparticle properties (Courtesy of Nanographene Inc.).

Graphene Nanoplatelets Properties	
Form	Powder
Purity	99.8%
Shape and size	Flakes 1.3 – 2.3 μm / Thickness < 3 nm
Density	0.13g/cm ³

3.1.3.2. Concentration limits for LCM and NP material. The maximum level of graphite was selected based on previous work that performed precipitation tests for graphite mixed in OBM (Contreras, 2014) as well as literature with real cases where graphite was used as a sealing agent in SBM drilling fluids (Goud, 2006). The first study found that graphite concentration above 2% by wt. can experience severe precipitation within the first 24 hrs. On the other hand, real cases implemented a maximum graphite concentration of 7 ppb to achieve wellbore strengthening, a concentration that is equivalent to the 2% by wt. The upper limit concentration for graphite in this research was then set as 2% by wt.

In the case of Silica NP researchers have been divided into two major groups. The first group has been using concentration above 5% by wt. in some cases as high as 10% or 30%. (Sensoy 2009, Cai 2012, Sharma 2012, Kang, 2016) Firstly, this concentration is costly and second difficult to upscale to real field trials. On the other hand, the second group has focused their research on the low concentration range (< 3% by wt.) (Boul, 2016; Fakoya, 2014; Mahmoud et al., 2018; Salih, 2016).

This work used the minimum NP concentration possible avoiding the inclusion of surfactants or special surface treatments that can increase the WBM cost. The same criteria were applied to graphene nanoplatelets. Previous studies conducted for the graphene nanoplatelets indicated that concentration above 4g/L (0.4%by wt.) can generate rheological problems to the WBM (Kosynkin, et al 2011).

3.1.3.3. NP-WBM preparation procedure. The NP-WBM mixing was divided into two steps. In the first step, the base drilling fluid prepared was mixed based on the pre-determined concentration in table 3.2. In the second step, the NP solutions were prepared and mixed with the base drilling fluid. There were few considerations for the mixing of the base drilling fluid.

- 1.) Volumes in the laboratory follow the concept that 350 ml of water correspond to 1 barrel at fields scale and concentration in pounds (field scale) are equal to grams at lab scale. The procedure described was used to prepare 925 ml (2.64 eq-barrel) of NP-WBM.
- 2.) The Wyoming Bentonite was added to 625 ml of deionized water and the pH of the was adjusted with KOH to 9.5 then the mixture was allowed to hydrate for 12 Hrs.

- 3.) After the hydration period, the other chemicals were added slowly to avoid the creation of ‘eye fish’ and was stirred for 10 minutes before adding the next product. This drilling fluid was named **Basic A**.
- 4.) In the last step, the selected concentration of graphite (LCM) based on individual test results was mixed with the Basic A fluid. The final slurry was stirred for an additional 20 minutes after adjusted pH to 9.5. Figure 3.23 presents the equipment used to prepare and mix the drilling fluid. KCL/PHPA drilling fluid was mixed using the same equipment and the concentrations described in Table 3.3.



Figure 3.23. Equipment used to prepare and mix the basic A fluid.

Preparation of silica NP and graphene NP solutions were carried individually to avoid cross-contamination. Below a summarized of the steps are described.

- 1.) NP was weighted using high-resolution balance ($\pm 0.0001\text{g}$) (clay lab) based on the desired concentration using non-absorbent weighting paper.
- 2.) 250 ml Erlenmeyer flask was filled with 150 ml of deionized water and a polymeric base with Xhantam gum was prepared with a magnetic stirrer. Then the NP weighted in step 1 was added slowly.

- 3.) NP dispersion was mixed at a high shear rate (22000 RPM) using a Hamilton Beach mixer for 15 minutes to help break large aggregates if present.
- 4.) NP dispersion was then covered with aluminum foil to avoid evaporation of the solution. Ultra-sonication was carried out at 40 kHz for 60 minutes using FS14H fisher scientific sonic bath. The water bath was changed every 20 minutes to avoid over-heated of the NP solution.
- 5.) Silica and Graphene NP solutions were mixed and stirred together with the same conditions used in step 3 for a period of 15 minutes. At the same time, the Basic A drilling fluid was stirred for the same period of time.
- 6.) Basic A drilling fluid was then added to the NP dispersion while mixing at a high shear rate (22000RPM) using a 100 ml Bstean plastic-steel syringe pump. The final NP-WBM was then stirred for an additional 20 minutes and the pH was adjusted with KOH to 9.5 if needed before any further characterization. Figure 3.24 shows the equipment used to prepare the NP solution and further mix with the Basic A fluid.

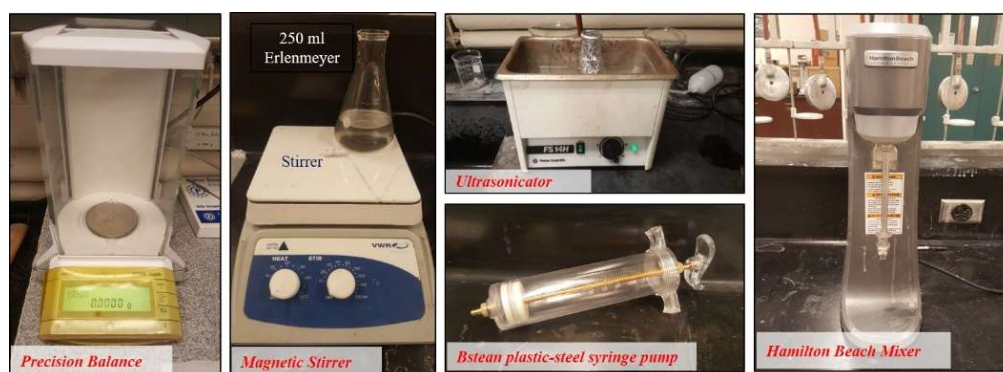


Figure 3.24. Equipment used to prepare and mix NP dispersion.

3.1.3.4. NP-WBM screening criteria. The NP-WBM screening criteria was design based on the limited concentration established previously. In the first stage of the screening criteria, different concentration of these particles was mixed with the Basic A drilling fluid individually. The best two performances of each nanomaterial were selected for the second stage. Table 3.7 presents the screening criteria design for the NP-WBM.

Table 3.7. Screening criteria design for the NP-WBM.

Screening Criteria Design for NP-WBM								
Silica Oxide Nanoparticle					Graphene Oxide Nanoplatelets			
NP [] %wt.	0.10%	0.25%	0.50%	1.00%	NP [] %wt.	0.10%	0.25%	0.40% 0.75%
Fluid Name	B	C	D	E	Fluid Name	G1	G2	G3 G4

During the second stage of the screening selection, the best two concentration of silica nanoparticles were mixed with the best two concentration of graphene nanoplatelets. From these 4 options, the best performance was selected as the new NP-WBM. In the following chapters, the best design will be analyzed and compared with the KCL/PHPA fluid.

3.1.3.5. API standard test evaluation. The standardized category is based on the “API recommended practice for field testing water-based drilling fluids 13 B-1”. The data obtained from each test provided the following characteristics of the drilling fluid system

tested: Drilling fluid density, pH, Rheology properties and static filtration both, LTLP and HTHP.

- **Density measurement.** The density of a drilling fluid is related to the total mass of the system both, liquid, and solids in a constant volume of the cup in the mud balance see Figure 3.25. The fluid density helps to control formation pressure and promotes the support of the wellbore wall if properly designed.



Figure 3.25. Mud balance instrument Missouri S&T.

For the scope of this research, the units for the fluid density used was lb /gal or ppg. The calibration of the balance was performed with fresh water at 70 °F adjusting the counterweight until the sliding-weight rider was 8.34 ppg. The correct weight was then determined when the level-bubble was centered and kept balance. The accuracy of the balance is within 0.1 ppg.

- **pH measurement.** pH measurements of the drilling fluids are an important property to control the drilling fluid performance. Basically, the pH of a drilling fluid measures the concentration of hydrogen ions in the fluid, $[H^+]$. For each individual concentration of hydrogen ions $[H^+]$ in the solution, there is an equivalent hydroxyl ion concentration $[OH^-]$ to preserve the equilibrium. The $[H^+]$ describes the acid component of

the solution while $[\text{OH}^-]$ the alkaline or basic section of the same system. For pure fresh water at 75 °F the concentration of $[\text{H}^+]$ and $[\text{OH}^-]$ are exactly the same, $[\text{H}^+] = [\text{OH}^-] = 1.0 \times 10^{-7}$ or which is the same a pH value of 7 (neutral pH). The first step to determine the pH of the drilling fluid was to calibrate the pH probe. a buffer solution with known pH (4, 7 and 10) was used for this process (Figure 3.26) following the manual of the eco-test pH2 equipment.



Figure 3.26. pH meter and buffer solutions. Missouri S&T.

Once calibrated, the pH meter was placed inside the drilling fluid at room temperature (75 ° F \pm 5 °F) until the pH reading stabilized at the same temperature. 3 different reading was performed for each fluid and the value was reordered to nearest 0.1 pH.

- **Rheology and gel strength test.** Rheological characteristics and drilling fluid gel strength properties provide vital information about the drilling fluid capacity to transport cuttings and also to suspend the same cuttings in the fluid column at static conditions. To determine the rheology behavior and gel strength of the drilling fluids under this research

an OFITE Viscometer model 800 was used (Figure 3.27). This viscometer has 8 different speeds 3, 6, 30, 60, 100, 200, 300, and 600 RPM.



Figure 3.27. 8-speed OFITE viscometer. Missouri S&T.

From the dial values collected for each shear rate, three values were obtained Plastic viscosity (PV), yield point (YP) and the gel strengths, which was measured at 3 different periods of time (10 sec, 10 min, and 30 min). The procedure followed to measure the rheology (PV, YP) and gel strength is described below:

- 1.) The test cup was filled with the desired drilling fluid up to the scribed line.
- 2.) The leg lock nut was loosed and the cup containing the drilling fluid was raised to the viscometer assembly until the scribed line indicated in the rotor sleeve.
- 3.) Once in position, the leg lock nut was tightening to secure the mud cup in place.

The viscometer was then started at 600 RPM until a steady value was reached in the indicator dial. The value was a record and the same procedure was repeated with the other 7 speeds recording the value for each shear rate.

- 4.) For the gel strength measurements, the drilling fluid was stirred at 600 RPM for 10 seconds. The viscometer was then stopped and kept undisturbed for 10 seconds, the viscometer was then initiated at 3 RPM and the maximum value reached in the dial was recorded as initial gel strength. The value was recorded in pascals and lb/100ft².
- 5.) The 10 min and 30 min gel strength were measured repeating the step 4. The drilling fluid was stirred for 10 seconds at 600 RPM then was stopped and the fluid was undisturbed for the period of time needed. Then the viscometer was then started at 3 RPM and the maximum values in the dial reading were recorded. The tests were performed at standard 120 °F.

• **Rheology calculations.** The plastic viscosity (PV), represents the resistance of the fluid to flow due to the internal mechanical conditions (Solids) inside the system. That resistance is most commonly affected by the solid concentration, size and shape and their relationship with the viscosity of the fluid phase in the system. It was calculated subtracting the 300 RPM dial reading from the 600 RPM,

$$PV = \theta_{300} - \theta_{600} \quad (10)$$

The yield point (YP) is based on the electrochemical interaction between the additives and the other solids present in the mud system while drilling (solids, clays). Also, gives an idea about the drilling fluid ability to carry or transport the drill cuttings to the surface. YP was calculated by subtracting the PV value from the 300 RPM dial reading,

$$YP = \theta_{300} - PV \quad (11)$$

- **Static drilling fluid filtration test.** There are two types of filtration test, static and dynamic. The first is experienced when the fluid is not in motion in the wellbore while the dynamic intent to replicate the condition when the drilling fluid is circulating in the wellbore. For the scope of this research, the Static filtrate was tested at LTLP and HTHP conditions.

- **Standard API filtration test.** The API test was run at room temperature and 100 PSI using a cylindrical press that contains the drilling fluid, see Figure 3.28. A filter paper (Whitman # 50, 3 ½” diameter) with 2.7 um particle retention was placed at the bottom of the cell. Then, the drilling fluid under test was poured into the cell within ½ inch from the top. The relieve valve was closed and the pressure was raised to 100 psi. The filtrate was collected in a graduated cylinder (10ml or 25 ml) located below the drain tube. The test was run for 30 minutes and the filtrate volume collected was recorded every 2 minutes and reported to the nearest 0.1 ml. After disassembling the cell, the filter cake was carefully washed, and its thickness was measured with a Vernier caliper to the nearest millimeter.



Figure 3.28. API LTLF filtrate press. Missouri S&T.

• **Static HTHP filtration test.** The HTHP test consists of a special cell with controlled pressure source of CO₂ with regulators with working pressures between 600 psi to 1300 psi, a heat jacket to adjust and a bottom pressurized collection cell for back-pressure to prevent the evaporation or flashing of the filtrate generated during the test. The filtrate medium can be filter paper (3 ½ inches - Whatman # 50 for temperatures up to 400 °F). The HTHP cell equipment is shown in Figure 3.29.



Figure 3.29. HTHP filtrate press. Missouri S&T.

The HTHP test was run under the following conditions: a differential pressure of 500 psi (600 psi above and 100 psi in the back-pressure cell) and 250 °F. The drilling fluid was stirred with a Hamilton beach mixer for 10 minutes before the test. First, the heating jacket was preheated at 250 °F ± 10°F for 30 minutes. Then the stirred drilling fluid was poured into the cell filled up to 0.6 inches from the top and the filter paper was installed, and the cell was closed.

Then, the pressure was set at 100 psi on both regulators and then the top stem valve was open to pressurize the drilling fluid until the 250 °F was stabilized in the thermometer connected to the cell. After 1 hour the pressure at the top regulator was increased to 600 psi while the bottom was conserved at 100 psi generating a 500-psi differential pressure. The bottom valve was open, and the filtrate volume was collected for 30 minutes in a graduated cylinder of 10 ml.

The area of the filter paper in the HTHP is half the area of the standard API LTLP filter paper, for this reason, the final filtrate volume collected in the HTHP test after 30 minutes was doubled to report as API loss. After the test, the filter cake was recovered, and its thickness measured with a Vernier caliper to the nearest millimeter.

To calculate the spurt loss of a drilling fluid the data from the filtration tests is plot vs. \sqrt{t} (square root of time) and extrapolate the result to zero to obtain the numerical value (Bourgoyne et al. Applied drilling engineering, SPE Textbook series, vol 2, 1986). Figure 3.30.

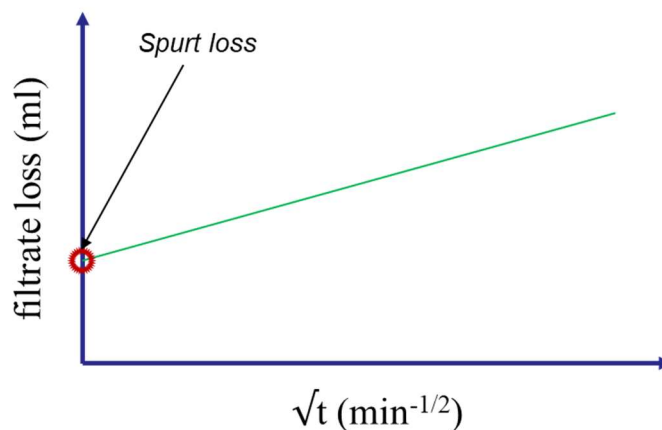


Figure 3.30. Graphical representation of spurt loss.

The other method is to calculate the spurt loss based on the following (Ofite HTHP instruction manual, 2017):

$$V_s = 2[V_{7.5} - (V_{30} - V_{7.5})] = 2(2V_{7.5} - V_{30}) = 4V_{7.5} - 2V_{30} \quad (12)$$

Where, V_s is spurt loss volume, $V_{7.5}$ filtrate volume collected after 7.5 minutes (doubled for HTHP), and V_{30} filtrate volume collected after 30 minutes (doubled for HTHP). Temperature and pressure can affect the behavior of polymers and chemical additives reducing the overall performance of the filter-cake build-up process. Thus, drilling fluids should be tested preferably at HTHP conditions.

3.1.3.6. Drilling fluid-formation chemical interaction tests. This second category of tests was designed to evaluate the ability of the drilling fluids to ‘shield’ the cutting and shale cores against the effects of water interactions that can cause swelling or sloughing effects. Bulk swelling test and dispersion test were selected in this research to test the protection capability of the NP-WBM and KCL/PHPA. The third test of this category is a visual analysis of small shale slabs exposed to drilling fluids to investigate how temperature and time affect the drilling fluid’s ability to control the opening of microfracture.

- **Cutting dispersion test.** The dispersion test provides a direct measurement of cuttings disintegration tendency. The test was performed with shale cuttings that passed through a # 5 mesh but were retained on a # 10 sieve. 25-30 grams of shale cuttings were added to 350 ml of the drilling fluid in an aging cell and then put inside the hot rolling oven (30RPM) Figure 3.31. For 16 Hrs. a 150 °F. The mass of shale retained in a # 35 sieve after the hot rolling was then compared with the initial mass and then the % of cutting

dispersion in the drilling fluid was calculated (Equation 13). Shale samples need to be complete dried before weight-balance after the hot roll process (Deville, 2011).



Figure 3.31. Cutting dispersion test.

$$\text{dispersion, \%} = \frac{\text{Initial mass of shale} - \text{recovered mass of shale}}{\text{Initial mass of shale}} * 100\% \quad (13)$$

- **Visual swelling analysis.** When shale formation interacts with WBM a degree of water absorption into the clay structure can take place. The severity of this phenomenon can overcome the internal stresses of the clay structure creating new microfractures or open natural microfractures present in the shale. To study this interaction a simple visual test was designed to determine if natural or new microfractures were created after exposing shale slabs for 14 days at 150 ° F. Deionized water was used as a blank fluid.

- **Sample preparation and test procedure.** A rectangular shale slab was cut from a 1- inch shale core using a slow diamond saw. Then, the shale piece was ultrasonicated

for 5 minutes and pictures of the shale initial conditions were taken using a Hirox optical digital microscope. The drilling fluid to be tested was poured in a 500 ml beaker and the oven was pre-heated to 150° F. Once the temperature was uniform the shale piece was immersed in the drilling fluid and the beaker was placed inside the oven. The beaker was continuously filled with drilling fluid to avoid extreme evaporation of the drilling fluid. The conditions of the shale sample were registered with the optical microscope after 7 and 14 days.

- **Bulk swelling test.** The bulk swelling test investigates the interactions effect of WBM on the shale rock during static conditions. The increase of shale volume due to the water absorption phenomenon into the clay structure is measured for 24 Hrs. The test is based on the Archimedes principle, and during the period of the test, several measurements of the shale sample, both immersed and air weights are collected to investigate the swelling behavior as a result of interacting with the drilling fluids.

- **Test equipment.** Figure 3.32 illustrates the equipment required for the experimental setup. A high resolution (0.001g) weight-balance with a hook option was used to take the measurements of the shale sample. A thin but strong plastic wire was used to hold to the sample and attached it to a clip that was used as a hook. 400 ml beaker containing the drilling fluid and a jack-up metal laboratory tray to raise or lower the beaker level respect to the suspended shale sample was implemented. It was important to zero the weight-balance to eliminated the plastic wire weight, hook (clip) weight, and just read the sample weight.

Also, the drilling fluid created a wet film in the sample, the weight of the wet film was subtracted from the air measurements to provide accuracy to the test, so just the volume

that is absorbed by the shale sample was read. A hair dryer was used to accelerate the drying process of the shale sample to measure the air-dry weight in each period.

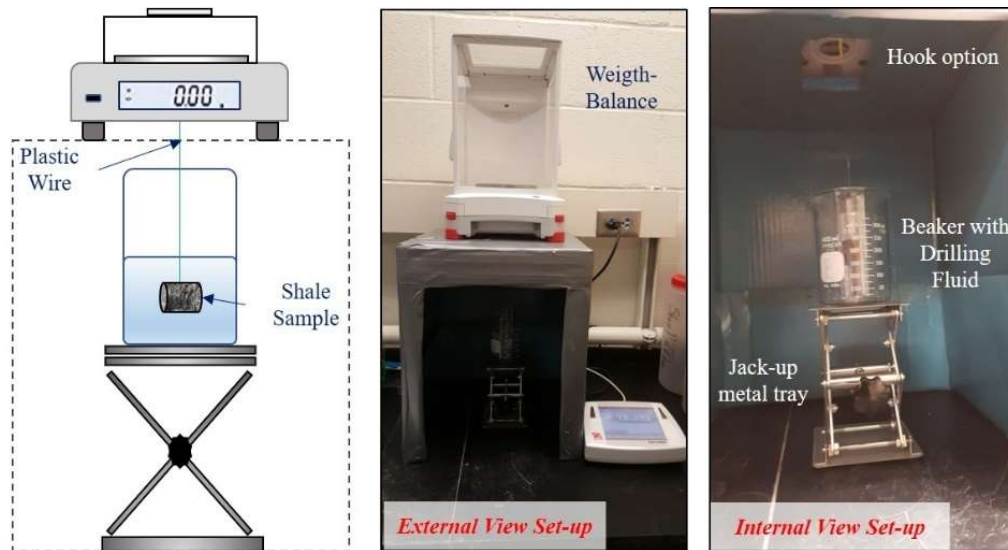


Figure 3.32. Experimental set-up for the bulk swelling test.

- **Test procedure.** The following procedure was adopted to perform the bulk swelling test:

- 1.) The plastic wire was tied to the paper clip and then attached to the hook located in the bottom of the weight balance. The weight of both wire and clip was registered.
- 2.) A fresh and clean shale sample was gently tied to the plastic wire and left suspended in air until the weight balance reading was stable. The initial air-dry weight was measured.
- 3.) The jack-up metal tray that holds the beaker full of drilling fluid was raised until the shale sample was totally immersed, and the initial immersed weight was registered. Then, the shale sample was immediately raised out of the fluid to

measure the weight of the initial wet condition. This value was subtracted for the air-dry weight to measure the weight of the wetting film. This value was reordered for each stage during the 24 Hrs.

- 4.) The last 2 steps were repeated to obtain the shale's air-dry and immersed weights for different immersion periods, 5, 15, 30, 60, 120, 180, 240, 720, and 1440 minutes. The increments in the volume of the shale sample due to the interactions with the drilling fluid were then calculated based on the Archimedes principle Equation (14).

$$\text{Volume} = (W_{\text{Dry}} - W_{\text{Immersed}}) / \rho_{\text{Mud}} \quad (14)$$

3.1.3.7. Dynamic aging test of WBM. The aging period can be set for several hours (usually 16 Hrs.) or days and can be performed either at ambient temperature or elevated temperatures depending on the objective of the test. The objective to include this test was to evaluate the ability of NP-WBM to withstand the effect of aging under elevated temperatures (150 °F, 200 °F, 250 °F) and its impact in its rheological and filtration behavior. The results were then compared with the impacts experienced in the conventional KCL/PHPA drilling fluid.

- **Test equipment.** 1000 ml Pyrex jar with temperature resistance up to 180 °C (356°F) and metallic aging cells with a capacity of 500 ml were used for dynamic aging and an oven with a maximum temperature of 400°F with the rolling option to simulated dynamic conditions of the drilling fluid.

• **Test procedure.** The guidelines to perform the dynamic aging followed the API standard procedure for laboratory testing drilling fluids (API RP 13-I, 2000). A summarize steps of the procedure are described below:

- 1.) The desired drilling fluid to test was poured into the aging cell leaving approximately 1 inch of empty space at the top. Next, the aging cell was closed.
- 2.) The roller oven was turned on and set on the required temperature. Enough time was allowed until the roller oven reached a uniform temperature.
- 3.) Once the temperature was reached, the aging cells were put on the rollers
- 4.) For dynamic aging, the roller power switch was set to the “On” position. This point was done to simulate the circulation condition of WBM downhole.
- 5.) After 16 Hrs. the oven was turned off and the aging cells were allowed to cool down to room temperature in a freshwater bath. After cooling down, the drilling fluid was extracted from the aging cells and stirred it in the mechanical mixer for 15 minutes to homogenize the sample.
- 6.) API standardized test describes previously in this chapter were performed to evaluate the rheology and filtration properties of the aged WBM.

3.2. RHEOLOGICAL MODEL OF THE NP-WBM

A rheological model describes the relationship between the shear stress and the shear rate. Most of the rheological models use in the industry were explained in section 2 and among all of them, the Hershel-Bulkley model (Equation 4) is the preferable method to evaluate drilling fluids. This model was considered in this research to analyze the NP-WBM and the influences of the NP on its rheological properties.

The initial step recorded all the data obtained with the rheological measurements at a defined temperature. then, an excel sheet was created for the Herschel-Bulkley model and the data were used as input to feed the model. The least square method was used to generate an approximate solution for the constants n , and K as well as to estimate the yield stress. Regression coefficient (R^2) and the sum of square errors were used to evaluate the fit between the calculated and the experimental data.

The method and process described were applied to the rheological measurements of each aging conditions of the NP-WBM. It helped to better understand how NP can influence the evolution and stability of the rheological properties of NP-WBM when it is exposed to high temperatures. Finally, the modeling results of both, NP-WBM and KCL/PHPA were used to compare the viscosity profile of each model.

4. RESULTS & DISCUSSION

Initially, the experimental analysis described the evaluation of the Woodford shale and registered the main characteristics of the rock, as mineral composition, porosity, pore size distribution. Based on the rock characterization the nanomaterials were selected and their characterization was evaluated to test their stability as a potential additive for WBM. Finally, the base drilling fluid, mostly water, and conventional additives were analyzed to understand the nature of the fluid loss and rheology, and later compared the behavior of the fluid when the NP were added to it. Needless to say, that low concentration were targeted to avoid the use of surfactants or surface treatments as well as to study large-application scale. In all cases, the NP-WBM were compared to the corresponding control sample and to the conventional KCL/PHPA. The characteristics of the drilling fluids were evaluated by the standardized API category, the chemical interactions tests and the aging tests as described in section 3.

4.1. WOODFORD SHALE CHARACTERIZATION

The Woodford shale was used for this research. Woodford shale is a late Devonian-early Mississippian, marine shale (Gupta, 2013). The sample was obtained through Samuel Coring & Technical Services located in Catoosa, Oklahoma. The cores obtained with the coring procedure described in chapter 3, were conserved in high-purity mineral oil (Therminol XP), to avoid any interaction with external moisture that could affect the analysis.

4.1.1. XRD Analysis. Three runs were performed on the shale sample according to the description in chapter 3. The interpretation of XRD was achieved based on the promises that each mineral has its unique diffraction pattern or peaks at specific angles (2θ) (Moore & Reynolds, 1997).

While dry shale sample gives a bulk analysis of the mineral composition, the glycol and heat-treated samples helped to identify the nature of the clays present in the Woodford shale. X-ray patterns (Figure 4.1.) revealed quartz as the most dominant clay-size mineral, identify at 3.35 Å and 4.27 Å. Following in decline order of abundance illite, chlorite, kaolinite, and pyrite. Illite was clearly identified by its 10.08 Å sharp peak being almost unaffected after glycolation and heat treatments Chlorite was identified by its peak at 14.24 Å and 3.53 Å peaks. Kaolinite was recognized from its 7.13 Å and 3.55 Å peak in the air-dried and glycolated patterns.

The heat-treatment allowed to confirm the presence of the kaolinite respect to the chlorite due to its peak disappearance in the XRD analysis There were no indicators of smectite or illite/smectite mixed layers in the samples. Pyrite was detected by a small peak at 2.71 Å and later confirmed with the SEM analysis. This result indicated that Woodford shale is composed mainly of two dominate minerals, quartz, and clays. Then, can be cataloged as a clay-rich siliceous mudstone (Figure 4.2).

Furthermore, the absent of swellable clays indicated that the Woodford shale is a 'hard' or brittle shale and it's more prone to suffer from cuttings dispersion due to the high content of illite as well as caving or sloughing tendency through hydraulic flow invasion. A quantitative estimation was obtained with the X'Pert software is summarized in Figure 4.3.

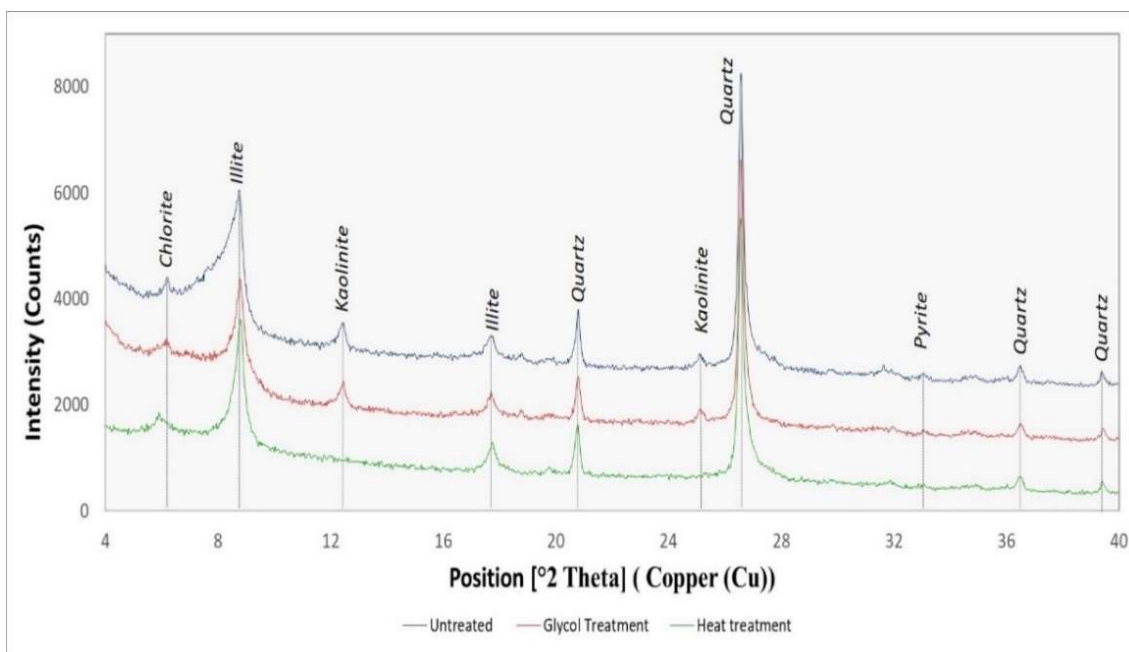


Figure 4.1. XRD analysis of the Woodford shale.

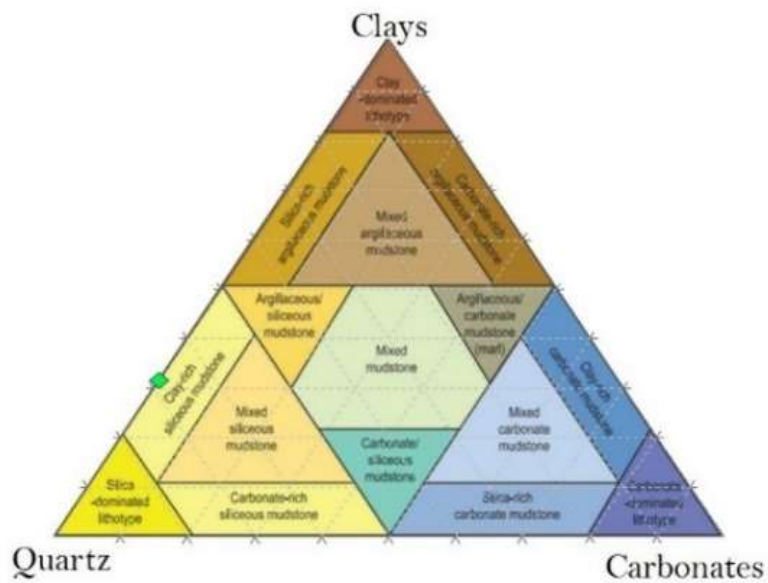


Figure 4.2. Ternary diagram of the Woodford shale.

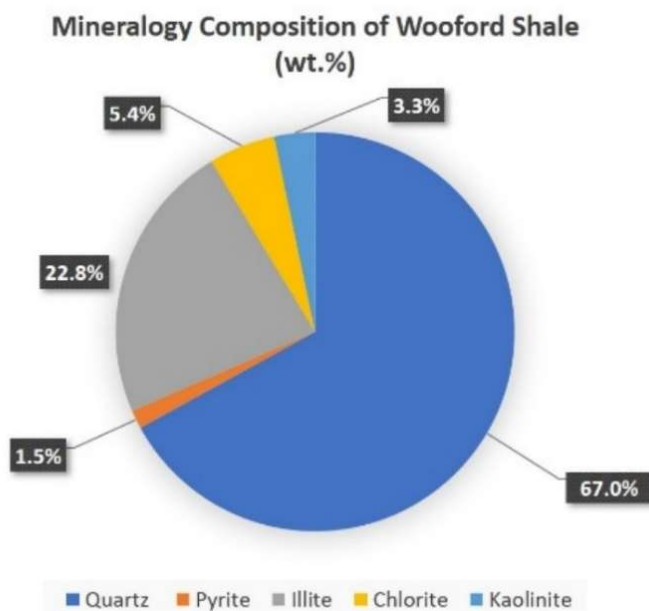


Figure 4.3. Mineral composition of the Woodford shale.

The later, confirm why conventional additives don't represent the most appropriated material since osmotic swelling rarely take place. On the other hand, KCL/PHPA drilling fluid are known to affect shales that have considerable presence of kaolinite (Boul, 2017), as it the case of the Woodford shale. A material that can provide a plugging effect to control the hydraulic flow should be the main characteristic to look for to design a WBM for the Woodford shale.

4.1.2. SEM Analysis. SEM analysis was conducted on Woodford shale in an attempt to characterize the complex nanopore structure of shales. The polished samples were prepared as described in chapter 3. Figures 4.4 shows a sequence of SEM images of the Woodford shale using the secondary electron (SE) to analyze the topographical characteristics of the shale. In the image (A) the zoom is equivalent to 250X, (B) 3K, (C) 7K, and (D) 30K times respect to the original size. From the image is it possible to

differentiate between the clay minerals and quartz as well as pyrite framboid with the back-scattering electron (BSE) useful for phase mineral identification (Figure 4.5).

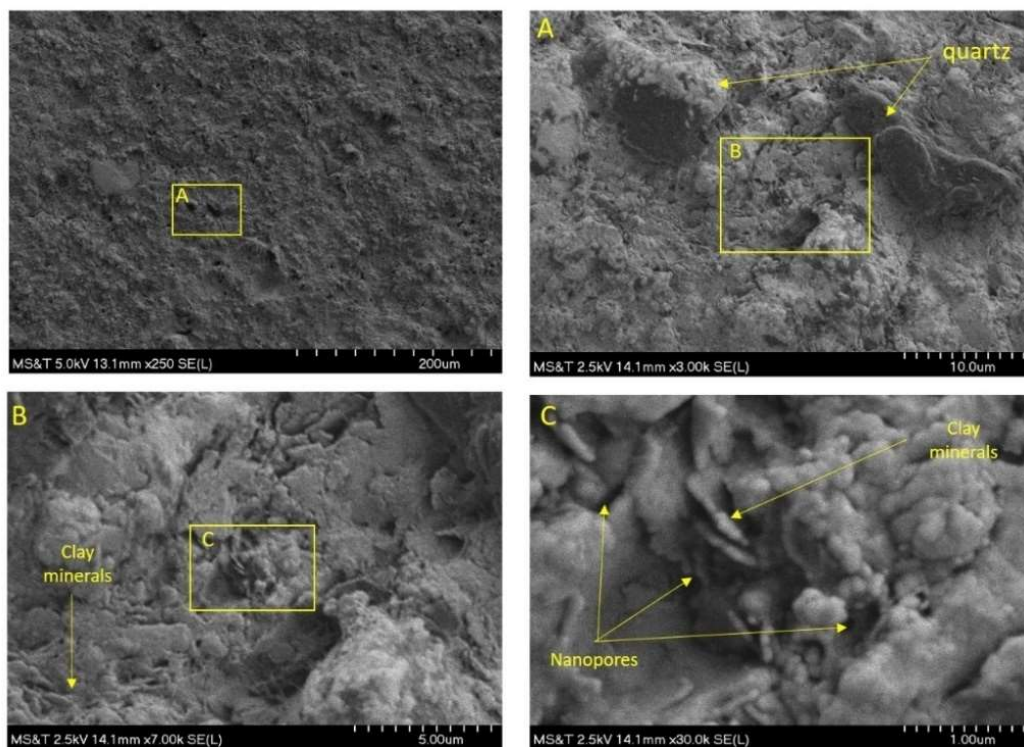


Figure 4.4. SEM Images of Woodford shale sample No 1.

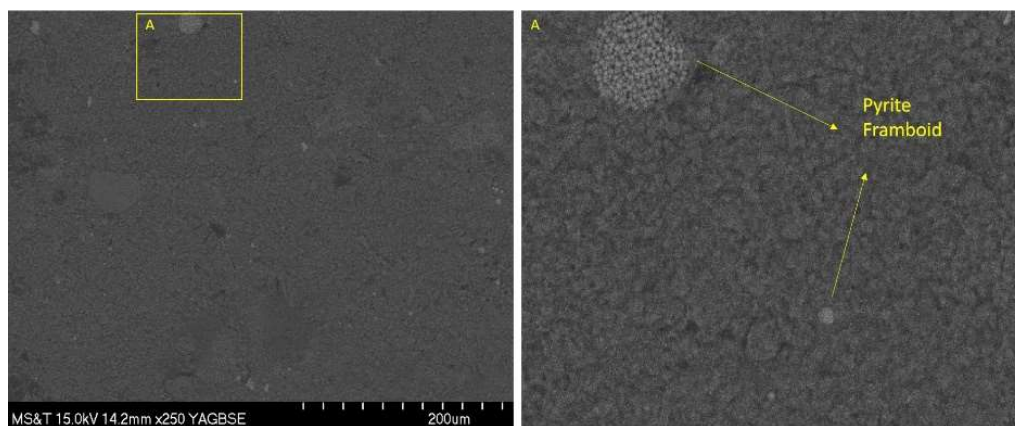


Figure 4.5. Pyrite framboid detected with BSE.

Another SEM image (Figure 4.6) also indicated the possible presence of pyrite between stacked clay sheets. These conditions are very sensitive because any interaction with fluid can affect the cementation between the minerals creating new micro-fractures that can increase the fluid invasion into the shale matrix.

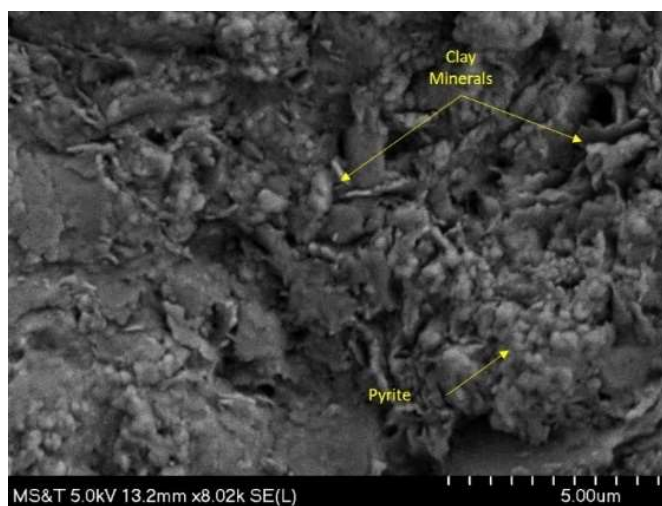


Figure 4.6. SEM image of the Woodford shale No 2.

A further analysis with the help of a commercial imaging software (ImageJ 1.51) allowed to estimate a pore size distribution of the Woodford sample. The pore size estimated falls according to the IUPAC classification in mesopore (2 – 50 nm) and macropore (> 50 nm) since no further ion-mill technique was applied to the sample the identification of pores in the micropore region (< 2nm) was not possible. However, for the purpose of the NP-WBM design, the most important range was covered due to the ability of the fluid to invade this type of pores. If effectively the nanomaterial selected can plug these pores in the near-wellbore region a filter cake could be formed reducing the risk of fluid invasion into the shale formation. The pore size range was from 21 nm to 435 nm

with a median of 112.84 nm and a standard error of 2.94 nm (Figure 4.7). according to Abrams plugging theory (1977), the required size of a NP to effectively plug the Woodford nanopores should be in the range between 16 nm to 37 nm. Thus, the selection of the silica NP with 20 nm size was appropriate for this purpose.

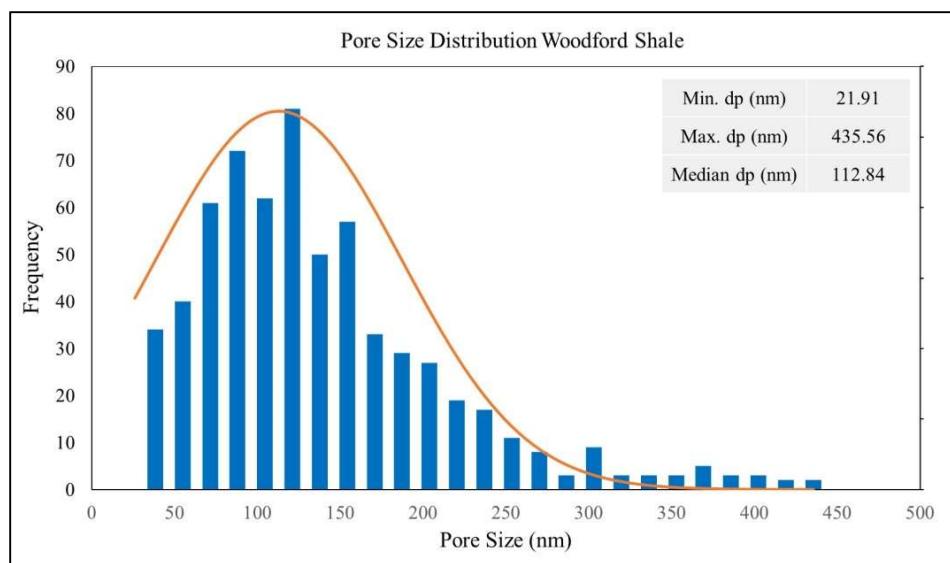


Figure 4.7. Estimation of pore size distribution in the Woodford shale.

there are some conditions that can affect the image quality and the further analysis. since rocks are not conductive some charge effect can take place reducing the quality of the data obtained. Also, the sample can suffer from contamination with materials used during the sample preparation that can create new voids or plug some features in the rock due to the interaction with the shale surface. In spite of all, SEM technique is believed to be a powerful tool that provides a direct measurement of the original pore structure and can give reliable data for the selection of the appropriate material in the design of a NP-WBM.

4.1.3. CEC Analysis. The cation exchange capacity test was performed to determine the reactivity of the Woodford shale. Based on the XRD results that indicated lack of smectite or mix-layer clays the CEC of the Woodford shale was assumed to be poor. The final CEC results confirmed this idea. Figure 4.8 shows the final endpoint of the test for the Woodford shale. The CEC was 1.5 meq/100g indicating a very poor tendency in the shale to experience an osmotic hydration that leads to clay swelling.

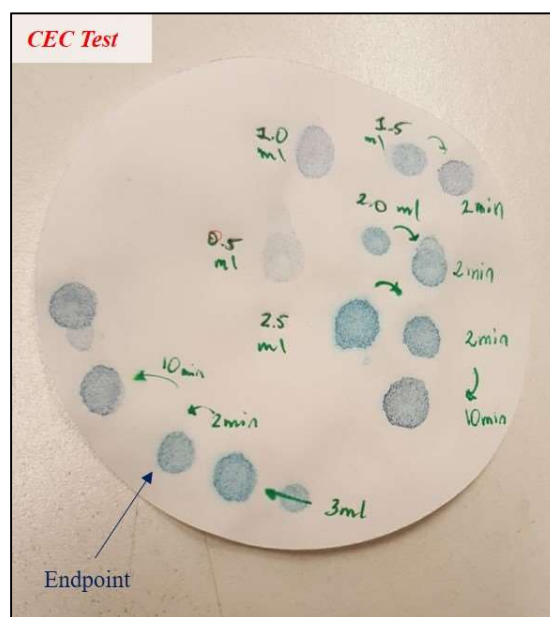


Figure 4.8. CEC test result for Woodford shale sample.

This condition seems not to be important, however, this value indicated why conventional additives initially design to control hydration effects on shales are not the most appropriated for brittle or ‘hard’ shales as in the case of the Woodford shale.

4.1.4. Porosity Analysis. Two different cores of 1-inch diameter were analyzed in this test. The Ultrapyc 1200e was used to estimate the grain volume and density. Table 4.1 shows the results obtained for each core.

Table 4.1. Grain volume and density of the Woodford shale samples.

Core	mass (g)	Grain volume (cc)	Grain density (g/cc)
1	11.865	4.8533	2.4448
2	8.692	3.471	2.5035

The second step calculates the bulk volume and bulk density of each core. This step was performed with the set-up form immersion test described in chapter 3. Table 4.2 shows the results for each core.

Table 4.2. Bulk volume and bulk density of the Woodford shale samples.

Core	Bulk Volume (cc)	Bulk density (g/cc)
1	5.372	2.21
2	3.85	2.26

Finally, by using the results obtained in both tests as an input in equation (8) the total porosity was calculated as registered in Table 4.3. It is vital to consider that this value is an estimation of the total porosity, not the effective porosity. Still, the values obtained were very similar to the total porosity estimated by other researchers (Agrawal, 2012; Gupta, 2013; Laughrey, 2017).

Table 4.3. Total porosity of the Woodford shale samples.

Core	Void Volume (cc)	Total porosity (%)
1	0.518	9.65
2	0.379	9.84

The importance of generating an efficient plugging effect relies on reducing the risk to cause dissolution or detachments of minerals from the pores in the near-wellbore region. This will control further communication with existing natural micro-fractures that lead to deeper invasion of the fluid inside the shale matrix.

4.2. SiO₂ & GRAPHENE OXIDE (GO) NP CHARACTERIZATION

Drilling fluids can experience different conditions downhole while drilling a well. Temperature, pH variations or an ionic strength gradient can be encountered when drilling fluids get in contact with brine formations or hydrocarbon fluids. These conditions can affect the stability of the NP selected causing them to aggregate destabilizing the system. During this section different environmental conditions were tested on both the NP system to qualitatively evaluate their stability. Zeta-potential measurements support quantitatively the behavior of the NP selected.

4.2.1. Aqueous Stability Test. Sedimentation photograph sequence was the first step to evaluate the NP against different environmental conditions. Deionized water was the base fluid for all the NP samples and the concentration used for both system was 0.1 % by wt. with the exception for graphene when tested with CaCl₂ (0.01% by wt.)

4.2.1.1 Effect of salt on SiO₂ & GO nanoparticle. Figure 4.9 shows the phase behavior of the silica NP dispersion in different NaCl and CaCl₂ concentration.

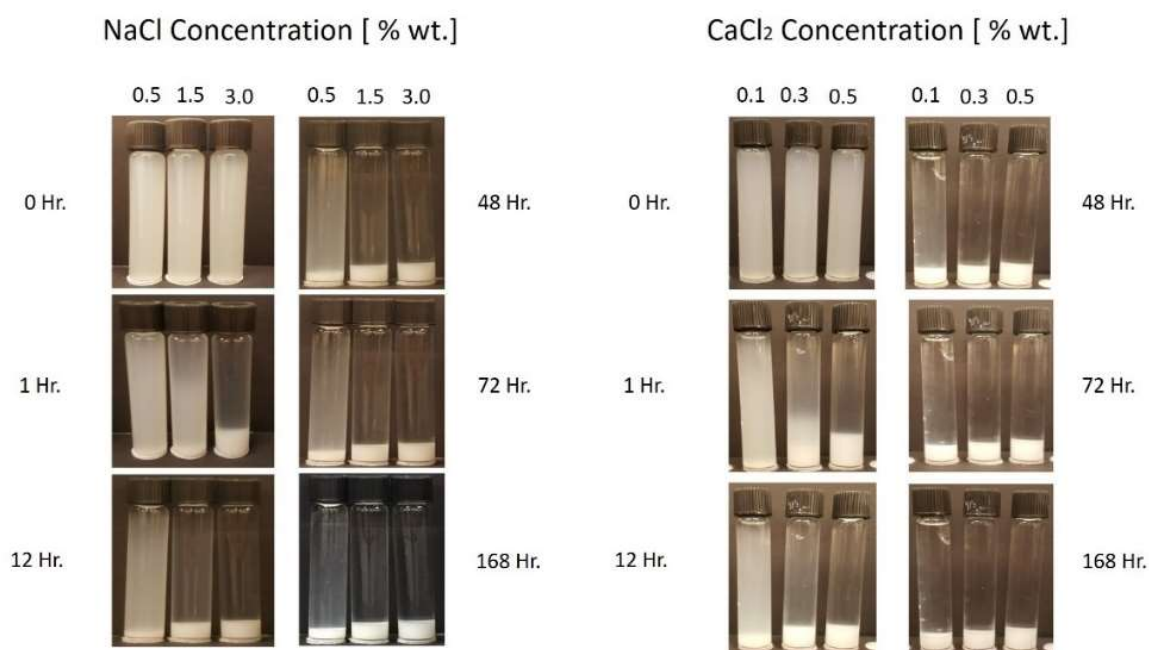


Figure 4.9. Effect of salt concentration and type on silica nanoparticles.

It can be seen that electrolytes, in general, affect the electrical double layer of the NP causing a compression effect that leads to aggregation. Basically, due to the increase of ions in the medium that tends to limit the repulsion ability of the NP (McElfresh, 2012). NP in NaCl solution started to experience a visual aggregation at 1.5 % wt. that lead to an increase in the sedimentation rate. The maximum concentration for NaCl represents a concentration similar to seawater (30000 ppm), at this condition the NP dispersion suffered aggressive aggregation and after 1 Hr. of exposure all the particles were settled down compared to lower concentrations. Still, the cut-off time for the NaCl conditions was 48

Hr., with some variation among the samples. after this period of time, all the NP that did not settle remains in solution up to 7 days.

In the case of CaCl_2 , the divalent salt has a stronger effect than the monovalent (NaCl) salts (Metin et al., 2011). At very low concentration the shrink effect is visually observed. However, the test indicated that after 48 Hrs. there was no further settling in a concentration below 0.3% wt. Finally, this test indicated that Silica NP can tolerate first the used of common water to prepare WBM at field scale with salinity < 500 ppm as well as sort of contamination with brine formation that has < 15000 ppm. Figure 4.10 shows the phase behavior of the graphene nanoplatelets dispersion in different NaCl and CaCl_2 concentration.

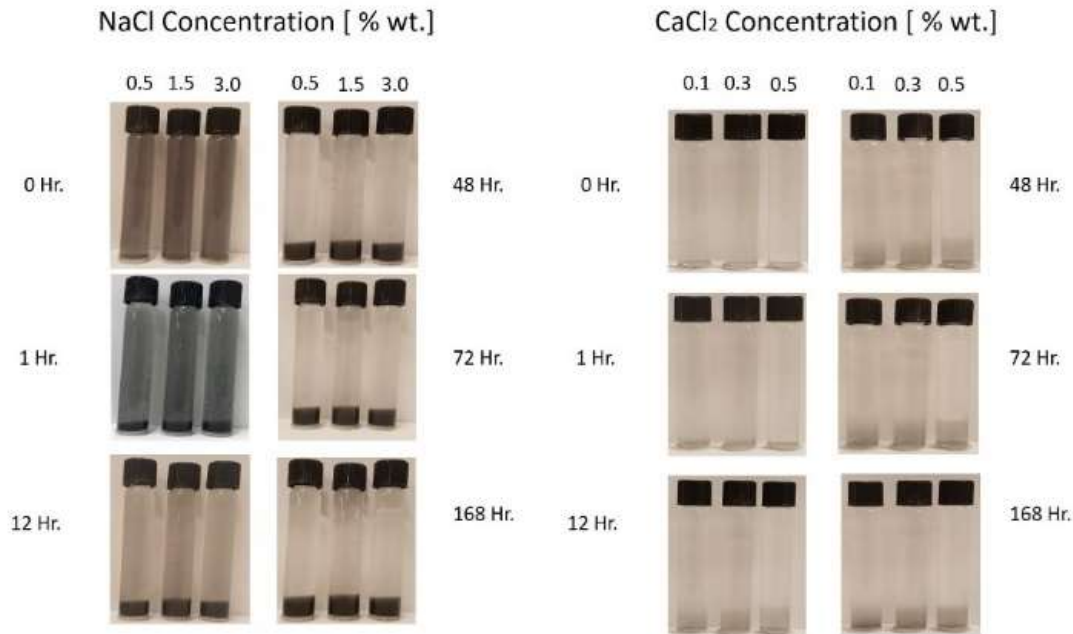


Figure 4.10. Effect of salt concentration and type on graphene NP.

In the case of graphene nanoplatelets, divalent salts also had a stronger effect than the monovalent salts. However, for graphene NP the aggregation and sedimentation rate were higher with a cut-off period of 12 Hrs. Two reasons can explain this phenomenon. First, the graphene nanoplatelets have a higher density than silica NP and second, due to their flake shape and lateral size in microns the gravity forces tend to have a greater effect on their sedimentation.

4.2.1.2. Effect of pH on SiO₂ & GO nanoparticle. Figure 4.11 illustrates the effect of acidic and alkali environments of the NP.

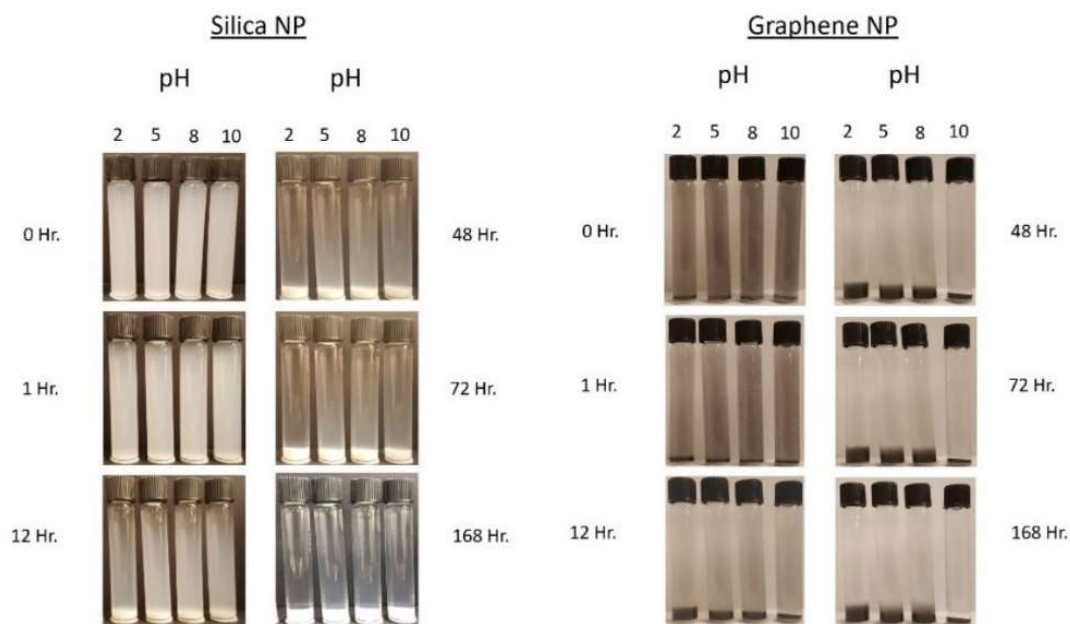


Figure 4.11. Effect of pH on nanoparticles.

The results indicated that when both types of NP are exposed to an acidic environment sedimentation rate increase respect to the other pH. The range of pH between 8 -10 covers the drilling fluid design in which most conventional additives improve their

performance. A visual response of the NP system to the alkali conditions indicated that NP are more stable and thus, the settling of particles out of solution decreases. The following tests were design based on this pH conditions since the NP-WBM will be adjusted pH around 9.5.

4.2.2. SiO₂ and GO Nanoparticle Zeta Potential Analysis. The ζ – potential measurements were included to assess the stability of both the NP system in the alkali region tested from a quantitative point of view. The advantage of this technique is that it evaluates the in-situ conditions of the dispersion. Table 4.4 shows the result of 3 ζ – potential measurements and the standard deviation for the silica and graphene NP.

Table 4.4. Zeta-potential measurements of silica and graphene nanoparticle.

zeta-potential (mV)	Silica Oxide	Graphene Oxide
Run 1	-35.3	-42.1
Run 2	-34.4	-41.2
Run 3	-34.3	-39.7
Std dev (mV)	0.55	1.21

The ζ – potential results below -30 mV for both, silica, and graphene was indicative of the potential stability of the NP that once mixed with the basic drilling fluid there should not be any aggregation tendencies. Figure 4.12 Figure 4.13 shows the ζ – potential distribution obtained for silica and graphene respectively.

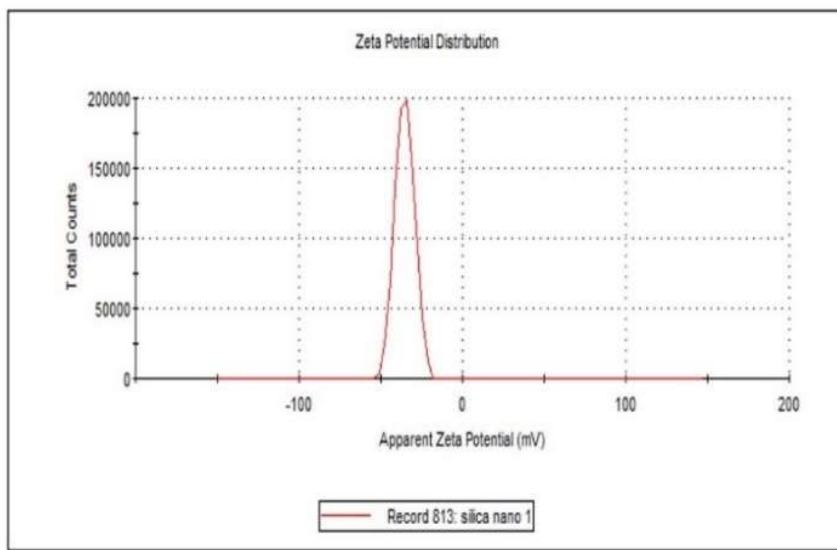


Figure 4.12. Zeta-potential distribution of silica NP.

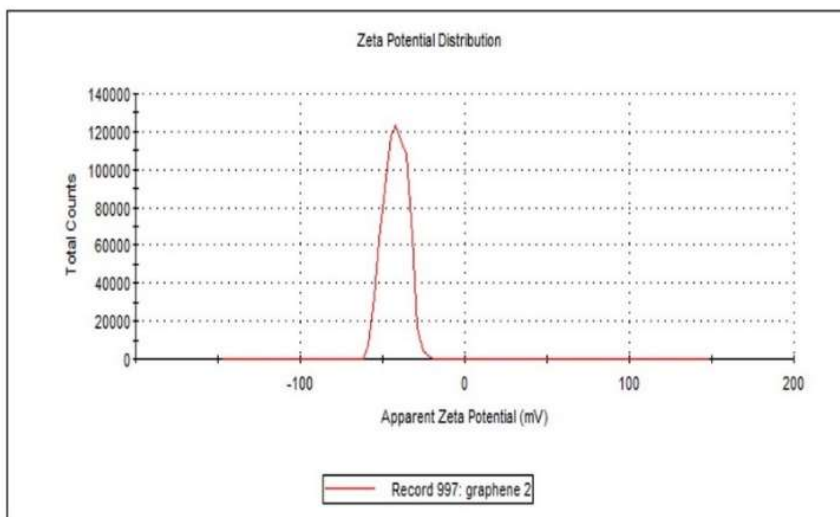


Figure 4.13. Zeta-potential distribution of graphene nanoplatelets.

4.3. NP-WBM DRILLING FLUID CHARACTERIZATION

The evaluation of NP in WBM for unconventional shales has been studied in the past years becoming nowadays more popular as documented in section 2. In this research,

the influence of silica NP and graphene nanoplatelets in filtration and rheology were evaluated as a function of pressure, temperature, and concentration. The effect on filtration properties was investigated under two different conditions: LTLP and HTHP. Both tests were performed based on the procedure explained in section 3 following the API standards. The Rheology of the fluids were compared to the base fluid (Basic A) at 120 °F and its effect on PV, YP, n, and K based on the Hershel-Buckley model.

The first part of the characterization evaluated the individual performance of each particle individually when added to the control fluid (Basic A). Then, the best two concentrations of each NP system were mixed together, and the tests were performed one more time to investigate the effect of combining both NP. Once the optimum formulation was identified, graphite (conventional LCM) was added at three different concentration to help in the filtration process and evaluated the synergistic effect with the NP if existed.

The individual effect of the graphite was also quantified separately with respect to the basic A fluid. The new NP-WBM was then exposed to different aging conditions (150 °F, 200°F, and 250°F) to investigate the possible NP influence on the stability of the WBM in terms of filtration and rheology. Finally, the new NP-WBM was tested against the Woodford shale to observed the chemical interactions between the rock and the fluid and analyzed the positive or negative effect in terms of inhibition capability.

4.3.1. NP-WBM Density and pH. Mud density is one of the important drilling fluid properties because it balances and controls formation pressure and wellbore stability. A mud density of 8.5 ppg was found to be constant for all samples with and without NP when mixed with the Basic A fluid as shown in Table 4.5.

Table 4.5. Density and pH values of drilling fluids with and without NP.

Drilling fluid composition	Properties	
	Density (ppg)	Final pH
Basic A	8.5	9.5
B	8.5	9.5
C	8.5	9.5
D	8.5	9.5
E	8.5	9.5
G1	8.5	9.5
G2	8.5	9.5
G3	8.5	9.5
G4	8.5	9.5
CG2	8.5	9.5
CG3	8.5	9.5
DG2	8.5	9.5
DG3	8.5	9.5
Basic A + 2 % graphite	8.6	9.5
DG2 + 2 % graphite	8.6	9.5

The addition of NP did not increase the drilling fluid density given the fact that their concentration was low. Only an increase of 0.1 ppg was registered when graphite at 2% wt. was added to the Basic A fluid with or without NP resulting in a density of 8.6 ppg, which still is considered a low density. A pH level of 8.7 was also found in all samples after mixing the NP with the Basic A fluid. The final pH of each formulation was raised to 9.5 with KOH to avoid the inclusion of sodium ions that could interact with the clays in the shale. No change reaction was observed due to the NP after the final pH was raised.

4.3.2. Effect of Nanoparticle on Static LTLP Filtration Test. Percentage of filtrate reduction under LPLT after 30 min for different silica and graphene NP concentrations in the Basic A drilling fluid are present in Figure 4.14. The percentages were calculated based on a filtration of 8.6 ml at 30 min for the control fluid (Basic A).

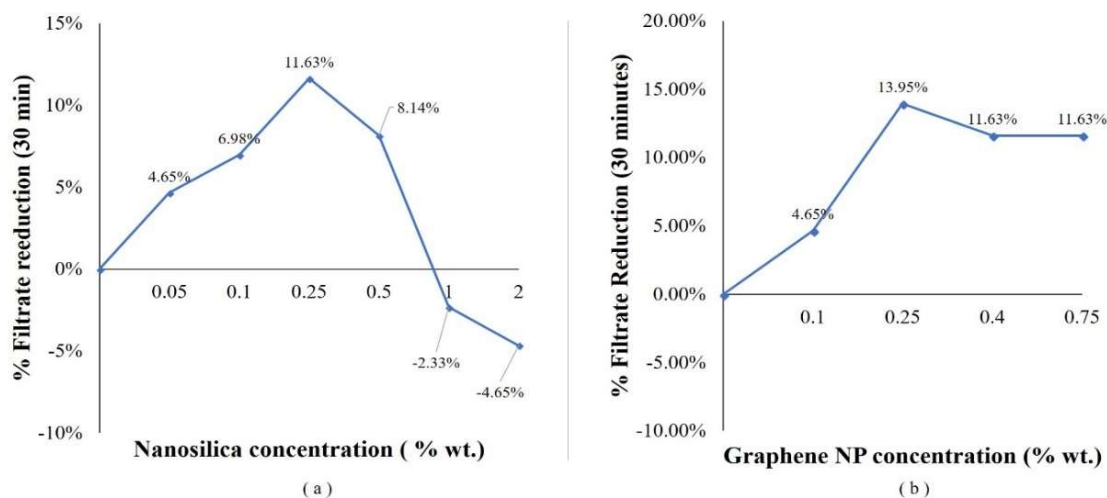


Figure 4.14. Percentage of reduction in LTLP filtrate for silica and graphene NP.

The results indicated in the case of silica that concentration above 0.5% wt. results in a negative impact in the drilling fluid filtration due to possible aggregation of particles that could lead to higher permeability in the filter cakes. In the case of the graphene nanoplatelets concentration above 0.4% wt. did not give further reductions in filtrate. The best concentration for silica was 0.25% wt. with a reduction of 11.63%, the same concentration gave the best results for graphene with a reduction of 13.95%, both with respect to the Basic A.

4.3.3. Effect of Nanoparticle on Static HTHP Filtration Test. A differential pressure of 500 psi and temperature of 250 ° F were selected to test the nanofluids under HTHP conditions. Figure 4.15 summarized the percentage of filtrate reduction of both, silica, and graphene NP relative to 27.2 ml of the Basic A fluid.

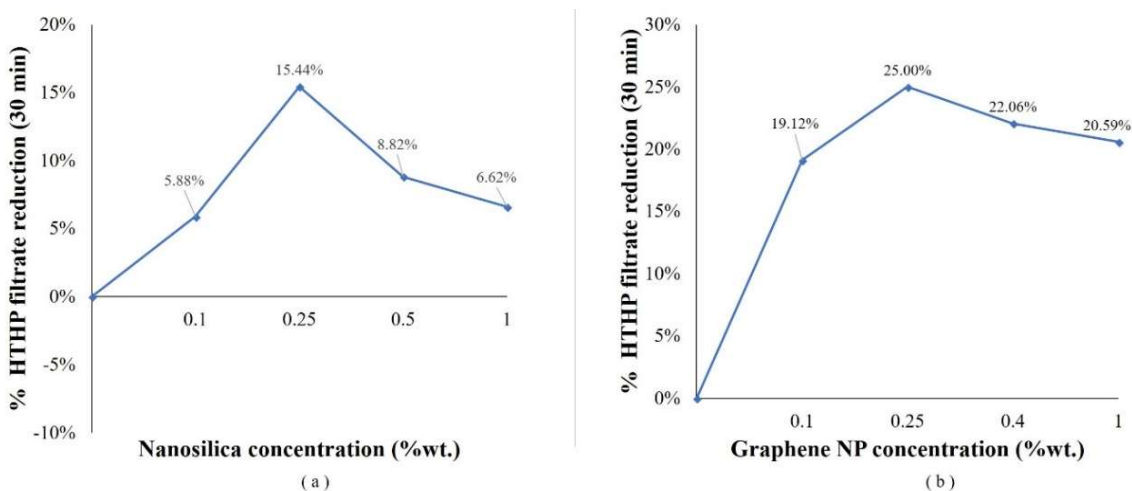


Figure 4.15. Percentage of reduction in HTHP filtrate for silica and graphene NP.

The HTHP results indicated that 0.25 % wt. gave the best performance for both types of NP. However, in the case of silica with higher concentration, the benefits of filtration started to reduce. The same effect was visualized with the graphene nanoplatelets; however, the reduction was much slower compared to the silica. In both, the system the performance of the NP at HTHP conditions were better compare to the LTLP conditions probably due to a better hydration of the system that allows them to be more dispersed in the system while their motion could be increased due to the high temperature.

4.3.4. Effect of Nanoparticle on the Rheology Behavior. The rheological properties of the different nanofluids were measured at the standard test temperature of

120°F. These included plastic viscosity (PV), yield point (YP), gel strength at 10 sec (10 s GS), 10 min (10 min GS) and 30 min (30 min GS). Table 4.6 shows the rheological results for each type of NP when mixed with the Basic A fluid.

Table 4.6. Rheology results for silica and graphene NP at 120 °F.

Rheological properties @ 120 ° F					
Drilling fluid composition	PV (cp)	YP (lbf/ft ²)	Gel 10 sec (lbf/100ft ²)	Gel 10 min (lbf/100ft ²)	Gel 30 mi (lbf/100ft ²)
BASIC A	19	15	3	9	12
B	19	17	4	11	15
C	19	17	4	10	14
D	20	18	4	9	12
E	21	16	3	11	15
G1	17	17	3	12	17
G2	19	19	4	14	19
G3	20	18	4	15	21
G4	20	19	4	15	22

In general, the rheology was not significantly affected by the addition of NP. The advantage of this behavior indicates that both NP system can be added to the fluids at low concentration without increasing the solid concentration in high proportions that could lead to higher PV representing a problem in the horizontal wells due to a decrease in the rate of penetration (Salhi, 2016). On the other hand, under static conditions, the gel strength was observed to be very uniform with respect to the basic fluid. the increments in the 10 min and 30 min gels were higher for the graphene than for the silica, due to their natural flake shape an orientation in the gel structure. However, none of them exhibit a progressive

condition that might lead to pump pressure increases in real operations increasing the risk of generating fractures in the formation. The previous test indicated very uniform rheological behavior among all NP concentration.

Nevertheless, the filtration performance of the nanofluids C, D, G2, and G3 reduce the final screening criteria and a matrix between these 4 concentrations was designed to evaluate the performance of silica and nanographene together and select the optimum formulation for the new NP-WBM.

4.3.5. Selection of Optimum Nanoparticle Concentration. The final screening criteria for the optimum NP-WBM was based on the previous results for each individual performance of both NP system. Table 4.7. Shows the final 4 formulations.

Table 4.7. Final screening criteria for NP-WBM.

Final Screening Criteria for NP-WBM						
NP Concentration % wt.		Silica Oxide Nanoparticle				
		0.00%	0.10%	0.25%	0.50%	1.00%
Graphene Oxide Nanoplatelets	0.00%	A	B	C	D	E
	0.10%	G1				
	0.25%	G2		CG2	DG2	
	0.40%	G3		CG3	DG3	
	0.75%	G4				

4.3.5.1. LTLP and HTHP filtration final screening of NP-WBM. Figure 4.16 represents the percentage of filtrate reduction for LTLP and HTHP conditions for the final matrix of the new NP-WBM.

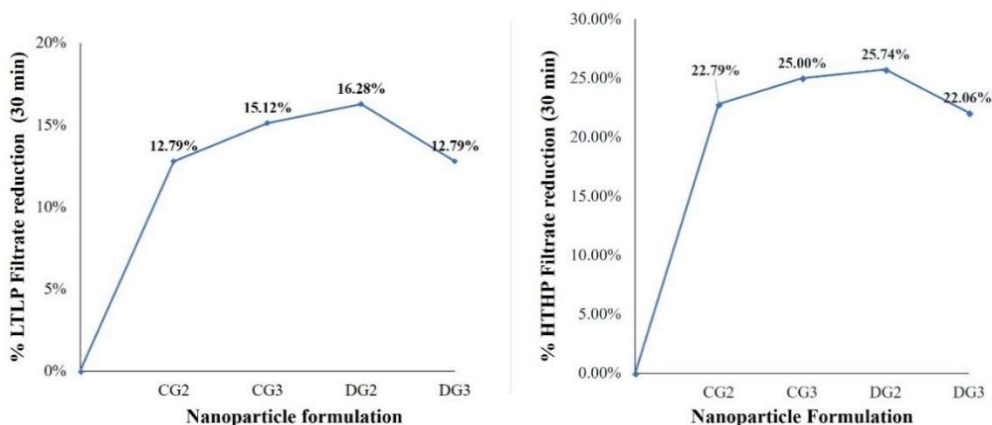


Figure 4.16. LTLP and HTHP filtration of the final screening for the NP-WBM.

The filtrate results indicated that the best formulation was the DG2 nanofluid (0.5% wt. silica and 0.25% wt. graphene). The improvement with respect to the basic fluid was 16.28% for the LTLP and 25.74% in the HTHP. Clearly, the condition of high temperature one more time indicated a better behavior of the NP system. Nevertheless, in terms of filtration, the higher quote belongs to the graphene oxide as its flake shapes in the x-axis are slightly below the 2.7 μm opening of the filter paper.

4.3.5.2. Rheology behavior for the final screening of NP-WBM. The same test used for the initial screening was applied for the final step. Table 4.8 shows the effect of adding both NP in a single system at 120 °F. The rheological behavior indicated a slight reduction of PV in all cases probably due to an effect of dispersion created by the negative

charges of both NP in the system that avoid clays to aggregated and increase particles in the mass. At the same time the improvement in the distribution of particles due to the presence of the NP in the fluid allow the polymers to hydrated properly at higher temperatures which result in a final increase of 4 to 5 (33.33%) units in the YP, improving the cleaning behavior of the NP-WBM mud respect to the basic fluid. Also, an increase in the 10 min and 30 min gel strength represent an improvement in the cutting suspension ability of the NP-WBM without creating progressive gels. Since the rheology improvements were very similar, the best performance of the nanofluid DG2 in filtration suggested that this one should be selected as the optimum formulation for the new NP-WBM and further evaluation against the shale cuttings.

Table 4.8. Rheology results for the final screening of NP-WBM at 120 °F.

Rheological properties @ 120 ° F					
Drilling fluid composition	PV (cp)	YP (lbf/ft ²)	Gel 10 sec (lbf/100ft ²)	Gel 10 min (lbf/100ft ²)	Gel 30 mi (lbf/100ft ²)
BASIC A	19	15	3	9	12
CG2	17	19	4	14	19
CG3	17	19	4	13	19
DG2	16	20	4	14	19
DG3	18	20	4	16	21

4.3.5.3. Filtration behavior of optimum NP-WBM. The last step prior to continuing with the chemical interaction tests was the inclusion of the conventional LCM

product. The graphite was mixed with the optimum fluid established previously at three different concentration (0.5%, 1.25% and 2% by wt.) to help the filtration process by including a wider spectrum of particles in the drilling fluid. Figure 4.17 represents the effect of mixing the NP DG2 system with the conventional graphite in LTLP and HTHP conditions.

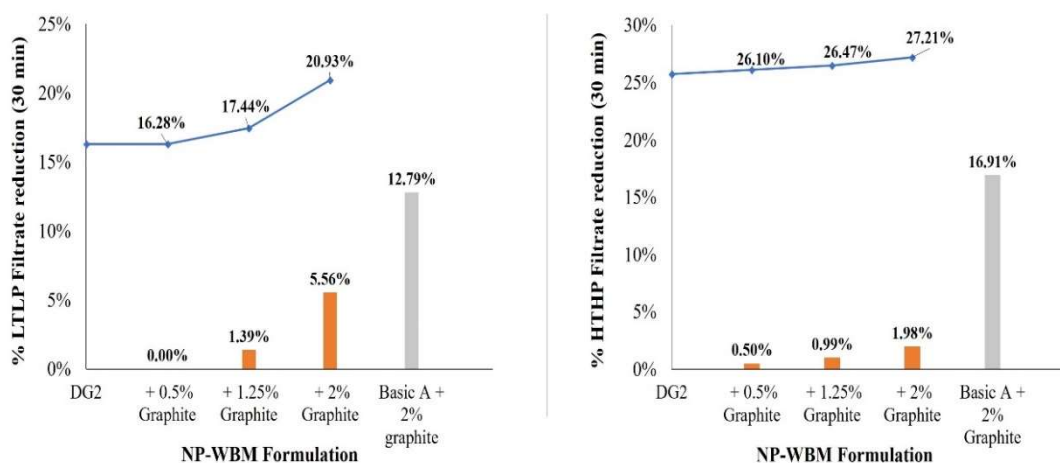


Figure 4.17. Final NP-WBM LTLP and HTHP filtrate.

A test with no NP were performed to evaluate the individual benefit of the graphite at its upper-limit concentration (2% wt.). The reduction in both, LTLP and HTHP were > 10% respect to the Basic A fluid. This behavior was also observed by previous researchers (Contreras, 2014). However, its benefit in filtration still below compared to the DG2 fluid. Still, a synergistic effect was reached by combining both systems, enhancing the filtration properties of the base NP-WBM in 20.93% and 27.21% for LTLP and HTHP filtrate test respectively. After the filtration experiments, the filter cake thickness was characterized to allow a comprehensive results analysis. Figure 4.18 presents photographs of filter cakes

collected following LPLT measurements. Cake thickness is quoted as one important characteristic of the filter cakes.





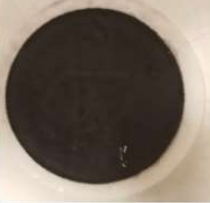
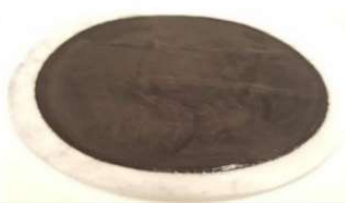
Sample description and thickness	Filter cake after 30 minutes (LTLP test)	
BASIC A (Control Sample) 0.9 ± 0.1 mm		
Basic A + NP (DG2) 0.7 ± 0.1 mm		
NP-WBM (+ 2% graphite) 0.81 ± 0.1 mm		

Figure 4.18. LTLP filtrate cake thickness and description.

The addition of NP yields to a 22.22% thickness reduction compared to the basic A fluid. likewise, the NP-WBM containing 2 % graphite concentration gave a reduction of 10% in thickness compare to the basic fluid. The reduction due to the presence of NP creates a less permeable filter-cakes which mean less filtrate can invade the formation. An increase of 15.7% in the thickness was the result of adding the graphite to the NP-WBM. Despite it, the overall fluid experiences a reduction in cake thickness.

Furthermore, filter cake characterization concluded that both NP and graphite are effective additives for filtration reduction in WBM while reducing the thickness of the filter cake preventing the occurrence of stuck pipe. In order to conduct an insightful interpretation of the HTHP results, the filter cake thickness after 30 min for each experiment was also characterized. Figure 4.19 presents the filter cake characterization for the HTHP conditions.



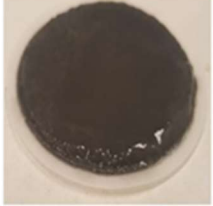
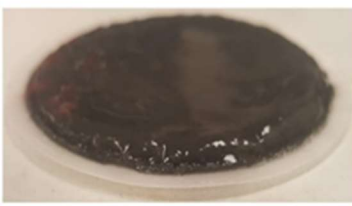
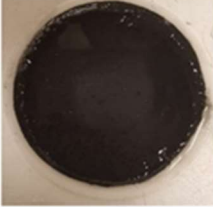
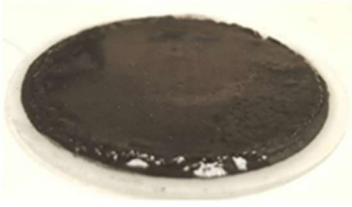
Sample description and thickness	Filter cake after 30 minutes (HTLP test)	
BASIC A (Control Sample) 2.92 ± 0.1 mm		
Basic A + NP (DG2) 2.37 ± 0.1 mm		
NP-WBM (+ 2% graphite) 2.61 ± 0.1 mm		

Figure 4.19. HTHP filtrate thickness and description.

Note that in comparison to the control sample, both additives experienced the same behavior as in the LTLP conditions. The inclusion of NP yields to an 18.83% reduction while the final formulation including the 2% wt. graphite a 10.61% reduction. Still, the

same benefits applied to the reduction of the filter cakes. Even more, when low NP concentration can interact with the free cations that clays release at higher temperatures, which helped to create a less permeable filter-cakes and protect the formation (Mahmoud, 2018). Finally, for field application purposes this result is a useful finding since it is always advisable to work under low-additives concentration for economic and environmental reasons. In general, similar findings have been observed in other studies that include NP as main additives (Ponmani, 2016)

4.3.5.4. Rheology behavior of the optimum NP-WBM. Table 4.9. describes the rheological properties of the optimum NP-WBM formulation as well as the benefit of the inclusion of the graphite at 120 °F.

Table 4.9. Rheological properties with optimum NP-WBM and graphite at 120 °F.

Rheological properties @ 120 ° F					
Drilling fluid composition	PV (cp)	YP (lbf/ft²)	Gel 10 sec (lbf/100ft²)	Gel 10 min (lbf/100ft²)	Gel 30 mi (lbf/100ft²)
DG2	16	20	4	14	19
+ 0.5% wt. graphite	18	20	4	13	19
+ 1.25% wt. graphite	18	22	4	15	21
+2% wt. graphite	19	24	4	16	22

The rheological behavior after adding the graphite to the optimum NP-WBM experience few improvements in a concentration above 1.25% wt. However, it can be concluded from the general behavior that the rheology of the basic A fluid is not affected

greatly either by the NP or the LCM material regardless the concentration used for this last one. The applicable improvements were observed in the filtration test previously analyzed indicating that all the products attached to the formulation of the NP-WBM could perform at field conditions with no affectation in the hydraulic design of the drilling phase. Table 4.10. summarized the optimum NP-WBM formulation including the graphite after all the analysis.

Table 4.10. Optimum NP-WBM formulation.

Optimum NP-WBM Formulation	
PRODUCT	CONCENTRATION
Bentonite	10 ppb
Xantham Gum	0.25 ppb
Pre-gelled Starch	1.85 ppb
PAC – LV	1.85 ppb
Silica nanoparticle	1.75 ppb (0.5 %wt.)
Graphene nanoplatelets	0.875 ppb (0.25%wt.)
Graphite	7 ppb (2% wt.)
KOH	Needed to raise pH to 9.5

4.3.6. NP-WBM Inhibition Capabilities in the Woodford Shale. During drilling operations in unconventional shales, the exposed formation (open-hole) usually interact with drilling fluid for a long period of time. The prolonged exposure can alter the petrophysical and mechanical properties of the shale and when WBM are use the effects can be more severe as explained in section 2. The degree of interaction between shale and WBM can impact directly in the future operations (e.g. completions, production). This

subsection was designed to test the effects of the optimum formulation of the new NP-WBM on the Woodford shale by analyzing the cutting erosion and the swelling effect.

4.3.6.1. NP-WBM dispersion test analysis. Inhibition capability of the new NP-WBM evaluated the effectiveness of the NP to control the disintegration tendency that Woodford shale can experience during the final stage of hydration when exposed to the fluids for 16 Hrs. at 150 °F. Distilled water was also used as a blank fluid. Figure 4.20 presents the results for the dispersion test in Woodford shale cuttings.

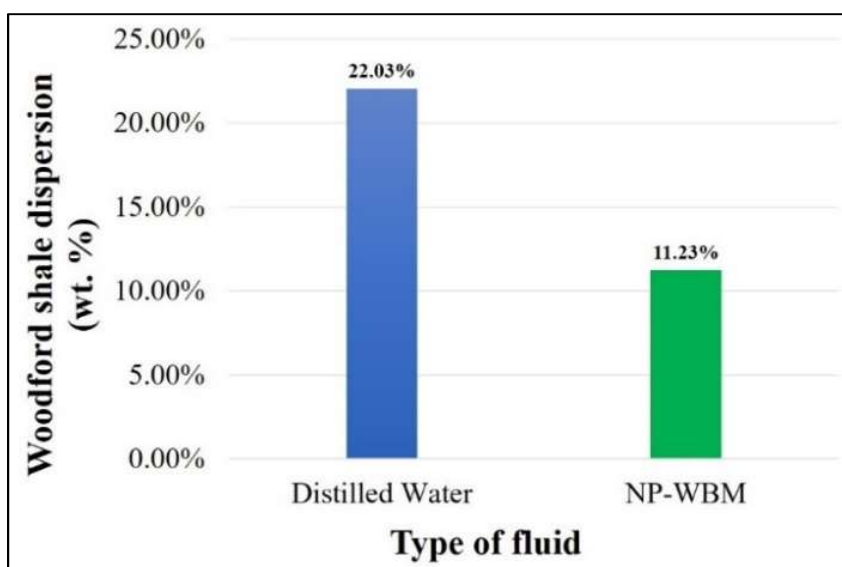


Figure 4.20. Woodford shale dispersion in distilled water and NP-WBM.

Mineralogical analysis of the XRD described previously revealed that no smectite is present in the Woodford shale that could lead to higher dispersion conditions. However, the high content of illite still represents a tendency of dispersion that needs to be controlled. From the results observed in the dispersion test, the NP-WBM yield to a 49.02% reduction

compares to the blank sample exposed to distilled water in the absence of a shale inhibitor and a pH of 10. It is clear that the final formulation of NP-WBM represents an improvement in the inhibition process. It is believed that the reason is due to the ability of NP to occupied pores in the surface area of the shale sample avoiding a further dissolution of minerals. On the other hand, the possible ‘shield’ that NP creates around the polymer structure extend their application at higher temperatures which might help in the process of inhibition.

4.3.6.2. NP-WBM visual swelling analysis. The effects of a surface hydration that took place in thin pieces of shale when exposed to distilled water and the NP-WBM was evaluated for a period of 14 days at 150 °F. Figure 4.21 describes a photograph sequence collected to analyzed the shale interaction with these fluids.



Figure 4.21. Woodford shale visual analysis.

The first thing noticed is that no change in shape was observed due to the interaction with these fluids. The reason goes back to the poor smectite content in the Woodford shale. Nevertheless, a closer analysis revealed the tendency of water to dissolve the silica-filled micro-fractures along the bedding planes (Figure 4.22 and Figure 4.23).

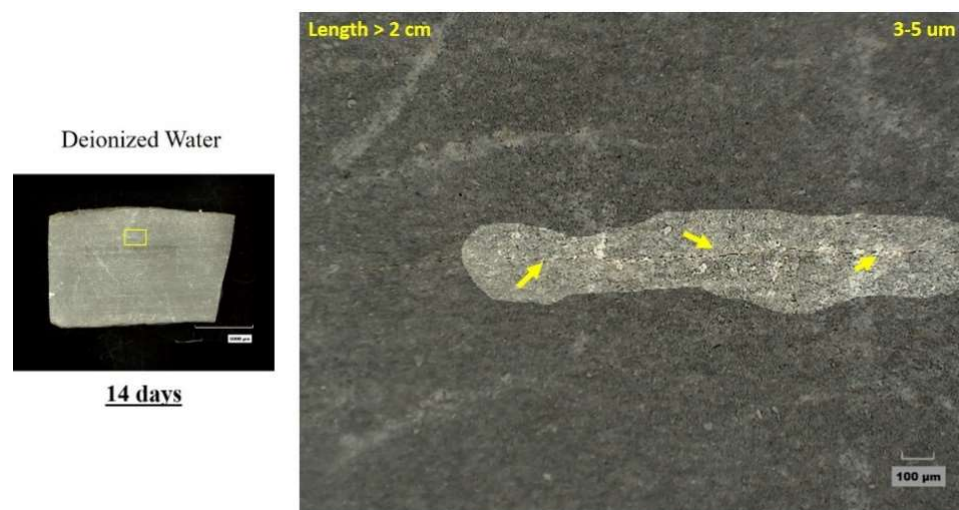


Figure 4.22. Micro-fracture in the Woodford shale due to water interaction No 1.

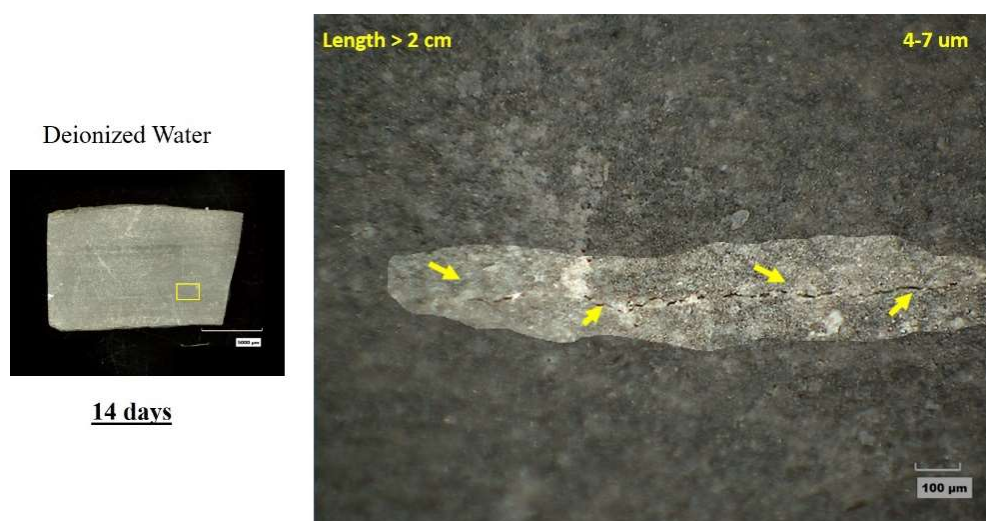


Figure 4.23. Micro-fracture in the Woodford shale due to water interaction No 2.

Figure 4.24. and Figure 4.25. shows the effect of NP-WBM on the surface of the shale sample.

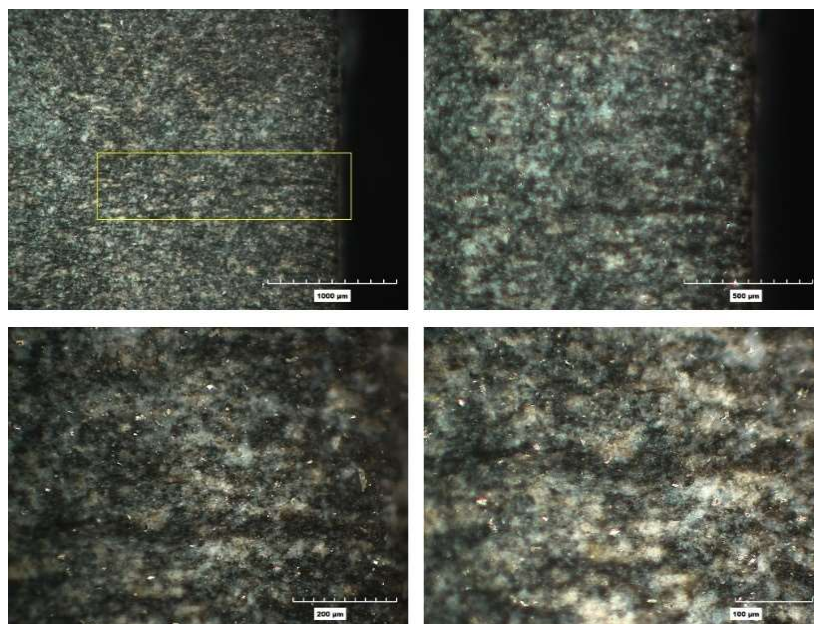


Figure 4.24. NP effect on the Woodford shale visual swelling analysis No 1.

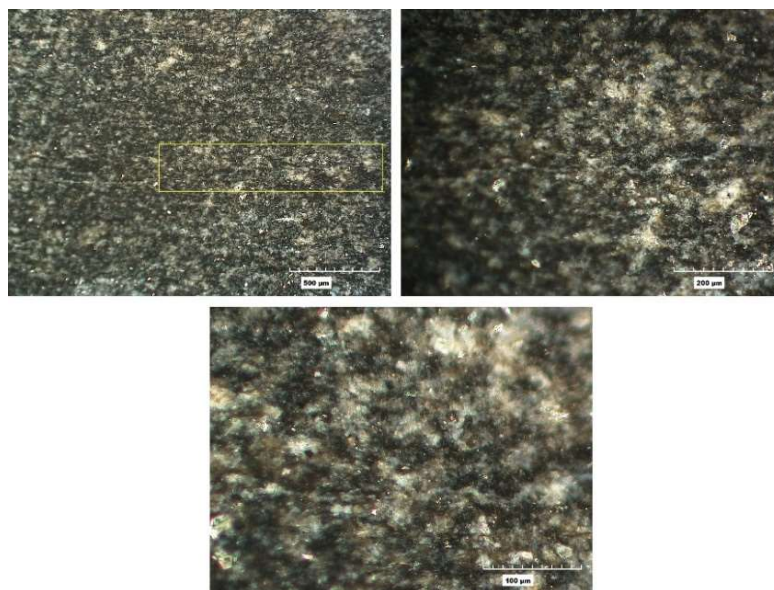


Figure 4.25. NP effect on the Woodford shale visual swelling analysis No 2.

It can be observed that NP both, silica and graphene oxide agglomerated along the bedding planes, especially covering the natural micro-fractures thus, reducing the dissolution tendency of the minerals and the opening of the fractures. This increase the protection against the fluid invasion that can cause the increase of pore pressure in the formation and finally the instability of the wellbore wall while drilling.

4.3.6.3. NP-WBM bulk swelling analysis. Following the procedure described in section 3. The extent of shale swelling of a small piece of the 1-inch core when immersed in the new NP-WBM and distilled water as a control sample was measured during a period of 24 Hrs. at room conditions. Figure 4.26. presents the bulk swelling behavior of the shale sample as a response to the interaction with the NP-WBM and the distilled water.

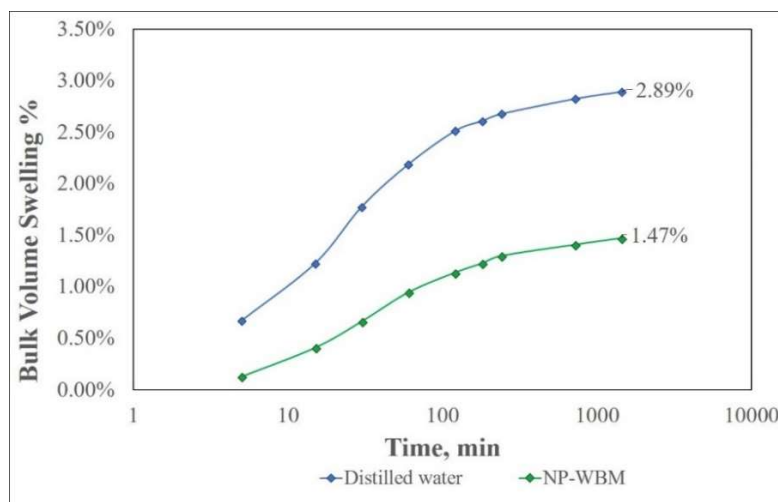


Figure 4.26. Bulk swelling of the Woodford shale in distilled water and NP-WBM.

In the absence of a chemical balance between the shale and WBM a water intake from the formation can be experienced. The degree of hydration is clearly connected with

the type of clay that composed the shale. However, the amount of water that can invade the shale is also directly proportional to the permeability and porosity of the rock sample, especially for 'hard shales'. In the previous tests developed in section 4.3.6.2. it was observed that distilled water with no chemical added caused sort of dissolution along the bedding planes that can lead to the opening of micro-fractures exposing more shale area for a future water or fluid invasion.

It is believed that this was one of the reasons why during the immersion tests the bulk swelling experienced was 2.89 %, whereas, the NP-WBM reduced the effect to a bulk swelling of 1.47% which is beneficial in terms of the design of the NP-WBM. Nevertheless, the fact that the bulk swelling test was conducted under atmospheric conditions, which do not represent the downhole condition also allow more water to interact with the rock since there is no confining or overbounded pressure that can somehow limit the opening of these fractures. Therefore, results from these tests were only used as a starting point and to check the initial compatibility between the NP-WBM and the Woodford shale.

5. NP-WBM VS. KCL-PHPA WBM AT AGING CONDITIONS

Dynamic aging tests were performed to determine whether NP could maintain the stability of WBM in terms of filtration and rheological properties. The same experiments evaluated the conventional KCL/PHPA for comparison purposes. Three different temperatures were analyzed 150 °F, 200 °F, and 250 °F. On the other hand, the inhibition capabilities of the NP-WBM previously described were compared with the inhibition properties of the KCL/PHPA under the same conditions.

5.1. FILTRATION CAPABILITIES

LTLP and HTHP static filtration test were carried out for the two systems to evaluate the ability of each one to withstand temperature effect. Figure 5.1. presents the results for LTLT static filtrate for both, KCL/PHPA and NP-WBM.

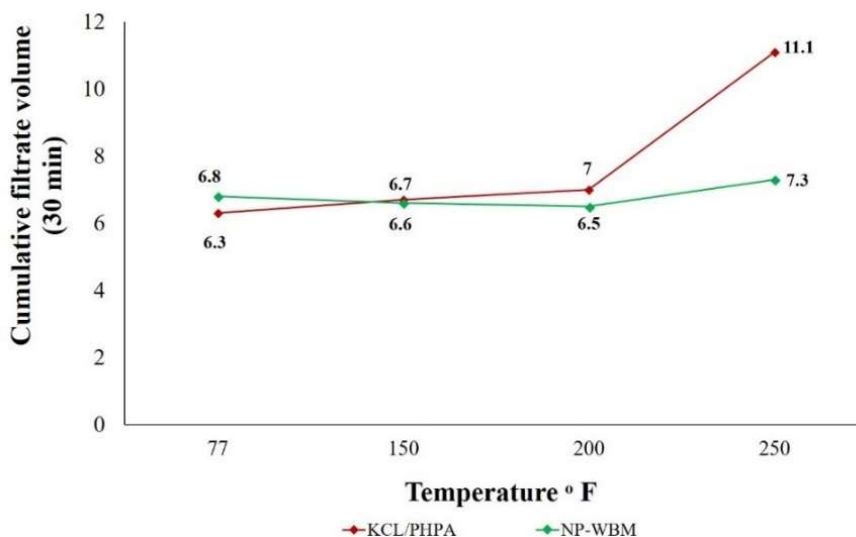


Figure 5.1. LTLP filtrate at aging conditions of KCL/PHPA and NP-WBM.

Initially, the KCL/PHPA at room temperature (77 °F) had a better performance at LTLF conditions with a filtrate volume of 6.3 ml compared to 6.8 ml of the NP-WBM representing a difference of 7.35%. However, as the aging conditions started to be more severe it was evident that at temperatures > 200 F°, clays in KCL/PHPA started to experience flocculation and polymers started to degrade at a faster rate compared to the NP-WBM. Thus, the KCL/PHPA experienced a sharp increase in its LTLF filtrate at 250 F° aged conditions with a filtrate volume of 11.1 ml representing a 52% increase compared to 7.3 ml registered with the NP-WBM. Nevertheless, no dramatic increments were experienced in cake thickness and spurt-loss was insignificant for both systems registered values below 0.

Figure 5.2 shows the results for HTHP static filtrate and Table 5.1 summarized the information related to filter cake and spurt loss for both fluids.

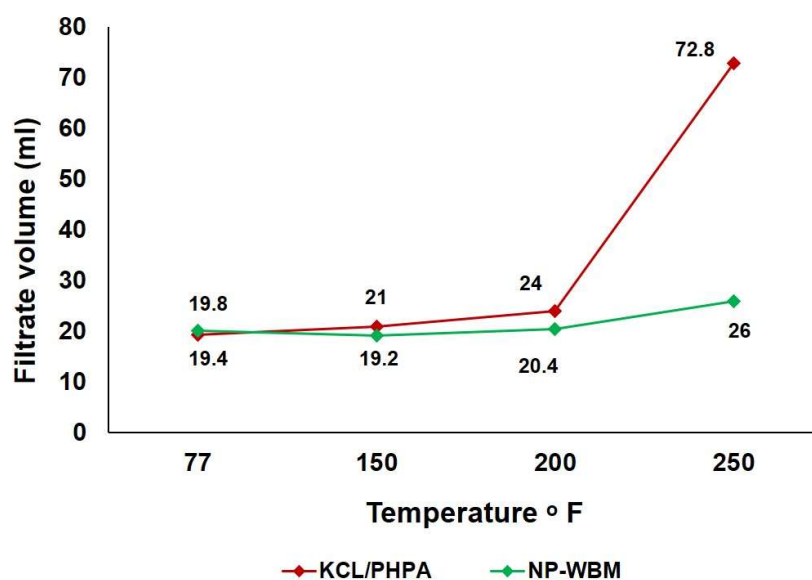


Figure 5.2. HTHP filtrate at aging conditions of KCL/PHPA and NP-WBM.

Table 5.1. Aging conditions summary for KCL/PHPA and WBM.

KCL/PHPA WBM HTHP summary aging conditions					
Aged Temperature (°F)	Filtrate (ml)	Change in filtrate volume(%)	Cake thickness (mm)	Change in filter cake thickness (%)	Spurt-loss volume (ml)
77 (No aged)	19.4	-	2.92	-	1.4
150	21	8.25%	2.96	1.37%	3.4
200	24	23.71%	3.11	6.51%	6
250	72.8	275.26%	6.32	116.44%	16.4
NP-WBM HTHP behavior summary aging conditions					
Aged Temperature (°F)	Filtrate (ml)	Change in filtrate volume(%)	Cake thickness (mm)	Change in filter cake thickness (%)	Spurt-loss volume (ml)
77 (No aged)	19.8	-	2.61	-	0
150	19.2	-3.03%	2.62	0.38%	0
200	20.4	3.03%	2.73	4.60%	0
250	26	31.31%	2.88	10.34%	0.4

The results of both fluids at aged conditions followed the same behavior observed at LTLP conditions. It seems that NP had a positive effect on dissipating the heat and maintain the stability of the conventional products in the WBM. Also, from the general trend, it was observed that NP provided a more stable fluid compared to the KCL/PHPA. A total breakdown of polymer chains in the KCL/PHPA reduced drastically the filtration at 250 °F aged condition experienced an increase of almost 275% confirming the total degradation of the entire system. Furthermore, as the temperature increases the filter cake thickness increases as well, which lead to higher spurt-loss as described in Table 5.1. compared to the NP-WBM than only 0.4 ml was registered at the highest aging temperature. The lower spurt-losses in NP-WBM suggested a more impermeable filter cake

as well as compacted due to the well-dispersed NP along the surface of the filter-cake. This indicated that NP-WBM might create external filter cakes even in the nanopore structure of shales which reduce fluid invasion and formation damage and at the same time these filter cake conditions are easier to remove prior cement jobs, which will help to increase the bonding between the formation and the cement (Amanullah, 2011). Figure 5.3. presents the filter cake for KCL/PHPA and NP-WBM at the different aging conditions.

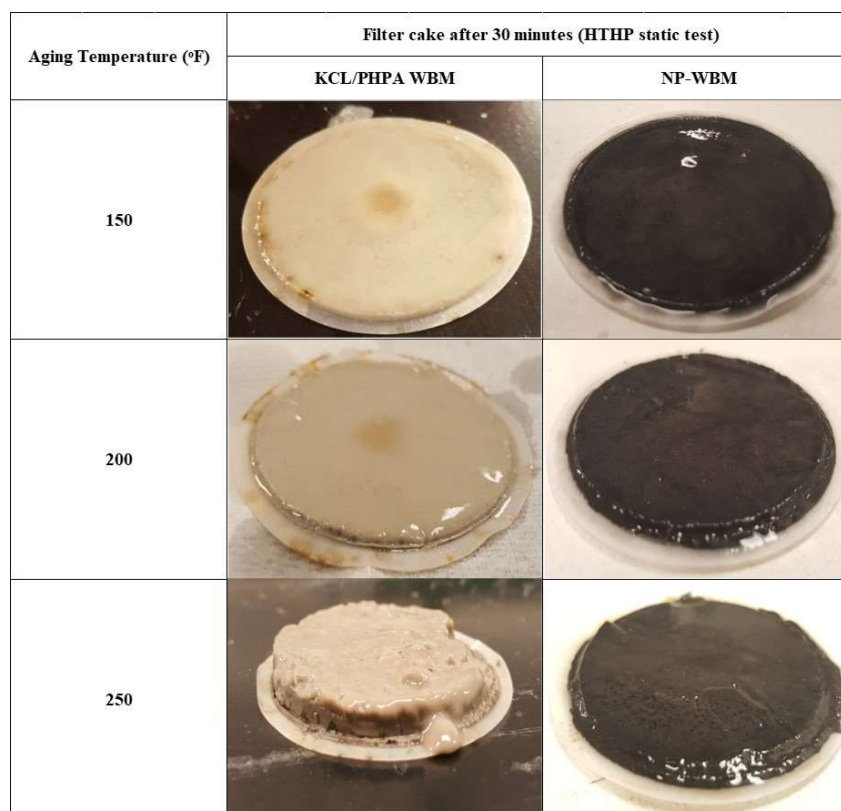


Figure 5.3. KCL/PHPA and NP-WBM filter cakes at HTHP after aging conditions.

Even that the conditions of the different filter cakes were very similar up to 200 °F the images show clearly the effect of degradation of chemicals at 250 °F and how it affected

the final condition of the KCL/PHPA filter-cake, leading to higher spurt-loss and filtrate volume compared to a more uniform and compact NP-WBM filter-cake.

5.2. RHEOLOGICAL BEHAVIOR ANALYSIS

Dynamic aging also helped to evaluate the response of NP to preserve the rheological stability of the WBM as well as the behavior of the KCL/PHPA fluid. Figure 5.4. and Figure 5.5 shows the rheograms of both systems at the different aging temperatures.

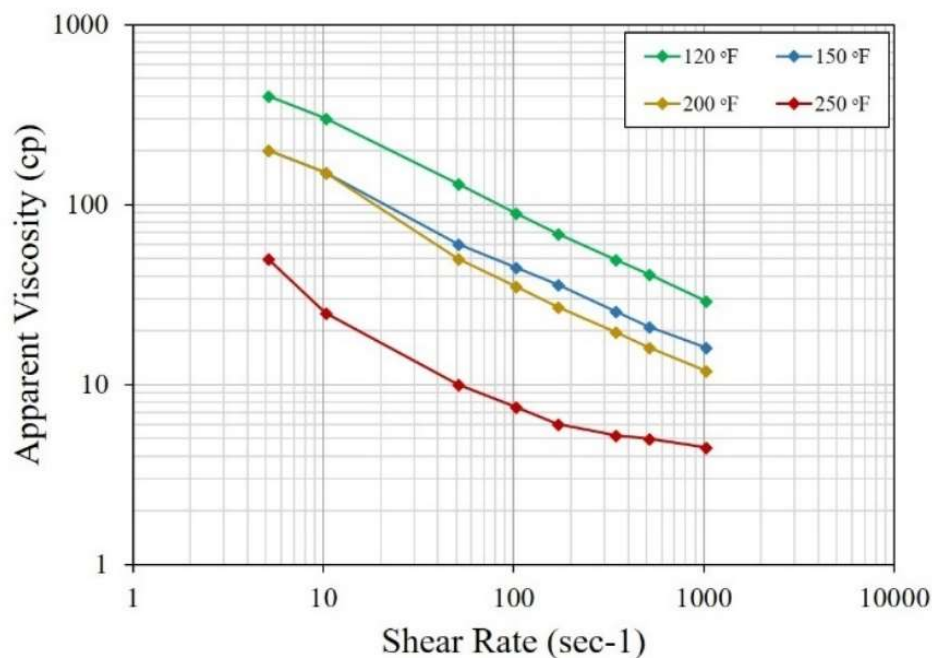


Figure 5.4. Rheogram of KCL/PHPA fluid at different aging conditions.

In general, the apparent viscosity of both fluids tested in this research experienced a decrease as the shear rate was increased which is desirable in drilling fluids (i.e. shear-thinning behavior). However, it became evident that the response of the KCL/PHPA fluid

was poor against the temperature increments losing all its rheological properties at 250 °F, adding products as lignosulfonates could improve the KCL/PHPA behavior at higher temperatures, but this will also add more environmental issues due to the increase of chemicals needed to treat the fluids and cuttings.

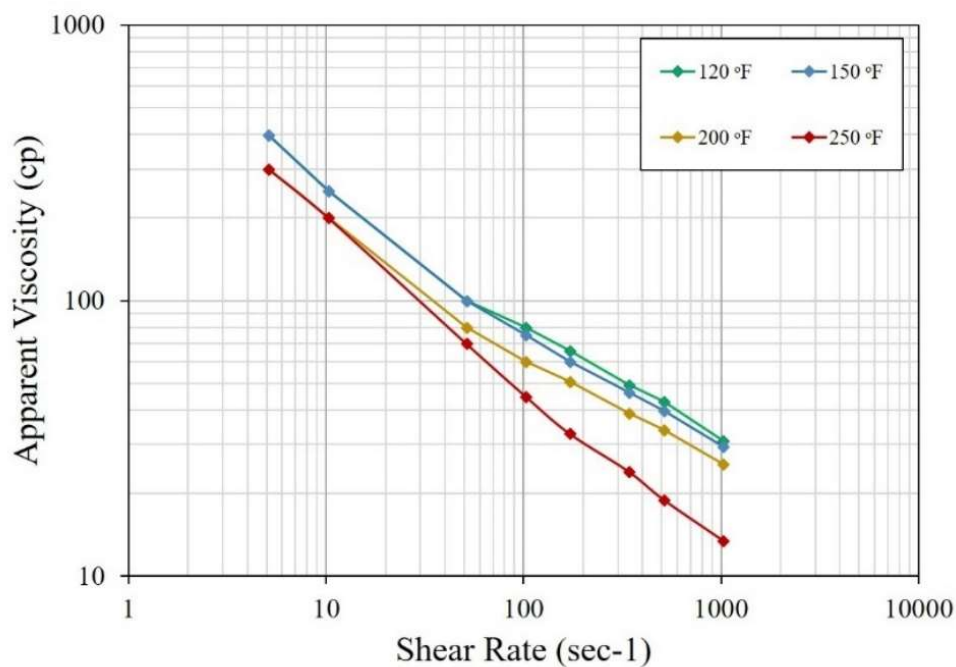


Figure 5.5. Rheogram of NP-WBM at different aging conditions.

On the other hand, the behavior observed for the NP-WBM was more stable along the different temperatures, which might indicate a potential ability of the NP to ‘shield’ the system against the temperature and its effects on the rheological properties. Figure 5.6 and Figure 5.7 illustrate the effect of temperature on the PV and YP behavior of KCL/PHPA and NP-WBM respectively due to different aging conditions. The rheology was measured at 120 °F as the standard of API.

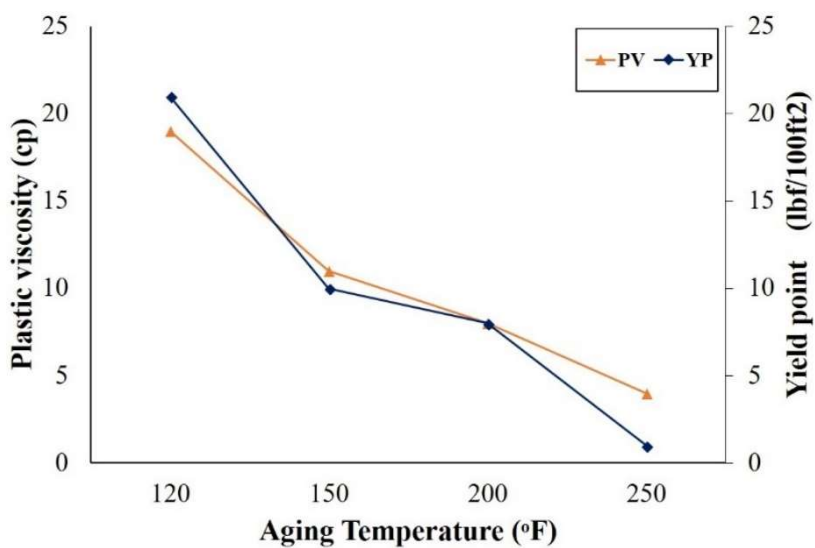


Figure 5.6. KCL/PHPA PV and YP at different aged conditions.

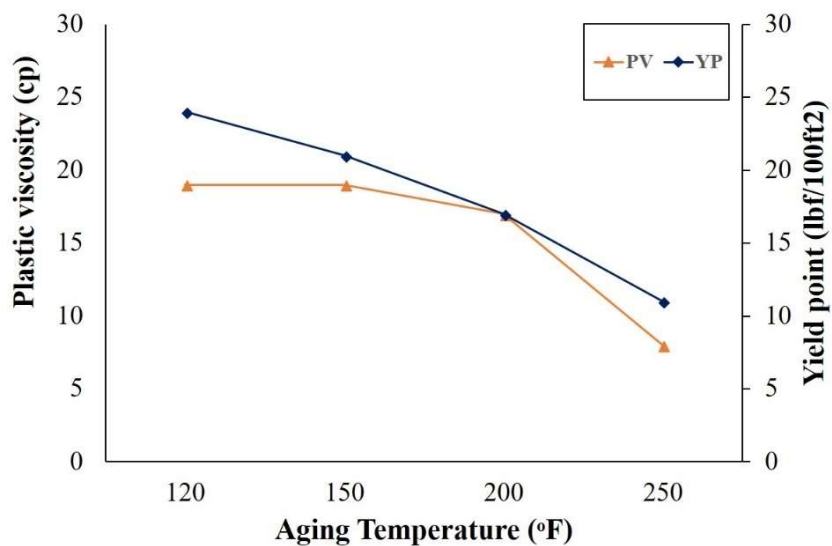


Figure 5.7. NP-WBM PV and YP at different aged conditions.

The decrease of PV and YP due to increases in temperatures are usually found in shear-thinning fluids. The critical zone started when the PV become higher than the YP, which can be understood as the capacity of the drilling fluid to transport cuttings to the

surface. At this point, the hole cleaning capabilities of the drilling fluid are diminished and can lead to different wellbore conditions (e.g. pack-off, increases in pump pressure). In the case of the KCL/PHPA, this condition was reached at 150 °F with a very steep slope, which might suggest a possible hydrolysis of polymers leading to a poor YP. The KCL/PHPA exhibited a transitional zone until 200 °F; still, the numerical values of the YP indicated no carrying capacity of the fluid and total loss of the rheological properties were experienced at 250 °F.

NP-WBM behavior was more stable as the aged temperature was increased. The YP was higher almost during the entire spectrum of temperature. The values suggested a good condition up to 200 °F. Despite that YP was higher than PV at 250 °F the decrease of the YP respect to the previous stage was almost a 35%. Still, the NP inclusion on the WBM formulation indicated a favorable ability to control the rate of decrease on YP.

In general, the NP-WBM ensured a better rheological behavior compared to the KCL/PHPA. NP-WBM used almost 60% fewer polymers to provide viscosity and increasing its concentration could lead to higher YP values at the 250°F temperature range. However, this can increase costs and reduce the interparticle spaces leading to a non-desirable condition of the NP. Thus, more studies should be performed on these type of fluids to improve the overall properties at higher temperatures without compromising the formulation and the NP stability.

Figure 5.8. and Figure 5.9. illustrate the gel strength of the NP-WBM and KCL/PHPA at different aged conditions.

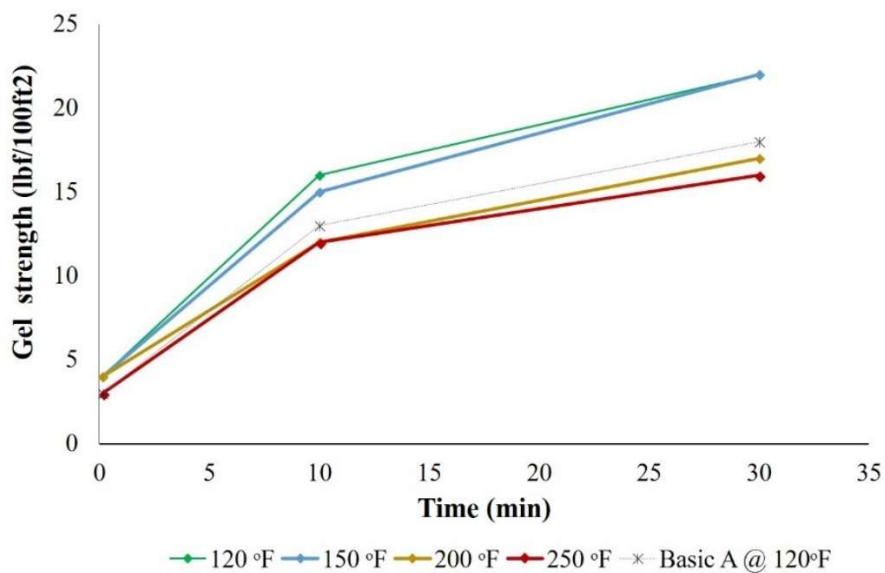


Figure 5.8. NP-WBM gel strength at different aging conditions.

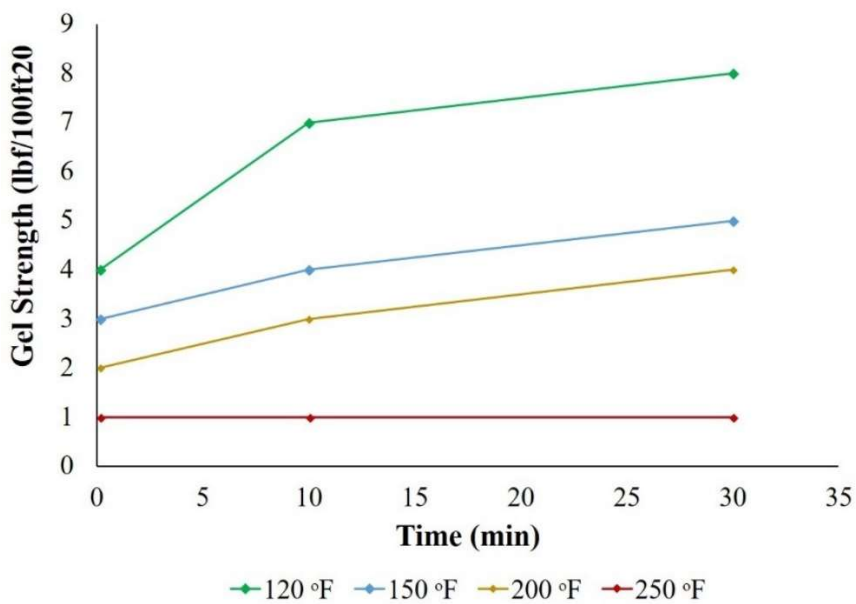


Figure 5.9. KCL/PHPA gel strength at different aging conditions.

The initial effect of NP on the gel strength of the Basic A fluid showed a slight increase probably due to the interaction between the negative charge surfaces of the clays

with the NP that have the same charge; and thus, under prolonged period of time with no excessive temperature the polymers and clays exhibit a better hydration process as well as thixotropy capability with no progressive gels. When the temperature started to increase above 150 °F, a decreased in gel strength was experienced. The latter could be caused by the dissociation of clay particles in smaller pieces and the same effect of differences in surface charge cause them to be keep dispersed in the drilling fluid, reducing the gel structure. Still, the values observed until 250 °F were able to form a gel structure under static conditions demonstrating the short and long-term stability of the NP-WBM to fulfill its functional task to suspend drilling cuttings under static conditions.

The capability of NP-WBM to avoid very high gel strength is a positive characteristic of the system because high gel conditions can difficult the separation of cuttings at the shakers as well as lose considerable volume of drilling fluid due to the high viscosity that the surface equipment cannot handle as well as a increments in the pressure required to re-establish circulation that can lead to a fracture into the formation. Other researchers found comparable results (Amanullah, 2011).

In the case of the KCL/PHPA, it is also observed that no tendency to form progressive gels exist, which is a positive characteristic as described before. However, the poor thermal stability attached to the degradation of chemicals lead to a poor gel structure that under static conditions might not suspend efficiently the drilling cuttings in the annular space. This can cause several attempts to drill string pack-off due to cuttings recirculated in the wellbore wall, especially in directional wells between 30° to 60° degrees of inclination where the bed cutting formation become a problem.

Finally, the experimental data obtained with the rheometer for each aged conditions were used as input parameters to fit the Herschel-Bulkley model and with the least square method estimated predicted rheological values as well as n (flow behavior index) and K (consistency index). Regression coefficient (R^2) and the sum of square errors were used to evaluate the fit between the calculated and the experimental data. Table 5.2 and Table 5.3 present the model constant that best described the fluid behavior at the different aged conditions for both, NP-WBM and KCL/PHPA.

Table 5.2. Herschel-Bulkley constants at different aging conditions for NP-WBM.

NP-WBM		Herschel-Bulkley Model			
Temperature (°F)	τ_0 (lbf/100ft ²)	K (lbf*sec ⁿ /100ft ²)	n	R^2	ΣQ^2 [(lbf/100ft ²) ²]
120	0.905	1.0212	0.593	0.9991	2.569
150	1.096	0.912	0.6	0.9991	2.309
200	0.863	0.649	0.629	0.9989	2.158
250	1.788	0.585	0.543	0.9992	0.346
BASIC A		Herschel-Bulkley Model			
Temperature (°F)	τ_0 (lbf/100ft ²)	K (lbf*sec ⁿ /100ft ²)	n	R^2	ΣQ^2 [(lbf/100ft ²) ²]
120	0.044	0.636	0.638	0.9991	0.206

In the case of the NP-WBM the addition of NP to the basic A fluid, improved the yield stress which warranty a better suspension of the drilled cutting while carrying them out to the surface providing a better integrity of the cuttings and hole-quality. Likewise, this advantage can help to reduce the erosion of cutting as well as the presence of

recirculated cuttings that might lead to particles with the higher surface area and sudden increases in fluid density.

Table 5.3. Herschel-Bulkley constants at different aging conditions for KCL/PHPA.

KCL/PHPA	Herschel-Bulkley Model				
	τ_0 (lbf/100ft ²)	K (lbf*sec ⁿ /100ft ²)	n	R ²	ΣQ^2 [(lbf/100ft ²) ²]
Temperature (°F)					
120	0.128	1.252	0.545	0.9992	1.88
150	0.795	0.532	0.587	0.9993	0.473
200	0.143	0.486	0.561	0.9977	0.974
250	0.49	0.009	0.99	0.9963	0.215

Also, the increase of K with the reduction of n is related to a better viscosity profile, which also improves the NP-WBM hydraulics, so needed in the horizontal sections of the unconventional shales. During the different aging conditions, it was observed that the NP helped to keep the non-Newtonian behavior as stable as possible while the temperature was increased. The latter suggested that at high temperatures the NP might absorb a great portion of the heat on the surrounding that otherwise could impact negatively in the polymers and/or bentonite structure affecting the overall performance of the drilling fluid.

In the case of the KCL/PHPA, its behavior indicated an acceptable performance to temperatures close to 200 °F. However, once the system is exposed during long periods of

time under these temperatures became evident that a total degradation of the system is experienced. The model indicated that practically the KCL/PHPA become a Newtonian fluid with n value almost equal to one and K to zero. In other words, it started to acts like water.

5.3. INHIBITION CHARACTERISTICS ON THE WOODFORD SHALE

Previously the NP-WBM inhibition capability was evaluated individually during its design. This subsection presents the results of the KCL/PHPA capabilities to protect the Woodford shale samples against inhibition. Figure 5.10 presents the result of the dispersion test on KCL/PHPA.

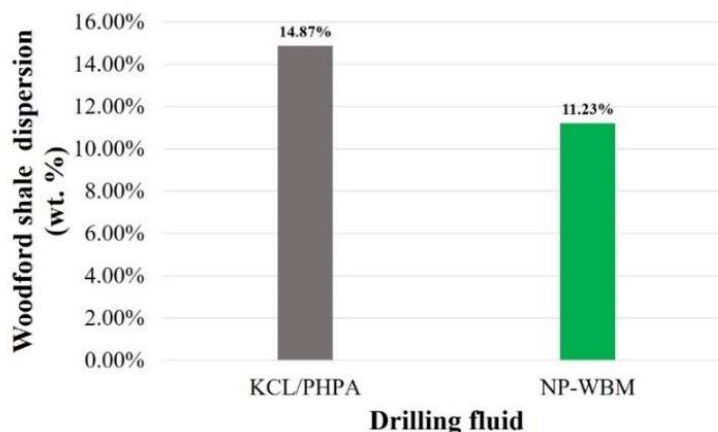


Figure 5.10. Woodford shale dispersion in KCL/PHPA.

The results indicated that 85.13% of the shale mass was recovered when the shale was exposed to KCL/PHPA. This is an acceptable result since it yields to a 32.5% reduction compared to distilled water analyzed before. Nevertheless, the situation with the

KCL/PHPA fluid goes back to its poor thermal stability that causes a decrease in pH conditions and generated the poor performance of polymers. Also, due to the absence of correct bridging agents, the fissures in the shale surface are exposed to the fluid invasion which aggravates the erosion effect if compared to the NP-WBM capability. Figure 5.11 and Figure 5.12 present the effect of temperature and time on the shale surface of the Woodford sample when exposed to KCL/PHPA for 14 days at 150°F.

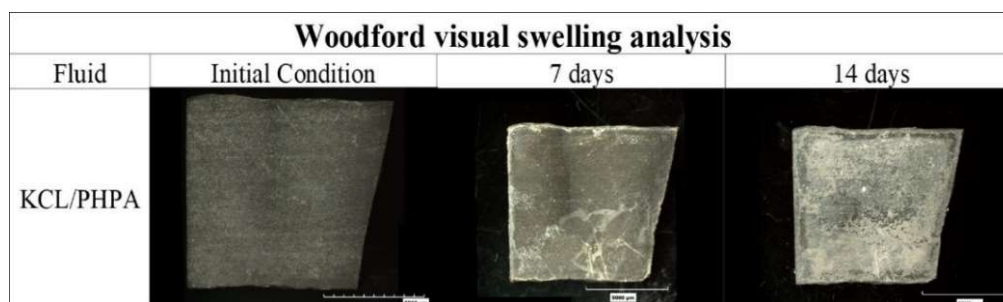


Figure 5.11. Woodford visual swelling in KCL/PHPA.

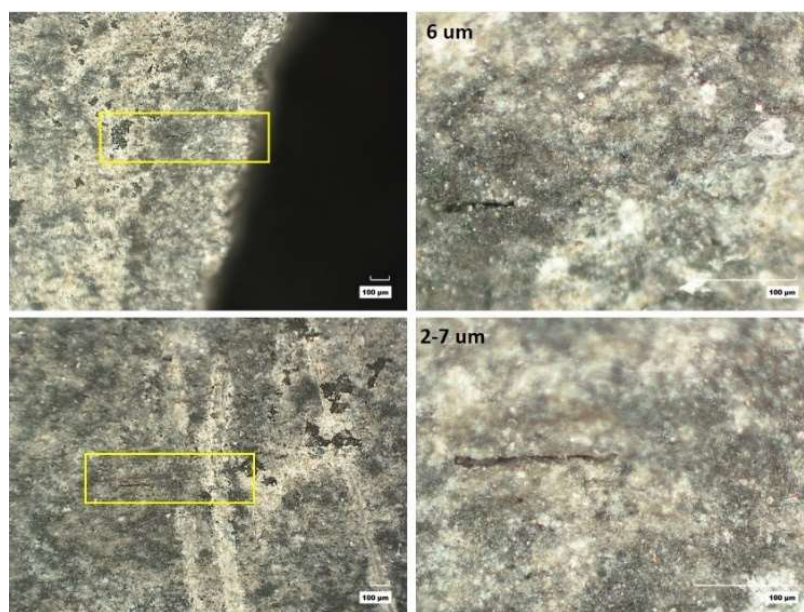


Figure 5.12. Micro-fractures exposed due to KCL/PHPA fluid.

Since the ions available in the Woodford shale are limited due to its mineralogical characteristics, the KCL has little effect on protecting the shale formation. The main actor of the system is the partially polyacrylamide cellulose (PHPA) that tend to coat the shale sample to restrict interaction with water. Samples immersed in distilled water experienced dissolution of minerals that exposed long micro-fractures (>2 cm) along the bedding planes (Section 4.3.6.2.), KCL/PHPA compared to this condition was able to protect most of the micro-fractures present in the shale surface. Just very small areas remain uncovered, which lead to a partial exposure of the micro-fracture as observed in Figure 5.12.

The solution could be addressed by increasing concentration of material; however, since the KCL/PHPA system does not include a correct bridging particle distribution the chances to dissolve the cementation in the silica-filled micro-fractures still represent a problem. This is one of the reasons NP-WBM might be more adequate to the formation, but only if a correct distribution between NP and conventional LCM additives are present in the formulation and a chemical compatibility exists. Finally, Figure 5.13. shows the bulk swelling experience in the Woodford shale sample when exposed to the KCL/PHPA fluid during 24 Hrs.

The reasons behind the results of the shale sample immersed in the KCL/PHPA compared to the one exposed to NP-WBM are all related to the fluid design considerations and conditions explained before in the visual and dispersion tests. Furthermore, this research might indicate that the drilling fluid design is the one that should fit the characteristics of the formation and not the opposite since one fluid does not fit all the formation (Lal, 1999).

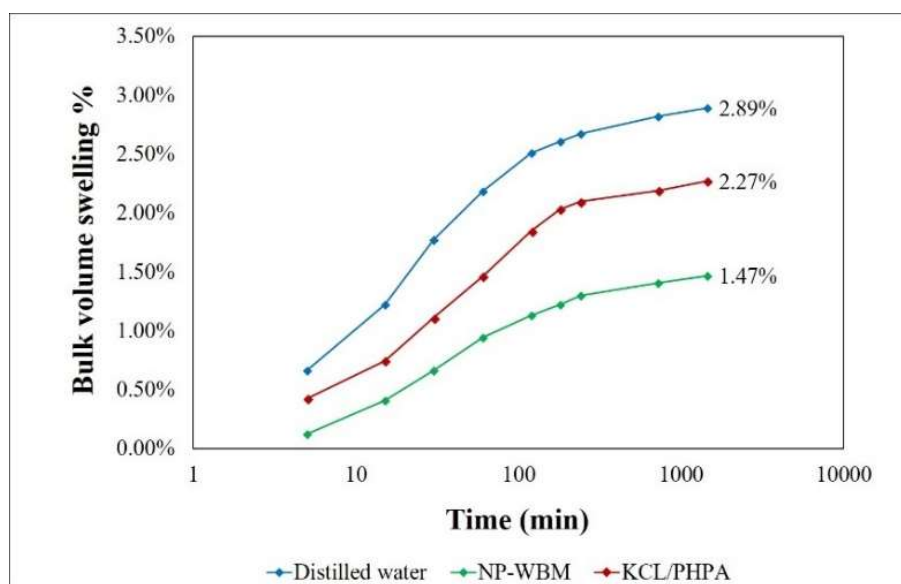


Figure 5.13. Bulk swelling of the Woodford shale in KCL/PHPA.

6. CONCLUSION AND RECOMMENDATIONS

6.1. CONCLUSIONS

This thesis provided an extensive laboratory analysis to evaluate the potential use of two different NP systems in a single formulation to improve the performance of WBM applied to unconventional reservoirs. The methodology was oriented on the premise that the drilling fluid should be design based on the characteristics of the formation intended to drill. Untreated NP were used at low concentration with no drastic alterations in pH or density of the drilling fluids. Despite the low concentration applied improvements were observed in terms of cutting integrity, filtrate reduction, and drilling fluid stability at different aging conditions. Furthermore, it was observed that a synergistic effect can take place between conventional LCM graphite and NP, which can contribute to cost reductions and design optimization of an environmental friendlier WBM. For clarity, the main points collected during the study and analysis results are presented below.

- 1.) Mineral composition of the Woodford shale helped to understand that the hydraulic flow was the predominant shale hydration mechanism. Additionally, the SEM results and the pore size estimation allowed to select the appropriate NP size and shape that yield to 49.13% bulk swelling reduction compared to the 21.45% reached with the KCL/PHPA mud.
- 2.) The NP stability tests suggested that the NP-WBM system might withstand brine or formation water contamination with salinity concentration up to 15000 ppm in the entire system. Also, indicating that NP-WBM should not experience any

instability issues when water sources at field condition are used as the aqueous phase.

- 3.) The preferable pH range of 8 to 10, increased the stability of NP in the drilling fluid as well as the compatibility with common filtrate control and rheological modifiers additives that are known to perform better in this range. So, no previous adjustments in pH should be made to mix NP with conventional products.
- 4.) In general, the results obtained with low NP concentration suggested that there is no need of surfactants to stabilize the colloidal solution as long as a zeta-potential measurement indicated absolute values above 30 mV, which was the case with both, silica, and graphene NP.
- 5.) The optimum NP-WBM formulation help to reduce the filtrate volume to 20.93% and 27.21% for LTLP and HTHP conditions respectively, which demonstrate the NP ability to reduce fluid invasion. Also, a reduction in cake thickness of about 10% in both test was observed, reducing the risk of stuck pipes.
- 6.) Initially, KCL/PHPA demonstrated a better filtrate capacity at room conditions. However, as temperature increased simulating wellbore conditions the response of the KCL/PHPA respect to the NP-WBM was very poor. It was evident how the polymers suffered from a high degradation rate, especially when aging conditions were > 200 °F showing a reduction in filtration capacity of the KCL/PHPA of 23.71% while NP-WBM only experienced 0.99% with no spurt-loss volume.
- 7.) The behavior of the NP-WBM during the aging tests confirmed the initial believed that NP can dissipate or absorb heat, and thus, protect the other chemicals in the

formulation. The impact on filtration and rheological properties was minimum until temperatures of 200 °F, which are above the 180 °F registered for Woodford.

- 8.) NP-WBM improved the shale cuttings integrity reducing their dispersion by 11.23% while KCL/PHPA system experienced an acceptable performance of 14.87%. this added to better rheological properties of the NP-WBM might help to improve the hole cleaning efficiency, reducing the risk of sudden pore pressure increments due to higher % LGS in the system resulted from a poor inhibition.
- 9.) Visual swelling tests allowed to identified the silica-filled micro-fractures along the bedding planes that can be exposed if an incorrect fluid formulation is used. Besides, it confirms the advantage of including the graphene nanoplatelets and the conventional graphite to help form a better bridge condition to avoid the dissolution of minerals in the micro-fracture and its further exposure to fluid invasion.
- 10.) Herschel-Bulkley model fitted the rheological behavior of the NP-WBM with an excellent precision with R^2 values > 0.99 . Also, the model indicated that NP increased the yield stress of the basic system as well as improving the viscosity profile, which leads to better hole cleaning condition in deviated and horizontal wells.
- 11.) Overall, the research indicated that NP might have a huge potential as HTHP drilling fluid additive, improving the characteristics of the WBM with minimum affectation in density and rheology. The advantage of NP to enhance the thermal stability of WBM system support the idea of a synergistic effect that can take place with the conventional additives, reducing the cost associated to the design of NP-

WBM and extending the WBM application to harsher environments while reducing the footprints of the drilling operations.

6.2. RECOMMENDATION FOR FUTURE WORK

The primary objective of this research was to evaluate the potential inclusion of NP at low concentration in WBM for unconventional shales. An experimental investigation of how NP affect mud properties and improve the inhibition capabilities were carried out following a methodology that initially characterizes the rock formation and the NP and later examined how these NP modified positively or negatively the mud's properties with respect to nanoparticle concentration, size, type, aging, and temperature. Even though the current study was thorough, it still has scope for extension and improvements in future. A few recommendations related to extending this work are presented below.

- 1.) Core flooding test to evaluate the NP capability to reduce the permeability of the near-wellbore region should be addressed to physically evaluate the ability of NP to plug nanopores. The inclusion of fractured cores will also extend the analysis of combining known LCM materials and NP.
- 2.) Uniaxial or Triaxial compression tests that simulated different overbore conditions, can help to better evaluate the effect of NP on the wellbore strengthening and related them to the plugging mechanism.
- 3.) Initially, difficulties were experienced with the NP-WBM preparation due to strong adhesion of NP in powder form. This issue was solved by including two steps, ultrasonication, and high shear rates. These are not available at field scale; a deep analysis should be addressed to find an easier mechanism to prepare NP-WBM than

can be replicated at field scale. A potential solution could be the generation of in-situ NP in WBM or evaluate the use of liquid formulation with no drying steps.

- 4.) Thermal conductivity tests of these NP and other ones should be included in a future project to better characterized the nanomaterials and estimate its real application at higher temperatures for WBM based on quantitative results that can estimated the improvement at aged conditions for the NP-WBM.
- 5.) Imaging techniques like SEM should be run to NP-WBM filter cake to evaluate the interactions of NP, conventional LCM, and other additives in the permeability reduction of the filter cake and its effects on filtrate reduction.
- 6.) Incorporate FIB-SEM techniques to refine the characterization of the pore structure of the Woodford shales that can lead to a more precise selection of the NP material. Also, the same analysis should be performed to cores already exposed to NP-WBM. The latter can help to better understand the plugging mechanism and capability of the NP.

REFERENCES

- Abdo, J., & Haneef, M. D. (2012). Nano-Enhanced Drilling Fluids: Pioneering Approach to Overcome Uncompromising Drilling Problems. *Journal of Energy Resources Technology*, 134(1), 14501. <https://doi.org/10.1115/1.4005244>.
- Abrams, A. (1977). Mud Design To Minimize Rock Impairment Due To Particle Invasion. *Journal of Petroleum Technology*, 29(5), 586–592. <https://doi.org/10.2118/5713-PA>.
- Aftab, A., Ismail, A. R., & Ibupoto, Z. H. (2017). Enhancing the rheological properties and shale inhibition behavior of water-based mud using nanosilica, multi-walled carbon nanotube, and graphene nanoplatelet. *Egyptian Journal of Petroleum*, 26(2), 291–299. <https://doi.org/10.1016/j.ejpe.2016.05.004>.
- Agrawal, A., Wei, Y., & Holditch, S. (2012). A Technical and Economic Study of Completion Techniques in Five Emerging US Gas Shales: A Woodford Shale Example. *SPE Drilling & Completion*, 27(1), 39–49. <https://doi.org/10.2118/135396-PA>.
- Al-Bazali, T. M., Chenevert, M. E., & Sharma, M. M. (2005). Experimental study of the membrane behavior of shale during interaction with water-based and oil-based muds, 3165086, 306-306.
- Al-marhoun, M. A. (1990). The Effect of High Temperature, High Pressure, and aging on Water-Based Drilling Fluids.
- Ali, M., Hascakir, B., & Texas, A. (2016). Water / Rock Interaction for Eagle Ford, Marcellus, Green River, and Barnett Shale Samples and Implications for Hydraulic-Fracturing-Fluid Engineering. *SPE Journal*, (February), 17–22. <https://doi.org/10.2118/177304-PA>.
- Amanullah, M., Al-Arfaj, M. K., & Al-Abdullatif, Z. (2011). Preliminary test results of nano-based drilling fluids for oil and gas field application. *SPE/IADC Drilling Conference, Proceedings*, 1(1965), 112–120. <https://doi.org/10.2118/139534-MS>.
- American Petroleum Institute, A. (2000). Recommended Practice Standard Procedure for Laboratory Testing Drilling Fluids Recommended Practice Standard Procedure for Laboratory Testing Drilling Fluids, (May).
- Anderson, R. L., Ratcliffe, I., Greenwell, H. C., Williams, P. A., Cliffe, S., & Coveney, P. V. (2010). Clay swelling - A challenge in the oilfield. *Earth-Science Reviews*, 98(3–4), 201–216. <https://doi.org/10.1016/j.earscirev.2009.11.003>.

- Arthur, J. D. (2009). Environmental Considerations of Modern Shale Gas Development. *Arthur, J. D. (2009). Environmental Considerations of Modern Shale Gas Development, 4–7.*, (October), 4–7. <https://doi.org/10.2118/122931-MS>.
- Aston, M. S., Alberty, M. W., Duncum, S. D., Bruton, J. R., Friedheim, J. E., & Sanders, M. W. (2007). A New Treatment for Wellbore Strengthening in Shale. *SPE Annual Technical Conference and Exhibition*. <https://doi.org/10.2118/110713-MS>.
- Aston, M. S., & Elliott, G. P. (1994). Water-based glycol drilling muds: Shale inhibition mechanisms. *European Petroleum Conference, (1/-)*, 107–113.
- Baker-Hughes. (n.d.). Drilling Fluids Reference Manual.
- Beihoffer. (1990). The Development of an Inhibitive Cationic Drilling Fluid for Slim-hole Coring Applications.
- Benaissa, S. (1997). Oil Field Applications of Aluminum Chemistry and Experience with Aluminum-Based Drilling Fluid Additive.
- Bhatia, K., & Chacko, L. (2011). Ni-Fe Nanoparticles: An Innovative Approach for Recovery of Hydrates. *Proceedings of SPE EUROPEC/EAGE Annual Conference and Exhibition, (May)*, 23–26. <https://doi.org/10.2118/143088-MS>.
- Bhattacharjee, S. (2016). DLS and zeta potential - What they are and what they are not? *Journal of Controlled Release, 235*, 337–351. <https://doi.org/10.1016/j.jconrel.2016.06.017>.
- Bol, G. M., Wong, S.-W., Davidson, C. J., & Woodland, D. C. (1994). Borehole Stability in Shales. *SPE Drilling & Completion, 9(2)*, 87–94. <https://doi.org/10.2118/24975-PA>.
- Boul, P. J., Reddy, B. R., Hillfiger, M., O'connell, T. P., & Thaemlitz, C. (2016). OTC-26902-MS Functionalized Nanosilicas as Shale Inhibitors in Water-Based Drilling Fluids, (January), 2–5. <https://doi.org/10.4043/26902-MS>.
- Bui, B. T., & Tutuncu, A. N. (2018). Modeling the swelling of shale matrix in unconventional reservoirs. *Journal of Petroleum Science and Engineering, 165(March)*, 596–615. <https://doi.org/10.1016/j.petrol.2018.01.043>.
- Bourgoyne, (1986). Applied drilling engineering, SPE Textbook series, vol 2.
- Bunch, J. S.; Verbridge, S. S.; Alden, J. S. Van der Z., & A. M.; Parpia, J. M.; Craighead, H. G.; McEuen, P. L. (2008). Impermeable Nano, Atomic Membranes from Graphene Sheets., *Lett.* 2008, 8, 2458–2462.

- Cademartri, L., & Geoffrey, A. O. (2009). Concepts of Nanochemistry. *Wiley-Vch Textbook*, 261. <https://doi.org/10.1039/c3cs60054h>.
- Caenn, R. & Chillingar G.V. Drilling fluids: State of the art. *Journal of Petroleum Science and Engineering*, Volume 14, Issues 3–4, 1996, Pages 221-230, [https://doi.org/10.1016/0920-4105\(95\)00051-8](https://doi.org/10.1016/0920-4105(95)00051-8).
- Cai, J., Chenevert, M. E., Sharma, M. M., & Friedheim, J. E. (2012). Decreasing Water Invasion Into Atoka Shale Using Nonmodified Silica Nanoparticles. *SPE Drilling & Completion*, 27(1), 103–112. <https://doi.org/10.2118/146979-PA>.
- Chakraborty, S., Agrawal, G., Digiovanni, A., & Scott, D. (2012). The Trick Is The Surface – Functionalized Nanodiamond PDC Technology. *SPE International Oilfield Nanotechnology Conference and Exhibition*, (June), 12–14. <https://doi.org/10.2118/157039-MS>.
- Charlez, P. A., & Delfiner, P. (2016). A Model for Evaluating the Commerciality of an Unconventional Factory Development Outside of North America. *SPE Economics & Management*, 8(2), 40–49. <https://doi.org/10.2118/179735-PA>.
- Chatterjee, S., Wang, J. W., Kuo, W. S., Tai, N. H., Salzmann, C., Li, W. L., ... Chu, B. T. T. (2012). Mechanical reinforcement and thermal conductivity in expanded graphene nanoplatelets reinforced epoxy composites. *Chemical Physics Letters*, 531, 6–10. <https://doi.org/10.1016/j.cplett.2012.02.006>.
- Chenevert, M. E. (1970). Shale Alteration by Water Adsorption. *Journal of Petroleum Technology*, 22(9), 1141–1148. <https://doi.org/10.2118/2401-PA>.
- Chenevert, M. E., & Osisanya, S. O. (1989). Shale/Mud Inhibition Defined With Rig-Site Methods. *SPE Drilling Engineering*, 4(3), 261–268. <https://doi.org/10.2118/16054-PA>.
- Chesser, B. G., Clark, D. E., & Wise, W. V. (1994). Dynamic and Static Filtrate-Loss Techniques for Monitoring Filter-Cake Quality Improves Drilling-Fluid Performance. *SPE Drilling & Completion*, 9(3), 89–92. <https://doi.org/10.2118/20439-PA>.
- Chesser, B. G., & Enright, D. P. (2013). High-Temperature Stabilization of Drilling Fluids With a Low-Molecular-Weight Copolymer. *Journal of Petroleum Technology*, 32(6), 950–956. <https://doi.org/10.2118/8224-PA>.
- Chilingar, G. V., & Haroun, M. (2014). Introduction to Electrokinetics.

- Contreras, O., Hareland, G., Husein, M., Nygaard, R., & Alsaba, M. (2014). Experimental Investigation on Wellbore Strengthening in Shales by Means of Nanoparticle-Based Drilling Fluids. *SPE Annual Technical Conference and Exhibition*, (August 2015), 1–16. <https://doi.org/10.2118/170589-MS>.
- Corbett, J. C. W., McNeil-Watson, F., Jack, R. O., & Howarth, M. (2012). Measuring surface zeta potential using phase analysis light scattering in a simple dip cell arrangement. *Colloids and Surfaces A: Physicochemical and Engineering Aspects*, 396, 169–176. <https://doi.org/10.1016/j.colsurfa.2011.12.065>.
- Craig, R. F. (2013). *Craig's Soil Mechanics. Journal of Chemical Information and Modeling* (Vol. 53). <https://doi.org/10.1017/CBO9781107415324.004>.
- Cullity. (1978). B.D. Cullity, *Elements of X-ray Diffraction*, 2nd ed., Addison Wesley, London, 1978.
- Deville, J. P., Fritz, B., & Jarrett, M. (2011). Development of Water-Based Drilling Fluids Customized for Shale Reservoirs. *SPE Drilling & Completion*, 26(4), 484–491. <https://doi.org/10.2118/140868-PA>.
- El-Diasty, A. I., & Ragab, A. M. S. (2013). Applications of Nanotechnology in the Oil & Gas Industry: Latest Trends Worldwide & Future Challenges in Egypt. *North Africa Technical Conference and Exhibition*, 1–13. <https://doi.org/10.2118/164716-MS>.
- Esmaceli, A. (2009). APPLICATIONS OF NANOTECHNOLOGY IN OIL AND GAS INDUSTRY Importance of Nanotechnology in Industry Nanotechnology and Gas Industry. *Nanotechnology*, (January), 1–6.
- Fakoya, M. F., & Shah, S. N. (2014). Enhancement of Filtration Properties in Surfactant-Based and Polymeric Fluids by Nanoparticles. *SPE Eastern Regional Meeting*, 1–12. Retrieved from <https://www.onepetro.org/download/conference-paper/SPE-171029-MS?id=conference-paper%2FSPE-171029-MS>.
- Fakoya, M. F., & Shah, S. N. (2017). Emergence of nanotechnology in the oil and gas industry: Emphasis on the application of silica nanoparticles. *Petroleum*, 1–15. <https://doi.org/10.1016/j.petlm.2017.03.001>.
- Gazaniol, D., Forsans, T., Boisson, M. J. F., & Piau, J. M. (1995). Wellbore Failure Mechanisms in Shales - Prediction and Prevention. *Journal of Petroleum Technology*, 47(7), 589–595. <https://doi.org/10.2118/28851-PA>.
- Geng, Y., Wang, S. J., & Kim, J. K. (2009). Preparation of graphite nanoplatelets and graphene sheets. *Journal of Colloid and Interface Science*, 336(2), 592–598. <https://doi.org/10.1016/j.jcis.2009.04.005>.

- Ghanbari, S., Kazemzadeh, E., Soleymani, M., & Naderifar, A. (2016). A facile method for synthesis and dispersion of silica nanoparticles in water-based drilling fluid. *Colloid and Polymer Science*, 294(2), 381–388. <https://doi.org/10.1007/s00396-015-3794-2>.
- Goud, M. C., & Joseph, G. (2006). Drilling Fluid Additives and Engineering to Improve Formation Integrity. *IADC/SPE Drilling Conference and Exhibition*.
- Gree, A. De. (2015). The History and Working Principle of the Scanning Electron Microscope (SEM), 1–8.
- Gupta, N., Rai, C. S., & Sondergeld, C. H. (2013). Petrophysical Characterization of the Woodford Shale. *Petrophysics*, 54(4), 368–382.
- He, S., Liang, L., Zeng, Y., Ding, Y., Lin, Y., & Liu, X. (2016). The influence of water-based drilling fluid on mechanical property of shale and the wellbore stability. *Petroleum*, 2(1), 61–66. <https://doi.org/10.1016/j.petlm.2015.12.002>.
- Hoelscher, K. P., De Stefano, G., Riley, M., & Young, S. (2012). Application of Nanotechnology in Drilling Fluids. *SPE International Oilfield Nanotechnology Conference and Exhibition*, (June), 12–14. <https://doi.org/10.2118/157031-MS>.
- Holditch, S. A. (2009). The Role of IOCs and NOCs in Developing Unconventional Oil and Gas Reservoirs. *The Way Ahead*, 5(3), 7–9.
- Horikoshi, S., & Serpone, N. (2013). *Introduction to Nanoparticles*. <https://doi.org/doi:10.1002/9783527648122.ch1>.
- Hoxha, B. B., Oort, E. van, & Daigle, H. (2017). How Do Nanoparticles Stabilize Shale? *SPE International Conference on Oilfield Chemistry*, (April), 3–5. <https://doi.org/10.2118/184574-MS>.
- Hoxha, B. B., Sullivan, G. J., Van Oort, E., Daigle, H., & Schindler, C. (2016). Determining the zeta potential of intact shales via electrophoresis. *78th EAGE Conference and Exhibition 2016: Efficient Use of Technology - Unlocking Potential*, (June).
- Jain, R., Mahto, V., & Sharma, V. P. (2015). Evaluation of polyacrylamide-grafted-polyethylene glycol/silica nanocomposite as potential additive in water-based drilling mud for reactive shale formation. *Journal of Natural Gas Science and Engineering*, 26, 526–537. <https://doi.org/10.1016/j.jngse.2015.06.051>.
- Jenkins, R. E. (1966). Accuracy of porosity determinations. *SPWLA 1st Annual Logging Symposium*, (July-August), 29–34.

- Ji, L., Guo, Q., Friedheim, J., Zhang, R., Chenevert, M., & Sharma, M. (2012). Laboratory Evaluation and Analysis of Physical Shale Inhibition of an Innovative Water-Based Drilling Fluid with Nanoparticles for Drilling Unconventional Shales. *SPE Asia Pacific Oil and Gas Conference and Exhibition*, (Sandrea 2006), 1–12. <https://doi.org/http://dx.doi.org/10.2118/158895-MS>.
- Kang, Y., She, J., Zhang, H., You, L., & Song, M. (2016). Strengthening shale wellbore with silica nanoparticles drilling fluid. *Petroleum*, 2(2), 189–195. <https://doi.org/10.1016/j.petlm.2016.03.005>.
- Korada, V. S. (2017). *Engineering Applications of Nanotechnology*. <https://doi.org/10.1007/978-3-319-29761-3>.
- Kosynkin, D. V., Ceriotti, G., Wilson, K. C., Lomeda, J. R., Scorsone, J. T., Patel, A. D., Tour, J. M. (2012). Graphene oxide as a high-performance fluid-loss-control additive in water-based drilling fluids. *ACS Applied Materials and Interfaces*, 4(1), 222–227. <https://doi.org/10.1021/am2012799>.
- Krishnamoorti, R. (2006). Extracting the Benefits of Nanotechnology for the Oil Industry. *Journal of Petroleum Technology*, 58(11), 24–26. <https://doi.org/10.2118/1106-0024-JPT>.
- Lal, M. (1999). Shale Stability: Drilling Fluid Interaction and Shale Strength. *SPE Asia Pacific Oil and Gas Conference and Exhibition*. <https://doi.org/10.2118/54356-MS>.
- Laughrey, C. D., Purrazzella, P., & Hooghan, K. (Bobby). (2017). Petroleum Geochemistry and Mudstone Diagenesis of the Woodford Shale, Anadarko Basin, USA – An Integrated Approach. In *Proceedings of the 5th Unconventional Resources Technology Conference*. <https://doi.org/10.15530/urtec-2017-2691776>.
- Li, S., Osisanya, S., & Haroun, M. (2016). Development of New Smart Drilling Fluids Using Nano-Materials for Unconventional Reservoirs Introduction and Previous Work Done on Smart Drilling Fluids Methodology. *Spe*.
- Mahmoud, O., Nasr-El-din, H. A., Vryzas, Z., & Kelessidis, V. C. (2018). Using ferric oxide and silica nanoparticles to develop modified calcium bentonite drilling fluids. *SPE Drilling and Completion*, 33(1), 24–26.
- Mahmoud, O., Nasr-El-Din, H. A., Vryzas, Z., & Kelessidis, V. C. (2016). Nanoparticle-Based Drilling Fluids for Minimizing Formation Damage in HP/HT Applications. *SPE International Conference and Exhibition on Formation Damage Control*. <https://doi.org/10.2118/178949-MS>.

- Maserati, G., Daturi, E., Del Gaudio, L., Belloni, A., Bolzoni, S., Lazzari, W., & Leo, G. (2010). Nano-emulsions as Cement Spacer Improve the Cleaning of Casing Bore During Cementing Operations. *SPE Annual Technical Conference and Exhibition*, 1–10. <https://doi.org/10.2118/133033-MS>.
- Mcelfresh, P. M., Wood, M., & Ector, D. (2012). Stabilizing Nano Particle Dispersions in High Salinity, High-Temperature Downhole Environments. *SPE International Oilfield Nanotechnology Conference*. <https://doi.org/10.2118/154758-MS>.
- McGill, M. (1997). Drilling Severely Depleted Sands in the Gulf of Mexico: The Benefits of Cloud Point Glycols.
- Metin, C. O., Lake, L. W., Miranda, C. R., & Nguyen, Q. P. (2011). Stability of aqueous silica nanoparticle dispersions. *Journal of Nanoparticle Research*, 13(2), 839–850. <https://doi.org/10.1007/s11051-010-0085-1>.
- Mi-Swaco. (1998). Mi-Swaco Drilling Fluid Manual.
- Miskimins, J. L. (2009). Design and Life-Cycle Considerations for Unconventional-Reservoir Wells, (May).
- Mody, F. K., & Hale, A. H. (1993). Borehole-Stability Model To Couple the Mechanics and Chemistry of Drilling-Fluid/Shale Interactions. *Journal of Petroleum Technology*, 45(11), 1093–1101. <https://doi.org/10.2118/25728-PA>.
- Myers, D. (1999). Surfaces, interfaces, and colloids, 4, 0–471. <https://doi.org/10.1002/0471234990>.
- O'Brien, D. E., & Chenevert, M. E. (1973). Stabilizing sensitive shales with inhibited, potassium-based drilling fluids. *Journal of Petroleum Technology*, 1089–1100. <https://doi.org/http://dx.doi.org/10.2118/4232-PA>.
- Ofite. (2017). HTHP Filter Press for Drilling Fluid Testing, 3(115 V), 0–33.
- Oleas, A., Osuji, C. E., Chenevert, M. E., & Sharma, M. M. (2008). Entrance Pressure of Oil-Based Mud Into Shale: Effect of Shale Water Activity and Mud Properties. *SPE Annual Technical Conference and Exhibition*, 25(1), 39–44. <https://doi.org/10.2118/116364-MS>.
- Patel, A., Stamatakis, S., Young, S., & Friedheim, J. (2007). Advances in Inhibitive Water-Based Drilling Fluids—Can They Replace Oil-Based Muds? *International Symposium on Oilfield Chemistry*. <https://doi.org/10.2118/106476-MS>.

- Peyvandi, A., Taleghani, A. D., Soroushian, P., & Cammarata, R. (2017). The Use of Low-Cost Graphite Nanomaterials to Enhance Zonal Isolation in Oil and Gas Wells. *SPE Annual Technical Conference and Exhibition*. <https://doi.org/10.2118/187105-MS>.
- Pham, H., & Nguyen, Q. P. (2014). Effect of silica nanoparticles on clay swelling and aqueous stability of nanoparticle dispersions. *Journal of Nanoparticle Research*, *16*(1). <https://doi.org/10.1007/s11051-013-2137-9>.
- Ponmani, S., Nagarajan, R., & Sangwai, J. S. (2016). Effect of Nanofluids of CuO and ZnO in Polyethylene Glycol and Polyvinylpyrrolidone on the Thermal, Electrical, and Filtration-Loss Properties of Water-Based Drilling Fluids. *SPE Journal*, *21*(2), 405–415. <https://doi.org/10.2118/178919-PA>.
- Rigaku. (1993). Theta / Theta Goniometer System With a Rotating Anode X-Ray Source (Ttr), *10*(1), 1–4.
- Riley, M., Young, S., Stamatakis, E., Guo, Q., Ji, L., De Stefano, G., ... Friedheim, J. (2012). Wellbore Stability in Unconventional Shales - The Design of a Nanoparticle Fluid. *SPE Oil and Gas India Conference and Exhibition*. <https://doi.org/10.2118/153729-MS>.
- Salih, A. H., & Bilgesu, H. (2017). Investigation of Rheological and Filtration Properties of Water-Based Drilling Fluids Using Various Anionic Nanoparticles. *SPE Western Regional Meeting*. <https://doi.org/10.2118/185638-MS>.
- Salih, A. H., Elshehabi, T. A., & Bilgesu, H. I. (2016). Impact of Nanomaterials on the Rheological and Filtration Properties of Water-Based Drilling Fluids. *SPE Eastern Regional Meeting*. <https://doi.org/10.2118/184067-MS>.
- Salles, F., Bildstein, O., Douillard, J. M., Jullien, M., & Van Damme, H. (2007). Determination of the driving force for the hydration of the swelling clays from computation of the hydration energy of the interlayer cations and the clay layer. *Journal of Physical Chemistry C*, *111*(35), 13170–13176. <https://doi.org/10.1021/jp0719762>.
- Santra, A. K., Boul, P., & Pang, X. (2012). Influence of Nanomaterials in Oilwell Cement Hydration and Mechanical Properties. *SPE International Oilfield Nanotechnology Conference and Exhibition*. <https://doi.org/10.2118/156937-MS>.
- Schlemmer, R., Friedheim, J., Growcock, F., Llc, M., Bloys, J., Headley, J., & Polnaszek, S. (2003). Chemical osmosis, shale, and drilling fluids. *SPE Drilling & Completion*, *18*(4), 318–331. <https://doi.org/10.2118/86912-PA>.

- Sensoy, T., Chenevert, M. E., & Sharma, M. M. (2009). Minimizing Water Invasion in Shale Using Nanoparticles. *SPE Annual Technical Conference and Exhibition*, (October), 1–16. <https://doi.org/10.2118/124429-MS>.
- Sharma, M. M., Zhang, R., & Chenevert, M. E. (2012). A New Family of Nanoparticle Based Drilling Fluids. *SPE Annual Technical Conference and Exhibition*, 1–13. <https://doi.org/10.2118/160045-MS>.
- Singh, V., Joung, D., Zhai, L., Das, S., Khondaker, S. I., & Seal, S. (2011). Graphene based materials: Past, present, and future. *Progress in Materials Science*, 56(8), 1178–1271. <https://doi.org/10.1016/j.pmatsci.2011.03.003>.
- SPE. (2007). Petroleum Resources Management System (PRMS). *Society of Petroleum Engineers*, 1–47.
- Srivatsa, J. T., & Ziaja, M. B. (2012). An experimental investigation on use of nanoparticles as fluid loss additives in a surfactant - Polymer based drilling fluid. *Society of Petroleum Engineers - International Petroleum Technology Conference 2012, IPTC 2012*, 3, 2436–2454. <https://doi.org/10.2523/IPTC-14952-MS>.
- Taha, N. M., & Lee, S. (2015). Nano Graphene Application Improving Drilling Fluids Performance. *International Petroleum Technology Conference*, (December), 6–9. <https://doi.org/10.2523/IPTC-18539-MS>.
- Taraghikhah, S., Kalhor Mohammadi, M., & Tahmasbi Nowtaraki, K. (2015). Multifunctional Nanoadditive in Water-Based Drilling Fluid for Improving Shale Stability. *International Petroleum Technology Conference*, 1–17. <https://doi.org/10.2523/IPTC-18323-MS>.
- Van Olphen, H. (1977). An introduction to clay colloid chemistry: for clay technologists, geologists, and soil scientists. New York: Wiley.
- Van Oort, E., Ripley, D., Ward, I., Chapman, J. W., Williamson, R., & Aston, M. (1996). Silicate-Based Drilling Fluids: Competent, Cost-effective and Benign Solutions to Wellbore Stability Problems. *SPE/IADC Drilling Conference*. <https://doi.org/10.2118/35059-MS>.
- Wahid, N., Carigali, P., Yusof, M. A., & Petronas, U. T. (2015). Optimum Nanosilica Concentration in Synthetic-Based Mud (SBM) for High-Temperature High-Pressure Well. <https://doi.org/10.2118/176036-MS>.
- Walker, B. H., & Black, A. D. (1993). Dynamic Spurt-Loss Beneath an Oilfield Bit. *Proceedings of SPE/IADC Drilling Conference*, 235–243. <https://doi.org/10.2523/25700-MS>.

- Ward, I., Chapman, J. W., & Williamson, R. (1999). Silicate Based Muds: Chemical Optimization Based on Field Experience. *SPE Drilling & Completion*, 14(1), 57–63. <https://doi.org/10.2118/55054-PA>.
- Zakaria, M., Husein, M., & Harland, G. (2012). Novel Nanoparticle-Based Drilling Fluid with Improved Characteristics. *Proceedings of SPE International Oilfield Nanotechnology Conference*, (November), 2013. <https://doi.org/10.2118/156992-MS>.
- Zamora, M., Broussard, P. N., & Stephens, M. P. (2000). The Top 10 Mud-Related Concerns in Deepwater Drilling Operations. *SPE International Petroleum Conference and Exhibition in Mexico*. <https://doi.org/10.2118/59019-MS>.
- Zamora, M., & Roy, S. (2000). The Top 10 Reasons to Rethink Hydraulics and Rheology. *IADC/SPE Asia Pacific Drilling Technology*, 1–8. <https://doi.org/10.2118/62731-MS>.
- Zeta-Meter, I. (1997). Zeta-Potential: A Complete Course in 5 Minutes. *Technical Note*, 1–8.
- Zeynali, M. E. (2012). Mechanical and physico-chemical aspects of wellbore stability during drilling operations. *Journal of Petroleum Science and Engineering*, 82–83, 120–124. <https://doi.org/10.1016/j.petrol.2012.01.006>.
- Zhang, J., Rojas, J. C., & Clark, D. E. (2008). Stressed-shale drilling strategy - Water-activity design improves drilling performance. *SPE Drilling and Completion*, 23(4), 385–393. <https://doi.org/10.2118/102498-PA>.

VITA

Jose Aramendiz Pacheco is from Valledupar, Colombia. He received his Bachelor of Science in Petroleum Engineering from the Universidad Industrial de Santander, Colombia in March 2008. After graduation, he worked mainly in the drilling and exploration area in Colombia for 8 and half years with different service companies as Baker Hughes, Weatherford, and Antonoil. During his career, Jose occupied different roles as drilling supervisor assistant, drilling fluids engineer, directional drilling field engineer and directional drilling coordinator. Jose joined Missouri University of Science & Technology in August 2016 and the Wellbore stability research group in May 2017. Jose received a degree of Master of Science in Petroleum Engineering from Missouri University of Science and Technology in December 2018.